THE TOG PROTEIN STU2/XMAP215 IS REGULATED BY ACETYLATION AND SUMOYLATION

By

MATT GREENLEE

Bachelor of Science in Biochemistry and Molecular Biology
Oklahoma State University
Stillwater, OK
May, 2011

Submitted to the Faculty of the
Graduate College of the
Oklahoma State University
in partial fulfillment of
the requirements for
the Degree of
DOCTOR OF PHILOSOPHY
May, 2021

THE TOG PROTEIN STU2/XMAP215 IS

REGULATED BY ACETYLATION AND

SUMOYLATION

Dissertation Approved:

Dr. Rita K. Miller

Dissertation Adviser

Dr. Junpeng Deng

Dr. Jose L. Soulages

Dr. Stephen Clarke

ACKNOWLEDGEMENTS

I would like to thank a number of truly inspiring people for their help during my time at Oklahoma State University. First, I would like to thank my parents, Joe and Tonya Greenlee, for their guidance, love, support, and the sense of purpose they have instilled in me. I would also like to thank my sister, Erin Greenlee, for her support over the years. I would like to thank Heather Phariss, for her unwavering love and support. I cannot say with any degree of certainty that this Ph.D. would have been possible without you.

I am grateful for the positive and motivational environment fostered by the Oklahoma State University department of Biochemistry and Molecular Biology. I have truly enjoyed the time I spent with other members of the Miller Lab. I will always remember the good times.

Lastly, I would like to thank my advisor, Dr. Rita K. Miller, for her help and support during my graduate career. You have my deepest gratitude for the great deal you taught me and the amazing opportunities you provided to expand my horizons.

Name: Matt Greenlee

Date of Degree: May, 2021

Title of Study: THE TOG PROTEIN STU2/XMAP215 IS REGULATED THROUGH ACETYLATION AND SUMOYLATION

Major Field: Biochemistry and Molecular Biology

Abstract:

Microtubules are an essential element of the cytoskeleton responsible for myriad functions which include cell shape, intra-cellular trafficking, cellular motility, and cellular division. The primary architects of these structures are the XMAP215 family of microtubule polymerases, which includes Stu2 in *S. cerevisiae*. XMAP215 family members are well known to function at four distinct locations on microtubules. During mitosis, XMAP215 members select for correct bi-oriented attachment with sister chromatid bound kinetochores in order to properly divide the genetic information found in chromosomes. XMAP215 is also found at the minus ends of microtubules at Microtubule Organizing Centers where it is believed to function in microtubule nucleation. In addition to these two locations, XMAP215 family members have been observed along the microtubule lattice as well as microtubule plus ends where they polymerize growing microtubules.

Here I demonstrate the XMAP215 family of microtubule polymerases are regulated by Small Ubiquitin-Like Modifiers (SUMO) and acetylation. Using two hybrid analysis, we mapped a minimal SUMO interacting region of Stu2 to its domain responsible for dimerization using yeast two-hybrid. With subsequent immunoprecipitation and SUMO affinity enrichment assays, we demonstrated with a high-degree of certainty that Stu2 is both covalently modified by SUMO and interacts with SUMO non-covalently. While searching by mass spectrometry for the lysines within Stu2 that are covalently modified by SUMO, we identified acetylated lysine residues. Immunoprecipitation and western blotting were used as a second method to demonstrate the acetylation of Stu2. Functional assays demonstrated that Stu2 acetylation regulates microtubule polymerization, chromosome segregation, and promoted interactions with γ-tubulin.

TABLE OF CONTENTS

Chapter Page

LIST OF TABLES

LIST OF FIGURES

Figure Page

CHAPTER I

INTRODUCTION

The XMAP215/Dis1/ch-TOG family of microtubule associated proteins are critical for kinetochore and spindle pole body processes, as well as microtubule polymerization. The human XMAP215 family member, CKAP5, is also known by its alias ch-TOG due to its overexpression in colon and hepatic tumors (Charrasse et al., 1998; Yu, Chen, Yu, Li, & Song, 2016). XMAP215 proteins contribute to microtubule dynamicity through their role in microtubule polymerization (Al-Bassam, van Breugel, Harrison, & Hyman, 2006; Pelin Ayaz et al., 2014; Brouhard et al., 2008; Podolski, Mahamdeh, & Howard, 2014; P. J. Wang & Huffaker, 1997). They are important for establishing correct kinetochore-centromere attachments and through microtubule depolymerization they facilitate "end on" microtubule capture by Ndc80 complexes to support correct sister chromatid distribution during mitosis (Asbury, Gestaut, Powers, Franck, & Davis, 2006; Humphrey, Felzer-Kim, & Joglekar, 2018; M. P. Miller, Asbury, & Biggins, 2016). They also play an important but poorly understood role in microtubule nucleation at microtubule organizing centers (MTOCs) (Chen, Yin, & Huffaker, 1998; Gunzelmann et al., 2018; Thawani, Kadzik, & Petry, 2018; Usui, Maekawa, Pereira, & Schiebel, 2003). It is therefore no surprise that the family of proteins is essential, and their absence is lethal amongst eukaryotes.

Sumoylation refers to the attachment of the Small Ubiquitin like MOdifier (SUMO) to substrate proteins via isopeptide linkages to lysine side chains. The SUMO moiety has been shown to control numerous cellular processes and responses to environmental stress. Prior to this work, Stu2 was not reported to interact with the sumoylation machinery or to be sumoylated.

Acetylation is a post-translational modification that can affect significant protein changes by masking the positive charges of lysine's ammonium-side chains with an acetyl group. Histone acetyl-transferases (HATs) transfer the acetyl-group of acetyl-CoA to the ε-ammonium group of lysine residues. This process is reversed by histone deacetylases (HDACs) which restore the positive charge of the lysine side chains. HATs and HDACs were originally named for the well-characterized process in which nucleosome histones are acetylated to expose DNA for transcription through heterochromatin to euchromatin transitions. However, since their naming, acetylation has also been shown to regulate many other proteins including cytoskeletal elements, protein turnover, the unfolded protein response, and protein transport. For this reason, the term lysine acetyl transferases, or KATs, and lysine deactylases or KDACs are often used instead of the classical HAT and HDAC terminology.

While the enzymology of acetylation and sumoylation pathways differ dramatically, both post-translational modifications are critical for environmental stress response, cell cycle progression, cellular trafficking of substrates, subcellular fractionation and orientation, protein expression, and protein-protein interactions. Learning how the functions of Stu2 are regulated by SUMO and acetylation will help to understand how the multiple roles of Stu2 are coordinated simultaneously.

The primary goal of this dissertation is to identify new regulatory mechanisms for the microtubule associated protein, Stu2. Evidence for phosphorylation mediated localization of the XMAP215/Dis1/Ch-TOG family of microtubule polymerases to the kinetochore was previously reported. Here I show that acetylation and sumoylation networks regulate the XMAP215/Dis1/Ch-

TOG member, Stu2, found in *S. cerevisiae*. My experiments directly implicate Stu2 acetylation and SUMO interactions in models of chromosome transmission fidelity. My work also identifies links between the acetylation state of Stu2 and its non-covalent interactions with SUMO. Furthermore, my data suggests that Stu2 acetylation and Stu2 interactions with SUMO might regulate Stu2 function at microtubule organizing centers. As my work is the first demonstration of sumoylation and acetylation for any member of the XMAP215 family, this work has wide ranging implications as a paradigm shift for this important family of MAPs and their downstream effect on the regulation of microtubules.

CHAPTER II

LITERATURE REVIEW

MICROTUBULES

Microtubules (MTs) are components of the cytoskeleton that form the structural cores for axonemes for cilium and flagellum for cell mobility. They also serve as tracks for several motor proteins to transport organelles, vesicles, and even chromosomes throughout the cell (reviewed in Barlan & Gelfand, 2017). During mitosis, microtubules comprise major elements of the mitotic spindle and serve as the primary force channels in concert with microtubule motors and various families of microtubule associated proteins (MAPs) to divide genetic material.

The bulk of microtubules originate from microtubule organizing centers (MTOCs) (Baas & Lin, 2011; Sanchez & Feldman, 2017; Wu & Akhmanova, 2017). In higher eukarya, the centrosome serves as the MTOC (reviewed in Tillery, Blake-Hedges, Zheng, Buchwalter, & Megraw, 2018) and in fungi the spindle pole body (SPB) serves as the MTOC (Winey & Bloom, 2012). MTs in metazoans, fission yeast, and filamentous yeast are nucleated from MTOCs through γ-tubulin ring complexes (γ-TURCs). Seven laterally interacting heterodimers consisting of 5 different GCP/Xgrip/Dgrip family proteins form the core of γ-TURCs. Each GCP/Xgrip/Dgrip family protein is capped by γ-tubulins to form the basic scaffold for αβ-tubulin

heterodimer addition for microtubule polymerization. The γ-tubulin small complex (γ-TuSC) found in budding yeast is often studied because of its simplified composition (Chen et al., 1998; Gunzelmann et al., 2018; Usui et al., 2003). The γ-TuSC consists of seven laterally interacting Spc97 and Spc98 heterodimers where each Spc protein is anteriorly capped by γ-tubulin (Geissler et al., 1996; Greenberg et al., 2016; Knop, Pereira, Geissler, Grein, & Schiebel, 1997; Kollman, Polka, Zelter, Davis, & Agard, 2010; Kollman et al., 2008; Nguyen, Vinh, Crawford, & Davis, 1998).

MTs are nucleated through γ-tubulin ring complexes found in MTOCs and project outwards to position cellular components (Kollman, Merdes, Mourey, & Agard, 2011; Teixidó-Travesa, Roig, & Lüders, 2012). MTs predominantly consist of 13 member protofilament rings that consist of alternating αβ-tubulin heterodimer chains. MT polarity enables uni-directional movement for long distance transport by end directed motors like dynein, which walks towards the MTOC which anchors the minus end of microtubules and the kinesins to transport cargo towards organelles or the cellular periphery where microtubule plus ends can be found.

Microtubules are further characterized by the role they perform in the cell. The astral MTs extend towards the cellular cortex from the MTOC. During mitosis, dynein that is anchored to the cellular cortex by Num1, walks towards the minus end of astral MTs to pull spindle pole bodies away from the metaphase plate (Eshel et al., 1993; Lee, Oberle, & Cooper, 2003). At the same time, kinetochore MTs interact with kinetochores to secure and divide sister chromatids (Biggins, 2013). Interpolar MTs, decorated with motor proteins, bridge the distance between MTOCs and provide tension during mitosis (Tolić, 2018).

TUBULINS

In *S. cerevisiae*, three types of tubulin serve as the building blocks responsible for microtubule networks. Of the three, α-tubulin, encoded by the *TUB1* and *TUB3* genes and β,

encoded by the *TUB2* gene, are responsible for the vast majority of microtubule structure. Heterodimers consisting of αβ-tubulin heterodimers form polarized microtubule protofilaments. The heterodimer is oriented within protofilaments such that the α-tubulins face the minus end of the microtubules at the spindle pole body, and the β-tubulins face the plus end of the microtubule (Desai & Mitchison, 1997). The majority of microtubules consist of thirteen laterally-interacting protofilaments that form a 25nm wide hollow tube.

Microtubule populations within cells contain individuals that are growing and shrinking regardless of cellular conditions. This inherent property of microtubules is termed "dynamic instability" (Mitchison & Kirschner, 1984a, 1984b). Growing microtubules undergo "catastrophe" during which growth halts and the microtubule plus end rapidly breaks down until it reaches an externally stabilized patch (Hyman, Salser, Drechsel, Unwin, & Mitchison, 1992). These stabilized patches are marked by the presence of microtubule associated proteins (MAPs) such as Bim1 (EB1 in humans) or Bik1 (CLIP-170 in humans) (Blake-Hodek, Cassimeris, & Huffaker, 2010). Upon stabilization, microtubules may undergo "rescue" whereby microtubules resume elongation through the addition of tubulin heterodimers to the plus end (Hyman et al., 1992).

Tubulin proteins undergo changes which contribute to this dynamic instability. While both α and β-tubulins bind GTP, only the GTP bound to β-tubulins undergoes hydrolysis (Hyman et al., 1992). GTP binds to α-tubulins in the N, or non-exchangeable site, and GTP binds to β-tubulins in the E, or exchangeable site. The E-site present on β-tubulins are adjacent to neighboring α-tubulins present in tubulin heterodimers (Lowe, Li, Downing, & Nogales, 2001; Nogales & Wang, 2006). Upon GTP-hydrolysis to GDP, β-tubulins twist and compress to impart torsional stress on the microtubule lattice (Alushin et al., 2014; Nogales & Wang, 2006; Wang & Nogales, 2005). Because only GTP bound αβ-tubulin heterodimers are incorporated into growing plus ends, growing microtubules are protected by a "GTP cap" (Carlier & Pantaloni, 1981).

In addition to α- and β-tubulins, yeast possess γ-tubulin. Although it shares significant structural similarities with the other tubulins, γ-tubulin is not incorporated into the microtubule lattice. Instead, it is essential for microtubule nucleation under physiological conditions (reviewed in Wiese & Zheng, 2006). Like β-tubulin, γ-tubulins perform GTP-hydrolysis. Basal GTP hydrolysis rates of β- and γ-tubulins are similar (Kollman et al., 2011) and interactions with α-tubulin further stimulate the GTPase activity of β- and γ-tubulins (Anders & Botstein, 2001; Gombos et al., 2013; Hyman et al., 1992; Nogales & Wang, 2006). Hydrolysis of GTP to GDP within γ-tubulin does not confer significant structural changes. Nevertheless, GTP-γ-tubulin nucleated microtubules nine times better than GDP-γ-tubulin when used in γ-TuSC microtubule nucleating templates (Gombos et al., 2013). In addition, GTP bound γ-tubulin was also reportedly essential for basal body nucleation (Shang, Tsao, & Gorovsky, 2005).

XMAP215/Stu2

XMAP215 proteins promote the assembly of α- and β-tubulin heterodimers into MTs. In addition to Stu2 found in *S. cerevisiae*, prominent XMAP215 family members include *S. pombe* Alp14 and Dis1, *A. thaliana* MOR1, *C. elegans* Zyg9, *D. melanogaster* MiniSpindles (msps), and human CKAP5/ch-TOG (Charrasse et al., 1998; Cullen, Deák, Glover, & Ohkura, 1999; Garcia, Vardy, Koonrugsa, & Toda, 2001; Rockmill & Fogel, 1988; Wang & Huffaker, 1997; Whittington et al., 2001). Members of the microtubule polymerase family are found at the kinetochore where they facilitate microtubule attachment (Humphrey et al., 2018; Miller et al., 2016; Miller et al., 2019), at MTOCs where they support microtubule nucleation (Gunzelmann et al., 2018; Thawani et al., 2018; Wang & Huffaker, 1997), at microtubule plus ends (Al-Bassam et al., 2006), and along the microtubule lattice (Al-Bassam et al., 2006; Humphrey et al., 2018; Wang & Huffaker, 1997). Depletion of these proteins significantly increases microtubule catastrophe and leads to shortened microtubules.

TOG domains

The XMAP215 family of proteins are most conserved in their N-terminal TOG domains, which bind directly to tubulins. Each protein contains between two and five 250 amino acid repeats known as Tumor Overexpressed Gene (TOG) domains (Al-Bassam et al., 2006). The number of TOG domains present in XMAP215 homologs vary based on the organism's relative complexity, with yeast having two TOG domains (Alp14, Dis1, Stu2). Worms have three TOG domains (Zyg9) and complex multicellular organisms including flies, plants, and humans have five TOG domains (msps, MOR1, and CKAP5) (reviewed in Al-Bassam & Chang, 2011). TOG domains are themselves comprised of 6 α-helical HEAT (Huntingtin, elongation factor 3, protein phosphatase 2A, TOR1) (Yoshimura & Hirano, 2016). These 6 HEAT repeats form a flat layer of α-helices that interacts with tubulins along their narrow edges (Al-Bassam, Larsen, Hyman, & Harrison, 2007; Ayaz, Ye, Huddleston, Brautigam, & Rice, 2012; Slep & Vale, 2007).

XMAP215/Stu2 and microtubule polymerization

Crystal structures indicate that TOG domains bind free tubulin heterodimers in a 1:1 ratio (Ayaz et al., 2014; P. Ayaz et al., 2012; Nithianantham et al., 2018). Through their MT binding domains, XMAP215 proteins are believed to touch and release the microtubule lattice until they find the microtubule plus-end. At the microtubule plus end, tubulins are incorporated into the MT lattice and the XMAP215 protein detaches (Brouhard et al., 2008; Widlund et al., 2011). While it is poorly understood whether other mechanisms enrich Stu2 at the plus end of microtubules, it is possible that interactions with plus end tracking proteins such as Bim1 (EB1) or Bik1 (CLIP-170) in humans may facilitate its plus-end localization (Wolyniak et al., 2006).

XMAP215/Stu2 and the kinetochore

Within the mitotic apparatus, Stu2 serves an important role in bridging kinetochores to microtubules. Stu2 helps secure attachments between kinetochores and a class of microtubules

termed K-fibers. When opposing K-fiber pairs fail to properly attach to sister chromatids, monopole kinetochore attachments experience low tension and are non-persistent, however, polarized attachments exert higher levels of tension and form persistent kinetochore interactions (Akiyoshi et al., 2010; Miller et al., 2016). Correct attachments between kinetochores and K-fibers are likely supported by Stu2 induced depolymerization of K-fibers at the kinetochore and subsequent "catch-bond" activity (Humphrey et al., 2018). The Dam1 ring then harnesses forces generated through microtubule catastrophe to secure these K-fiber attachments (Grishchuk et al., 2008; Volkov et al., 2013).

The propensity for the Dam1 ring to track microtubule plus ends has also been well characterized in vitro (Asbury et al., 2006; Lampert, Hornung, & Westermann, 2010; Powers et al., 2009; Tien et al., 2010). As tension of kinetochore attachments to k-fibers increases, so too does the probability of microtubule rescue (Franck et al., 2007). K-fiber elongation may represent an additional protective measure that cells employ to ensure that correct kinetochore attachments are maintained during transient periods of excessive tension.

XMAP215/Stu2 and microtubule organizing centers

XMAP215/Stu2 serves as a microtubule nucleation factor at the SPB. While research in this area is still ongoing, XMAP215 family members have long been observed in MTOCs. Interactions between XMAP215 family proteins and MTOC proteins have been shown between Stu2 and Spc72 in *S. cerevisiae* (Chen et al., 1998), Alp14 and Alp7 in *S. pombe* (Sato, Vardy, Garcia, Koonrugsa, & Toda, 2004), msps and D-TACC in *D. melanogaster* (Fiona, Cullen & Ohkura, 2001; Lee, Gergely, Jeffers, Peak-Chew, & Raff, 2001), and ckap5-a and tacc3 in *X. laevis* (Kinoshita et al., 2005). Localization of XMAP215 family members to MTOCs correlates with increases in microtubule numbers (Bellanger & Gönczy, 2003; Kinoshita et al.,

2005; Lee et al., 2001). Most recently, XMAP215 family members synergistically nucleated microtubules with γ-TuSCs and γ-TuRCs (Gunzelmann et al., 2018; Thawani et al., 2018).

THE SUMO PROTEIN

SUMO, the Small Ubiquitin like MOdifier, is a member of the ubiquitin family of proteins that are known for their covalent attachment and subsequent regulation of proteins (Bayer et al., 1998). The SUMO protein is encoded by the *SMT3* gene in *S. cerevisiae* and is 101 amino acids long and approximately 11.6 kDa in size. While SUMO shares only about 18% of sequence identity with ubiquitin, the tertiary structures of both proteins possess a common ββαββαβ tertiary structure known as the β-grasp fold (Bayer et al., 1998).

SUMO is expressed solely as a pro-protein monomer by the *SMT3* gene in *S. cerevisiae*. In contrast, ubiquitin pro-proteins are co-expressed with other proteins by the *UB11*, *UB12*, and *UB13* genes and as a poly-ubiquitin precursor protein by the *UB14* gene (Ozkaynak, Finley, Solomon, & Varshavsky, 1987). In each case, the c-terminus of the pro-protein is proteolytically processed to expose the glycine residues necessary for activation and conjugation. Initial SUMO processing is carried out by the Ubl-specific protease (ULP) Ulp1 (Li & Hochstrasser, 1999; Mevissen & Komander, 2017; Ronau, Beckmann, & Hochstrasser, 2016), whereas ubiquitin activation is performed by deubiquitinating enzymes (Fang & Weissman, 2004; Larsen, Krantz, & Wilkinson, 1998; Li & Ye, 2008; Ozkaynak et al., 1987; Wilkinson, 1997).

Sumoylation

Sumoylation describes the covalent attachment of SUMO to substrate proteins via an isopeptide bond to the ε-amine group of lysine residues. Sumoylation plays important roles in myriad cellular processes including cell cycle progression (Finkbeiner, Haindl, Raman, & Muller, 2011; Pinder, McQuaid, & Dobson, 2013; Stead et al., 2003; Yong-Gonzales, Hang, Castellucci, Branzei, & Zhao, 2012), environmental adaptation (Garcia-Domiquez & Reyes, 2009; Ouyang,

Valin, & Gill, 2009), protein trafficking (Wang, Pernet, & Lee, 2012), and stress responses such as DNA repair (Nagai, Davoodi, & Gasser, 2011; Prudden et al., 2011). The roles of sumoylation have also been extensively reviewed (Alonso et al., 2015; Bergink & Jentsch, 2009; Dasso, 2008; Gareau & Lima, 2010; Nagai et al., 2011; Praefcke, Hofmann, & Dohmen, 2012; Stehmeier & Muller, 2009). Classically, SUMO conjugation to substrates occurs at a canonical ΦKXE/D consensus site, where Φ is a hydrophobic residue and X can be any amino acid (Johnson, 2004; Melchior, 2000). Yet, only about half of observed sumoylation sites match the ΦKXE/D motif (Hendriks et al., 2017).

The diverse function of ubiquitin's modification of protein substrates is specified by its ability to "chain itself" in different configurations (reviewed in Akutsu, Dikic, & Bremm, 2016). Perhaps the most prominent function of ubiquitin is protein turn-over (Ciechanover, 1994; Rock et al., 1994) (reviewed in Walters, Goh, Wang, Wagner, & Howley, 2004)(Pickart & Fushman, 2004). Protein turnover is mediated by a specific ubiquitin configuration consisting of at least four lysine 48-linked ubiquitin molecules. Proteins labeled with these chains of K48-linked ubiquitin are recognized by S5a/Rpn10's c-terminal ubiquitin interacting motif (UIM) at the 26S proteasome and degraded (Hofmann & Falquet, 2001; Young, Deveraux, Beal, Pickart, & Rechsteiner, 1998). Additionally, K11 chaining by the anaphase-promoting complex (APC) targets specific protein substrates protein degradation during mitosis (Matsumoto et al., 2010). The role of ubiquitin in regulating endocytic trafficking, inflammation, translation, and DNA repair is dictated by its ability to form ubiquitin chains through lysine 63 (Acconcia, Sigismund, & Polo, 2009; Miranda & Sorkin, 2007; Pickart & Fushman, 2004). K6 linkages are reportedly associated with DNA repair responses and increase in abundance following UV challenges (Elia et al., 2015; Morris & Solomon; Nishikawa et al., 2004). Furthermore, K6 linkages aren't anticipated to be related to protein turnover since their abundance does not increase with proteasome inhibition (Kim et al., 2011; Wagner et al., 2011).

The sumoylation pathway

Unlike the ubiquitin family which relies on three classes of enzymes, addition of mature SUMO requires only two classes of enzymes, the E1 SUMO activating enzymes and E2 conjugating enzyme, albeit the third class of SUMO enzymes, the E3 SUMO ligating enzymes, are believed to enhance the process and provide some specificity (Gareau & Lima, 2010; Takahashi, Toh-e, & Kikuchi, 2001). E1 SUMO activating enzymes consume ATP to produce a high-energy thioester bond with the c-terminal glycine of mature SUMO. The E1 holoenzyme consists of an evolutionarily conserved Aos1p and Uba2p heterodimer (Desterro, Rodriguez, Kemp, & Hay, 1999; Dohmen et al., 1995; Johnson, Schwienhorst, Dohmen, & and Blobel, 1997).

SUMO E2 enzymes are responsible for attachment of SUMO moieties to lysine residues. The single E2 SUMO conjugating enzyme is Ubc9p (reviewed in Gareau & Lima, 2010 and Alonso et al., 2015). It is evolutionarily conserved and yeast Ubc9 shares 56% sequence similarity with human Ubc9 (Johnson & Blobel, 1997; Schwarz, Matuschewski, Liakopoulos, Scheffner, & Jentsch, 1998). Ubc9 is regulated by post-translational modifications that modulate its conjugation activity and regulate its substrate specificity. Ubc9 sumoylation impairs RanGAP1 sumoylation but leads to significant increases in sumoylation of the transcriptional regulator Sp100 (Knipscheer et al., 2008). Ubc9 recognition of specific substrates was also reportedly enhanced through Cdk1 phosphorylation in a cell cycle dependent manner (Su, Yang, Huang, Liu, & Hwang, 2012). Acetylation of Ubc9 also down regulates sumoylation of substrates possessing the negatively charged amino acid-dependent sumoylation motif (NDSM) (Naik et al., 2017).

In addition to E1s and E2s, a final class of SUMO ligating enzymes (E3s) expand the range of potential SUMO substrates and improves efficiency. E3s accomplish this task by either

recruiting E2-SUMO and substrates into complexes to promote specificity and proximity, or they can promote SUMO removal from E2 enzymes to increase efficiencies (Desterro et al., 1999; Gareau & Lima, 2010; Okuma, Honda, Ichikawa, Tsumagari, & Yasuda; Takahashi, Toh-e, et al., 2001). Humans possess several classes of E3 SUMO ligases including, the protein inhibitor of activated STAT (the PIAS family) (Shuai, 2000), the polycomb group protein Pc2 (Kagey, Melhuish, & Wotton, 2003), and the cytoplasmically exposed nucleoporin RanBP2/Nup358 (Pichler, Gast, Seeler, Dejean, & Melchior, 2002).

While there are several classes of E3 ligases found in humans, there are only four E3 ligases in yeast; Siz1, Siz2/Nfi1, Mms21/Nse2, and Cst9/Zip3 (Duan, Holmes, & Ye, 2011; Heideker, Prudden, Perry, Tainer, & Boddy, 2011; Johnson & Gupta, 2001; Reindle et al., 2006; Stephan, Kliszczak, & Morrison, 2011). Siz1, Siz2/Nfi1, and Mms21/Nse2 all possess RING domains responsible for ligation activities and belong to the PIAS family of E3 ligases. The Siz/PIAS family SUMO E3s interact with their E2s similarly to how ubiquitin E3-ligases interact with ubiquitin E2 conjugation enzymes (Hochstrasser, 2001; Johnson & Gupta, 2001). Based on predictions from ubiquitin E2/E3 complex studies, SUMO Siz/PIAS E3 ligating enzymes were mutated to disrupt SUMO E2/E3 interactions and subsequently failed to support SUMO conjugation to substrates (Yunus & Lima, 2009). In yeast, Siz1 and Siz2 account for a majority of sumoylation where Siz1 plays a larger role in global sumoylation in the cell and Siz2 activity correlates more strongly with DNA repair mechanisms (Horigome et al., 2016; Johnson & Gupta, 2001; Takahashi, Kahyo, Toh-E., Yasuda, & Kikuchi, 2001).

Mms21 supports Siz2 functions in DNA repair and was first identified while screening for mutants that are sensitive to methyl methanesulfonate (MMS) (Horigome et al., 2016; Prakash & Prakash, 1977). MMS methylates DNA at N7-deoxyguanosine, N3-deoxyadenosine, to a lesser extent other oxygen and nitrogen atoms in other bases, and phosphodiester linkages to stall replication forks during DNA replication (Lundin et al., 2005). Mms21 is part of the SMC5-

SMC6 complex and Mms21 mediated sumoylation events are important for nucleolar formation and function (Kim et al., 2016; Zhao & Blobel, 2005). Additionally, Mms21 regulates sister chromatid segregation, localization of dsDNA breaks to the nuclear periphery, and suppresses spontaneous mutation and mitotic recombination (Bermúdez-López et al., 2010; Horigome et al., 2016; Montelone & Koelliker, 1995; Prakash & Prakash, 1977). Cst9 is essential for synaptonemal complex formation and localizes to programmed DNA double-strand breaks (DSBs) to facilitate targeted gene recombination during meiosis (Agarwal & Roeder, 2000; Cheng et al., 2006; Ouspenski, Elledge, & Brinkley, 1999; Serrentino, Chaplais, Sommermeyer, & Borde, 2013).

SUMO noncovalent interactions

In addition to covalent attachment to substrates, SUMO can bind proteins non-covalently. These non-covalent interactions occur through SUMO interaction motifs (SIMs) (Kroetz & Hochstrasser, 2009; Minty, Dumont, Kaghad, & Caput, 2000; J. Song, Durrin, Wilkinson, Krontiris, & Chen, 2004). The SIM motif consists of a 4 amino-acid long stretch of hydrophobic residues with the pattern (I/L/V) X (I/L/V) (I/L/V) where the X position is occupied by any amino acid (Kroetz & Hochstrasser, 2009; Song et al., 2004). Protein SIMs bind to SUMO at a hydrophobic patch found between β-sheet two and α-helix one (Song, et al., 2004). Upon interaction with SUMO, the SIM adopts a beta sheet confirmation that extends the N-terminal beta sheet of SUMO (Chang et al., 2011; Hecker, Rabiller, Haglund, Bayer, & Dikic, 2006; Namanja et al., 2012; Sekiyama et al., 2008; Song, Zhang, Hu, & Chen, 2005; Xu et al., 2014).

The functional analysis of SIMs is an expanding field that recently has revealed new roles in DNA repair, DNA replication, and substrate sumoylation. SIMs facilitate recruitment of RAP80 to damaged DNA where it facilitates repair of double-strand DNA Breaks (Anamika & Spyracopoulos, 2016; Guzzo et al., 2012; Hu, Paul, & Wang, 2012). Sumoylated PCNA also

recruits Srs2 helicase to replication forks for error free DNA replication (Hannich et al., 2005; Hoege, Pfander, Moldovan, Pyrowolakis, & Jentsch, 2002; Kerscher, 2007; Papouli et al., 2005). Sumoylation of Ubc9 has also been shown to enhance its ability to covalently attach SUMO to proteins containing SIMs (Kim, Kim, Matunis, & Ahn, 2009; Knipscheer et al., 2008; Tatham et al., 2005).

Phosphorylation and acetylation regulate noncovalent interactions between SUMO and SIMs. Phosphorylation of serine or threonine residues flanking SIMs improve electrostatic interactions between SUMO and non-covalently interacting proteins (Cappadocia et al., 2015; Chang et al., 2011; Stehmeier & Muller, 2009). PML protein, named for its association with promyelocytic leukemia nuclear bodies, contains one such phosphoSIM. PML interactions with SUMO are facilitated by phosphorylation of Serines 565, 560, 561, and 562 (Cappadocia et al., 2015; Rabellino et al., 2012; Scaglioni et al., 2006). SUMO interactions with RAP80 are enhanced by SIM phosphorylation and may play a role in RAP80 recruitment to damaged DNA (Anamika & Spyracopoulos, 2016). Acetylation of lysine residues in SUMO1 and SUMO2 reduce their affinity for SIMs by eliminating electrostatic interactions between SUMO lysines and phosphoserines, phosphothreonines, aspartates, and glutamates that often flank SIM motifs (Ullmann, Chien, Avantaggiati, & Muller, 2012).

SUMO targeted ubiquitin ligases

SUMO targeted ubiquitin ligases (STUbLs) are an important group of proteins responsible for protein turnover of sumoylated proteins. These proteins interact with sumoylated proteins in order to ubiquitinate them. STUbLs are able to carry out this process since they are a special class of Ubiquitin E3 ligases with SIMS (Perry, Tainer, & Boddy, 2008). In yeast, there are two STUbLs. One STUbL consists of the heterodimer formed by Slx5 and Slx8. The Slx5-Slx8 heterodimer is essential for cellular survival in the absence of the Sgs1 DNA helicase

(Mullen, Kaliraman, Ibrahim, & Brill, 2001). The second STUbL, Ris1, is important for preventing telomeric fusions by preventing their erroneous recognition as double-strand breaks (Chung & Zhao, 2013; Lescasse, Pobiega, Callebaut, & Marcand, 2013).

SUMO isopeptidases

Because of SUMO isopeptidases, sumoylation is a reversible process. SUMO can be cleaved from the ε-amine group of lysine to restore proteins to their non-sumoylated state. This is important since many SUMO substrates are rapidly sumoylated and desumoylated in response to environmental stresses. Yeast use three enzymes to desumoylate proteins; Ulp1, Ulp2, and Wss1. Ulp1 and Ulp2 are responsible for removing SUMO from different populations of substrates (Johnson & Blobel, 1999; Li & Hochstrasser, 2000). While Ulp2 is not essential, deletion of Ulp1 is lethal. This may be explained by demonstrations where Ulp1 could cleave Ulp2 specific SUMO conjugates while Ulp2 failed to cleave Ulp1 substrates (Li & Hochstrasser, 2000). However, Ulp2 showed significantly more activity in regulating SUMO chains compared to Ulp1. (Schwienhorst, Johnson, & Dohmen, 2000). The third SUMO isopeptidases, Wss1, exhibits SUMO ligase activity in addition to its role as a SUMO isopeptidase (Balakirev et al., 2015). While Wss1 has been shown to predominantly remove SUMO, it is able to remove ubiquitin from substrates as well. (Su & Hochstrasser, 2010).

ACETYLATION

Acetylation is a post-translational modification that regulates protein-protein and protein-nucleic acid interactions by masking the positive charge of lysine ε-ammonium groups. Defects in acetylation regulatory enzymes, HDAC and HATs correlate strongly with major diseases including cancer, neurodegenerative disorders, and cardiovascular disease (Barbier et al., 2019; Blander & Guarente, 2004; Carrozza, Utley, Workman, & Côté, 2003; Irwin et al., 2012; Irwin, Lee, & Trojanowski, 2013; Kim et al., 2011; Li et al., 2014; McKinsey & Olson, 2004; Min et al.,

2010, 2015; Tracy et al., 2016; Yang, 2004). The first proteins discovered to undergo acetylation were histones, a discovery made in 1968 (Vidali, Gershey, & Allfrey, 1968). It took nearly three decades to identify the first acetylation sites in a non-histone protein, p53 (Gu & Roeder, 1997). However, genomic and proteomic approaches have identified many non-histone acetylation events in proteins which demonstrate acetylation roles beyond histones regulation (Choudhary et al., 2009; Duffy et al., 2012; Henriksen et al., 2012; Kim et al., 2006; Lin et al., 2009). Acetylation is now known to regulate DNA-protein interactions, subcellular localization, the cell cycle, transcriptional activity, chromatin remodeling, RNA metabolism, cytoskeleton dynamics, membrane trafficking, and protein stability (Choudhary et al., 2009).

Lysine acetyl-transferases and lysine deacetylases

Histone acetyl-transferases (HATs) or lysine acetyl-transferases (KATs) use the acetyl moiety in Acetyl-CoA for the transfer of acetyl groups to the ε-ammonium group of lysine residues. Acetylation by KATs involves the formation of a ternary complex including KAT–acetyl-CoA–substrate followed by deprotonation of the ε-amino group of lysine by glutamate or aspartate within the KAT catalytic site, and is completed through a nucleophilic attack on the carbonyl group of acetyl-CoA (Albaugh, Arnold, Lee, & Denu, 2011; Berndsen, Albaugh, Tan, & Denu, 2007; Tanner, Langer, Kim, & Denu, 2000). Histone deacetylases (HDACs) or lysine deacetylases (KDACs) hydrolyze the amide linkage between acetyl groups and amino groups of lysine residues to yield acetate. Most KATs and HDACs function as multi subunit complexes (Millar & Grunstein, 2006; Roth, Denu, & Allis, 2001; Sterner & Berger, 2000). Spontaneous protein acetylation also occurs in the absence of KATs, especially in the mitochondrion where the concentrations of acetyl-CoA and the pH is higher (Poulsen et al., 2013; Weinert et al., 2014).

Acetyl-coenzyme A (CoA) is a central metabolite processed from pyruvate following glycolysis. Unsurprisingly, Acetyl-CoA levels are highest during exponential growth in the

presence of glucose. Since protein acetylation levels often match the concentration of Acetyl-CoA concentration, protein acetylation has been extensively studied as metabolic rheostats for cells (Cai, Sutter, Li, & Tu, 2011; Ramaswamy, Williams, Robinson, Sopko, & Schultz, 2003; Sandmeier et al., 2002; Seker, Møller, & Nielsen, 2005; Takahashi, McCaffery, Irizarry, & Boeke; Weinert et al., 2014; Wellen et al., 2009).

Currently, seven KATS and nine KDACs have been identified in yeast. KATs are classified by their cellular localization where A-types are found in the nucleus and B-types are found in the cytoplasm (Galdieri, Zhang, Rogerson, Lleshi, & Vancura, 2014). KDACs however, are divided into structural classes as Class I, Class II, and Class III enzymes. Class I and Class II KDACs have similar catalytic domains, whereas Class III KDACs share no sequence similarity to Classes I and II and are instead a member of the family of sirtuins that require NAD^+ to function. Similar to KDACs, KATs are also classified based on their structural conservation. In *S. cerevisiae*, the Gcn5-related N-acetyltransferase (GNAT) superfamily consists of Gcn5, Hat1, and Elp3 while the MYST group which is named after its founding members (MOZ, Ybf2/Sas3, Sas2, and Tip 60) also includes Esa1, Sas2, and Sas3.

A-type KATs

Yeast A-type KATs include Gcn5, Esa1, Sas2, Sas3, Rtt109 and Elp3. While there are a significant number of KATs that share substrates, they have strikingly limited overlap in lysine recognition as summarized by Table 1 of (Galdieri et al., 2014). Gcn5 is found in the SAGA complex, the SLIK/SALSA, ADA, HAT-A2, and HATB3.1 complexes which acetylate multiple lysine residues of Histone 3 to facilitate nucleosome assembly (Burgess, Zhou, Han, & Zhang, 2010; Krebs, 2007; Millar & Grunstein, 2006; Rando & Winston, 2012; Shahbazian & Grunstein, 2007). Additionally, newly synthesized Histone 3 is acetylated at lysine 56 by Rtt109p to facilitate DNA replication and repair when Asf1 is present (Adkins, Carson, English, Ramey, &

Tyler, 2007; Driscoll, Hudson, & Jackson, 2007). Unlike other KATs, Esa1, is essential for viability. Esa1 is the catalytic subunit of the NuA4 HAT complex (Reifsnyder, Lowell, Clarke, & Pillus, 1996; Smith et al., 1998). Sas2 is responsible for H4 at K16 acetylation which creates boundary regions separating heterochromatin and adjoining euchromatin (Kimura, Umehara, & Horikoshi, 2002; Suka, Luo, & Grunstein, 2002). Additionally, loss of Histone 3 acetylation in Gcn5 and Sas3 double knockouts leads to cell cycle arrest in the G2/M phase of the cell cycle (Howe et al., 2001). Lastly, Elp3 functions in the Elongator HAT complex, which was first identified by its association with RNA PolII holoenzyme during transcriptional elongation (Saunders, Core, & Lis, 2006). Recent studies suggest Elp3 stability is reliant on Elp1, and compromising Elp3 HAT stability leads to the autonomic neuropathy familial dysautonomia (Slaugenhaupt et al., 2001; Svejstrup, 2007).

B-type KATs

The only B-type KAT found in *S cerevisiae* is Hat1. Hat1 is well known for its role in the rapid acetylation of newly synthesized cytoplasmic histone H4 at lysines 5 and 12 (Sobel, Cook, Perry, Annunziato, & Allis, 1995). However, inactivation of Hat1 did not reveal a role for Hat1 in chromatin assembly (Parthun, Widom, & Gottschling, 1996).

Multiple KAT complexes are regulated through autoacetylation

Esa1 autoacetylates a conserved lysine residue to activate the NuA4 HAT complex (Yuan et al., 2012). It also acetylates Yng2, another subunit of the NuA4 complex, which when mutated to abolish this acetylation leads to hypersensitivity to benomyl and methyl methanesulfonate. Rtt109 enzymatic activity is also reliant on autoacetylation of a lysine residue present in its active site (Albaugh et al., 2011). Lastly, Gcn5 acetylates several subunits found in the SAGA HAT complex, which correlates strongly with the complex's activity (Cai et al., 2011). Together, these

observations indicate autoacetylation of HAT complexes represent another means through which nutrient abundance regulates acetylation levels in the cell.

Class I KDACs

Class I KDACs are found predominantly in the nucleus and include Rpd3, Hos2, and Hos1. Rpd3 works to deacetylate Yng2 following its acetylation by Esa1 (Lin et al., 2008). Along with the Class II KDAC, Hda1, Rpd3 works to counteract the acetylation of the NuA4 and SAGA HAT complexes (Lin et al., 2008). Furthermore, the activities of the NuA4, SAGA, Hda1 and Rpd3 complexes represent a majority of cellular histone acetylation and deacetylation. Hos1 functions in the acetylation cycle of Smc3, a member of the chromosomal cohesin complex. This entails routine Smc3 deacetylation by Hos1 during anaphase to prepare for subsequent cellular division, a process that requires non-acetylated Smc3 (Borges et al., 2010). The final Class I KDAC member, Hos2 complexes in the Rpd3L complex as well as its own SET3 complex. Hos2 functions along with the Class III Hst1 to suppress yeast sporulation (Pijnappel et al., 2001).

Class II KDACs

Class II KDACs including Hda1 and Hos3 are found in the nucleus and cytoplasm. As previously discussed, Hda1 represents one of the more active KDACs and deacetylates a diverse range of substrate proteins. Hda1 deacetylation of K27 and K270 in the *S. cerevisiae* protein Hsp90 promotes resistance to the azole miconazole (Robbins, Leach, & Cowen, 2012). Unlike other KDACs, Hos3 possesses basal histone deacetylase activity even in the absence of a complex (Carmen et al., 1999). Additionally, Hos3 is not inhibited by the pan-deacetylase inhibitor Trichostatin A (Carmen et al., 1999). Even when expressed in *E. coli*, Hos3 possessed intrinsic deacetylase activity leading investigators to believe that interacting proteins likely sequester Hos3 to reduce its activity, rather than activate it like most other KATs or KDACs (Carmen et al., 1999).

Class III KDACs/sirtuins

Lastly, Class III KDACs (sirtuins), including Sir2, Hst1, Hst2, Hst3, and Hst4 seem to be localized based on amino- and carboxyl-terminal extensions that also regulate their catalytic activity (North & Verdin, 2004). Sirtuins activity closely mirrors glucose abundance under high glucose conditions. When glucose is high, cytosolic NAD^+ essential for sirtuin deacetylation is largely converted into NADH (Finkel, Deng, & Mostoslavsky, 2009). The sirtuin Hst1 is also implicated in NAD^+ synthesis since NAD^+ abundance is increased in the absence of a functional *HST1* gene (Bedalov, Hirao, Posakony, Nelson, & Simon, 2003). Lastly, disruption of the *HST3* and *HST4* genes lead to a growth defects in yeast grown on the non-fermentable carbon source, acetate (Starai, Takahashi, Boeke, & Escalante-Semerena, 2003).

Acetylation of MAP proteins

Acetylation of K212 in the human plus end tracking protein EB1, the human homologue of Bim1 in yeast, was shown to regulate interactions with CLIP-170, p150glued, and APC (Xie et al., 2018). Also, CLIP-170, the human homolog of the yeast protein BIK1, has been shown to be acetylated, however the function and modified residues have yet to be identified (Li et al., 2014). It is not known how or if acetylation regulates other microtubule associated proteins (MAPs). In this report, we examine the acetylation of the XMAP215 protein Stu2 in yeast. We found that Stu2 TOG domain acetylation mediates cellular growth, microtubule stress responses, modulates non-covalent interactions between Stu2 and SUMO, and impacts chromosome stability.

Acetylation was previously shown to regulate the microtubule network. Aged MTs contain K40 acetylated α-tubulin, but it is not known if K40 acetylation is responsible for MT longevity. While the function of K40 acetylation remains inconclusive, (Kaul, Soppina, & Verhey, 2014), it has been reported that inhibition of K40 acetylation is necessary for contact inhibition during cell proliferation (Aguilar et al., 2014).

Recent structural studies indicate that extensive α-tubulin K40 acetylation weakens lateral contacts formed by adjacent protofilaments while strengthening longitudinal interactions of αβ-tubulin heterodimers within protofilaments (Eshun-Wilson et al., 2019; Manka & Moores, 2018). Tau acetylation suppresses its interactions with MTs (Cohen et al., 2011). Additionally, acetylation impairs phosphorylation mediated degradation of tau, implicating tau acetylation in neurodegenerative diseases often referred to as tauopathies (Barbier et al., 2019; Irwin et al., 2012; Irwin et al., 2013; Min et al., 2010, 2015; Tracy et al., 2016). Such neurodegenerative diseases characterized by hyperphosphorylated tau include frontotemporal dementia and parkinsonism linked to chromosome 17 (FTDP-17), as well as Alzheimer's disease (AD) (Cairns et al., 2007; Hutton et al., 1998; Ludolph et al., 2009; Spillantini et al., 1998).

Acetylation has also been shown to compete with sumoylation of proteins, (Escobar-Ramirez et al., 2015; Stankovic-Valentin et al., 2007; Ullmann et al., 2012; Zheng & Yang, 2005). This raises the possibility that there may be an antagonistic relationship between Stu2 sumoylation (Greenlee et al., 2018) and Stu2 acetylation (this report).

CHAPTER III

THE TOG PROTEIN STU2/XMAP215 INTERACTS COVALENTLY AND NONCOVALENTLY WITH SUMO

It is becoming increasingly apparent that SUMO regulates different classes of microtubule-associated proteins, which include tau (Dorval & Fraser, 2006), Ndc80 (Montpetit, Hazbun, Fields, & Hieter, 2006), CENP-E (Zhang et al., 2008), Kar9 (Leisner et al., 2008; Schweiggert, Stevermann, Panigada, Kammerer, & Liakopoulos, 2016), Bim1 (Meednu et al., 2008), Pac1, and Bik1 (Alonso et al., 2012). For that reason, we asked whether the XMAP215 family of microtubule polymerases and tubulins themselves may also be regulated by sumoylation pathways. XMAP215 microtubule polymerases and tubulins are some of the most evolutionarily conserved proteins across eukarya. This is largely due to their roles in maintaining the microtubule apparatus that is so critical for cellular division.

Stu2, the XMAP215 family member found in *S. cerevisiae* interacts with 5 out of the 8 classes of MAPs that are known to interact with SUMO. These classes include tau (Dorval & Fraser, 2006), Ndc80 (Montpetit et al., 2006), CENP-E (Zhang et al., 2008), Kar9 and Bim1/EB1 (Leisner et al., 2008; Meednu et al., 2008; Schweiggert et al., 2016), Pac1/Lis1, and Bik1/CLIP-170 (Alonso et al., 2012). In this chapter, we investigate whether Stu2 and tubulins are also regulated by SUMO. Further, we demonstrate that tubulin can bind to SUMO noncovalently and directly.

SUMMARY OF MANUSCRIPT

Stu2 and SUMO

In this paper, we demonstrate that Stu2 interacts covalently and non-covalently with SUMO through yeast two-hybrid, *in vitro* sumoylation, co-immunoprecipitation, and affinity purification assays. We first used yeast two-hybrid to demonstrate that Stu2 interacts with SUMO, the SUMO conjugating E2 enzyme Ubc9, the SUMO ligating E3 enzyme Nfi1, and two MAPs previously shown to be sumoylated, Bik1 and Bim1 (Alonso et al., 2012). In addition to interacting with SUMO and the sumoylation machinery, we find that Ris1 and Wss1, a STUbL and SUMO isopeptidases, interact with Stu2. This finding represented a clear indication that Stu2 is sumoylated. Using a series of two hybrid-Stu2 truncations, we mapped SUMO and the sumoylation machinery's interactions with Stu2 to a short region within Stu2 that encompasses the c-terminal half of the microtubule binding domain and the dimerization domain. Second, we demonstrated that Stu2 was sumoylated *in vitro* following incubation with reconstituted SUMO E1 holoenzyme Aos1/Uba2, the SUMO E2 conjugating enzyme Ubc9, activated SUMO-GG, and ATP. Third, we performed co-immunoprecipitation experiments that showed Stu2 bands cross-react with SUMO antibodies. In addition, we enriched histidine tagged Stu2 under chaotropic conditions using 8M urea. Despite extensive protein denaturation, anti-SUMO continued reacting with Stu2 bands in western blots. Lastly, we demonstrated that Stu2 interacts non-covalently with SUMO using GST-SUMO-GA affinity enrichment columns.

Tubulins and SUMO

While investigating Stu2 covalent and non-covalent interactions with SUMO, we also tested whether tubulins, key binding partners of Stu2, would interact with SUMO. Yeast two-hybrid experiments demonstrated that tubulins did indeed interact with SUMO and the sumoylation machinery. Tubulins, like Stu2, interacted with the STUbL, Ris1, but not with the isopeptidases Wss1. While performing pull-downs with SUMO-GST fusion proteins to test for non-covalent interactions between Stu2 and SUMO,

we also probed for Tub1. These western blots revealed that tubulins too might interact non-covalently with SUMO. Because the possibility existed for Stu2 to bridge an interaction between Tub1 and SUMO, we repeated the experiment using a degron tagged Stu2. Even in the absence of full-length Stu2, tubulin continued interacting non-covalently with SUMO.

Acknowledgements

From the subject matter of chapter 3 in this dissertation, a manuscript was prepared, submitted, and published in the journal *Cytoskeleton*. This article, titled "The TOG protein Stu2/XMAP215 interacts covalently and noncovalently with SUMO," was co-authored by Matt Greenlee, Annabel Alonso, Maliha Rahman, Nida Meednu, Kayla Davis, Victoria Tabb, River Cook, and Rita K. Miller.

Discussion

This work demonstrates that Stu2, a member of the XMAP215 family of microtubule polymerases, and tubulins, the constitutive proteins of microtubules themselves, interact with SUMO covalently and non-covalently. These findings indicate that Stu2 and tubulins are among a growing list of MAPs regulated by SUMO. It will be important to discern how SUMO interactions control the multiple roles of this microtubule polymerase during mitosis and meiosis. Additional work lies ahead in determining what specific processes are regulated by SUMO interactions with Stu2 and tubulin. One key task that still remains is to identify Stu2's sumoylation sites. Identifying and mutating to prevent Stu2 sumoylation will provide powerful insights into what Stu2 sumoylation is responsible for amongst the numerous functions in which Stu2 participates. Another burning question is whether SUMO regulates XMAP215 family proteins from other organisms.

Figure	Contributed by . . .
2a, 2b, 2c, 2d, 5b, 6a, 6b	**Annabel Alonso**
3	**River Cook**
2a, 2b, 2c, 2d	**Kayla Davis**
5a, 6c, 7a, 7b, 7c, 8a, 8b, 8c, 8d, 9a, 9b, 9c, 9d	**Matt Greenlee**
4	**Nida Meednu**
1a, 1b, 1c, 3	**Maliha Rahman**
3	**Victoria Tabb**

Table A The figure and panel contributions of each author for the Greenlee et. Al., 2018 manuscript. This manuscript includes figures and panels submitted by the following authors: Matt Greenlee, Annabel Alonso, Maliha Rahman, Nida Meednu, Kayla Davis, Victoria Tabb, and River Cook.

Purified tubulins bind directly to SUMO columns.

Following the completion of this manuscript, additional efforts were made to confirm that tubulin does indeed interact with SUMO in the absence of Stu2. *In vitro* binding experiments demonstrated that purified αβ-tubulin heterodimer (a kind gift from Jeff Moore) are affinity purified by our 5x-poly-SUMO columns even in the absence of detectable levels of Stu2 protein (Figure 3-A). When 500 ng (2.5 ng/μL) of tubulin was applied to the 5x-SUMO-GST columns, only about 20% appeared to bind to SUMO (compare 500 ng and 100 ng tubulin control lanes). At the lowest concentration where 250 pg/uL (50 ng) was used, at least 20% bound to the column based on the minimal amount of tubulin shown to interact with our anti-Tub1 antibody (compare 50 ng panel A with 10 ng panel C). Additionally, we confirmed the absence of Stu2 in purified tubulin aliquots using anti-Stu2 antibodies from the Huffaker lab (Figure A panel b). The finding that tubulins bind SUMO directly is significant because it provides an additional way in which sumoylated MAPs might interact with microtubules. In the instance of these studies, it suggests that Stu2 is not responsible for all the tubulin binding to the 5x-poly-SUMO column. Furthermore, human tubulin sumoylation sites were identified in recent mass spectrometry experiments (Hendriks et al., 2017). This suggests tubulins bind SUMO non-covalently and covalently and has a wide range of applications for many different systems.

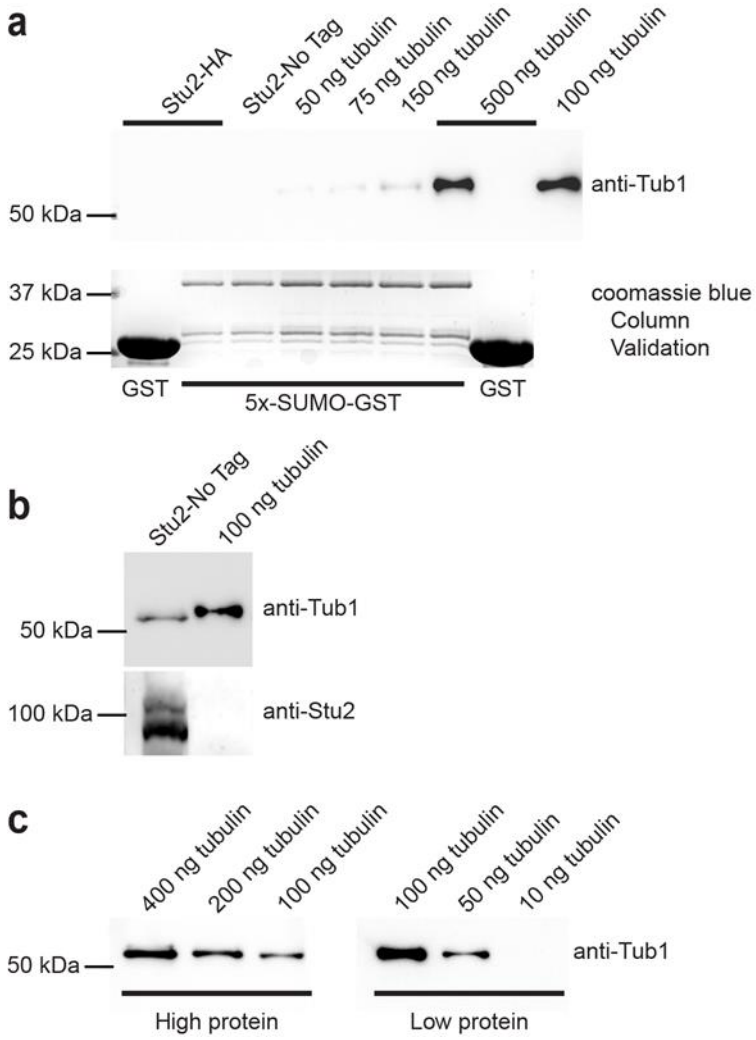

Figure A Purified tubulin binds directly to the 5x-SUMO-GST column even in the absence of detectable levels of Stu2. (a) Untagged Stu2 (yRM12359) and a series of αβ-tubulin heterodimer (a gift from Jeff Moore) titrations were incubated in the presence of GST and 5x-SUMO-GST columns (first image). GST and 5x-SUMO-GST proteins bound to glutathione agarose were run on SDS-PAGE and coomassie stained to evaluate equal loading of affinity columns (second image). (b) To confirm the absence of Stu2 in 5x-SUMO-GST tubulin pulldowns, we western blotted untagged Stu2 and purified tubulin with anti-Tub1 and anti-Stu2 antibodies. A small molecular weight shift in the anti-Tub1 blot represents the affinity tagging of tubulin used for its purification. (c) Lastly, we determined the minimal sensitivity of our anti-Tub1 antibody to be about 50 ng when known quantities of purified tubulins were western blotted.

The TOG protein Stu2/XMAP215 interacts Covalently and non-covalently with SUMO.

Matt Greenlee*, Annabel Alonso*, Maliha Rahman*, Nida Meednu‡, Kayla Davis*, Victoria Tabb*, River Cook* and Rita K. Miller*

* Department of Biochemistry and Molecular Biology
Oklahoma State University
Stillwater, OK 74078

‡ Department of Biology
University of Rochester
Rochester, New York 14627

Corresponding author:
Rita K. Miller
248A Noble Research Center
Department of Biochemistry and Molecular Biology
Oklahoma State University
Stillwater, Oklahoma 74078

Phone: 405-744-7732
Fax: 405-744-7799

Email: rita.miller@okstate.edu

Key words: *STU2, XMAP215, ubiquitin, microtubules, SUMO, tubulin*
Running Head: Stu2p interacts with SUMO

Abbreviations:
AD, Activation domain
BD, DNA binding domain
MAP, microtubule-associated protein
SC, synthetic complete
SPB, spindle pole body
STUbL, SUMO-Targeted Ubiquitin Ligase
TBS, Tris buffered saline
YPD, yeast peptone dextrose

ABSTRACT:

Stu2p is the yeast member of the XMAP215/Dis1/ch-TOG family of microtubule-associated proteins that promote microtubule polymerization. However, the factors that regulate its activity are not clearly understood. Here we report that Stu2p in the budding yeast *Saccharomyces cerevisiae* interacts with SUMO by covalent and non-covalent mechanisms. Stu2p interacted by two-hybrid analysis with the yeast SUMO Smt3p, its E2 Ubc9p, and the E3 Nfi1p. A region of Stu2p containing the dimerization domain was both necessary and sufficient for interaction with SUMO and Ubc9p. Stu2p was found to be sumoylated both *in vitro* and *in vivo*. Stu2p co-purified with SUMO in a pull-down assay and vice versa. Stu2p also bound to a non-conjugatable form of SUMO, suggesting that Stu2p can interact non-covalently with SUMO. In addition, Stu2p interacted with the STUbL enzyme Ris1p. Stu2p also co-purified with ubiquitin in a pull-down assay, suggesting that it can be modified by both SUMO and ubiquitin. Tubulin, a major binding partner of Stu2p, also interacted non-covalently with SUMO. By two-hybrid analysis, the beta-tubulin Tub2p interacted with SUMO independently of the microtubule stressor, benomyl. Together, these findings raise the possibility that the microtubule polymerization activities mediated by Stu2p are regulated through sumoylation pathways.

INTRODUCTION:

Stu2p is the yeast member of the highly conserved XMAP215 / Dis1/ ch-TOG family of microtubule associated proteins (MAPs) that stimulate microtubule growth and block catastrophe (Al-Bassam et al., 2006) (Podolski et al., 2014) (Wang and Huffaker, 1997) (Brouhard et al., 2008) (reviewed in (Al-Bassam and Chang, 2011)). The molecular basis of this property lies in the dual ability of Stu2p to bind free tubulin dimers and microtubule polymer. Binding to alpha-beta dimers occurs through its two TOG (Tumor Overexpressed Gene) domains (Ayaz et al., 2012) (Al-Bassam et al., 2006) (Slep and Vale, 2007) (Al-Bassam et al., 2007), and binding to the microtubule lattice occurs through its basic microtubule binding domain (Wang and Huffaker, 1997) (Al-Bassam et al., 2006). Through a conformational change, Stu2p/ch-TOG facilitates the addition of dimers onto the plus end of the microtubule polymer (Al-Bassam et al., 2006). Although in most cases it has been seen to act as a microtubule polymerase (Podolski et al., 2014), in a few specific instances it has also been characterized as having a destabilizing effect (van Breugel et al., 2003) (Shirasu-Hiza et al., 2003) (Brouhard et al., 2008) (Al-Bassam et al., 2006) (Al-Bassam and Chang, 2011).

Stu2p and XMAP215 homologues function on multiple types of microtubules within the cell. On the plus end of cytoplasmic microtubules, Stu2p functions in cytoplasmic microtubule orientation to facilitate positioning of the mitotic spindle (Kosco et al., 2001a). XMAP215 is a dynamic component of the kinetochore that functions in metaphase chromosome alignment by helping to attach microtubules to the kinetochore (Aravamudhan et al., 2014) (Kitamura et al., 2010) (Ma et al., 2007). In addition to regulating microtubule dynamics, the yeast Stu2p can stabilize tension-bearing microtubule attachments at the kinetochore (Miller et al., 2016). Stu2p, like other XMAP215 members, is a component of the MTOC and interacts with TACC complex proteins (Wang and Huffaker, 1997) (Al-Bassam and Chang, 2011). While the role of Stu2p at the yeast MTOC remains unclear, it is known that XMAP215 can promote microtubule nucleation (Wieczorek et al., 2015).

The signal transduction systems that regulate the various functions of Stu2p and TOG proteins are not well understood. Stu2 can be modulated by phosphorylation (Park et al., 2008). The phosphorylation of TOG binding-partners proteins is also a mode of regulating its localization and activity in *Drosophila* and fission yeast (Okada et al., 2014) (Trogden and Rogers, 2015). However, less is known about the regulation of Stu2p by other types of post-translational modifications. In this paper we show that Stu2p interacts with the small ubiquitin-like modifier termed SUMO, encoded by *SMT3*.

The SUMO moiety is well known to attach to lysine residues through the action of an E2 conjugation enzyme and an E3 ligase (reviewed in (Gareau and Lima, 2010) and (Alonso et al., 2015)). Unlike ubiquitin, there is a single E2 enzyme for sumoylation, called Ubc9p (Johnson and Blobel, 1997) (Kersher et al., 2006). In contrast to higher eukaryotes, there are four E3 enzymes for sumoylation in yeasts, the best characterized of which are Siz1p and Nfi1p/Siz2p (Johnson and Gupta, 2001) (Takahashi et al., 2001). Attachment of SUMO to target proteins is reversible through the action of two SUMO specific proteases, Ulp1p and Ulp2p (Bylebyl et al., 2003) (Kroetz and Hochstrasser, 2009) (Li and Hochstrasser, 1999; Li and Hochstrasser, 2000). The WLM metalloprotease Wss1p is thought to remove SUMO from targets (Mullen et al., 2010), but may remove ubiquitin as well (Su and Hochstrasser, 2010).

SUMO can interact with a partner protein in two ways, covalently or non-covalently. For covalent interactions, SUMO is often attached to the lysine residue within the canonical consensus site, ΦKXD/E, where Φ is a hydrophobic residue and X can be any amino acid. However, degenerate consensus sites are also used frequently, which can confound the identification of modified lysines (Hendriks et al., 2017). SUMO can also interact non-covalently with a protein. This occurs though the conserved SUMO Interacting Motif (SIM) found in SUMO's binding partners. The SIM motif consists of a stretch of hydrophobic amino acids in the pattern (I/L/V) X (I/L/V) (I/LV) with the X position being occupied by any amino acid (Kroetz and Hochstrasser, 2009) (Song et al., 2004), although the consensus sequence may be more complex (Jardin et al., 2015).

In this work, we show that Stu2p/XMAP215 interacts both covalently and non-covalently with SUMO, as well as with the Ris1p STUbL enzyme. A major binding partner of Stu2p is the tubulin dimer. Here, we show that beta-tubulin encoded by *TUB2* also interacts with SUMO and Ris1p.

RESULTS:

Stu2p interacts with SUMO and the SUMO machinery.

Stu2p is important for spindle positioning (Kosco et al., 2001a). Stu2p also interacts with several other microtubule-associated proteins, including the spindle positioning protein Kar9p, the CLIP-170 homologue Bik1p, the EB1 homolog Bim1p, and the kinetochore protein Ndc80p (Miller et al., 2000) (Wolyniak et al., 2006) (Alonso et al., 2015) (Blake-Hodek et al., 2010) (Wong et al., 2007). Each of these interacts with SUMO (Montpetit et al., 2006) (Meednu et al., 2008) (Alonso et al., 2012) (Leisner et al., 2008). Therefore, we tested whether *STU2* might also interact with SUMO using a two-hybrid assay. For this, we employed three forms of SUMO*;* a full-length SUMO, a preprocessed form in which the terminal three amino acids were removed from the coding DNA *(SUMO*-GG), and a conjugation incompetent form SUMO in which the glycine used in conjugation was mutated to an alanine *(*SUMO-GA). As shown in Figure 1A, *STU2* interacted with full-length SUMO and with SUMO-GG, but not with SUMO-GA.

As conjugation of SUMO to a target protein requires several enzymes in the sumoylation pathway (Praefcke et al., 2012), we asked whether *STU2* could interact with other components of the sumoylation pathway. We found that *STU2* interacted with the E2 conjugating enzyme encoded by *UBC9,* confirming a previous two-hybrid screen (Wong et al., 2007). Extending this observation, we also found that *STU2* interacted with the E3 ligase enzyme encoded by *NFI1/SIZ2* (Figure 1B). As discussed in more detail below, these two-hybrid interactions do not distinguish between covalent and non-covalent interactions between Stu2p and SUMO.

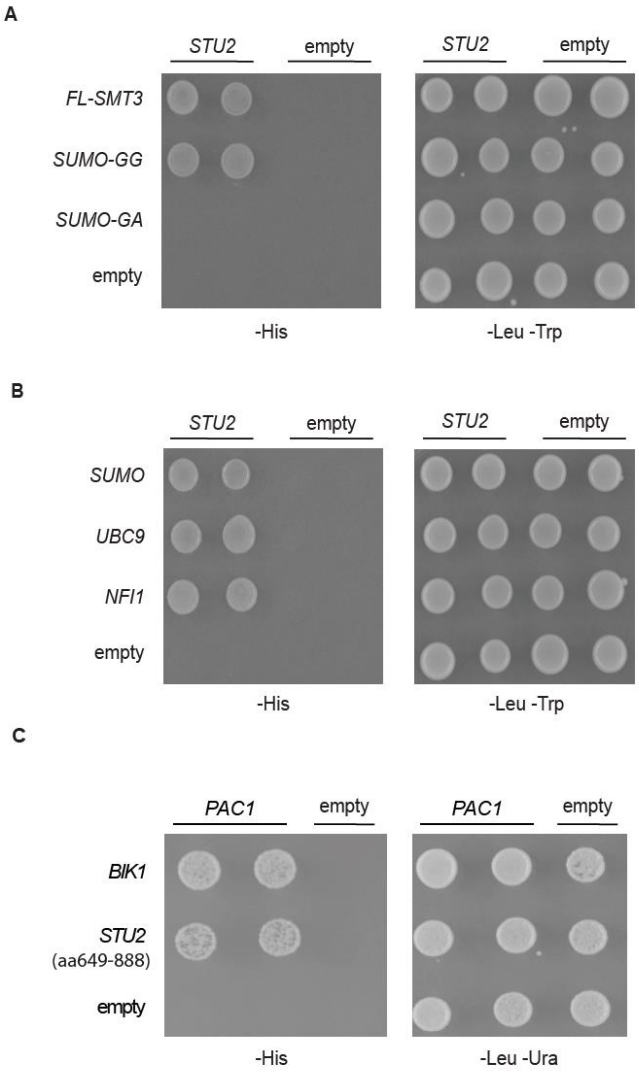

Figure 1 *STU2* interacts with the sumoylation machinery and *PAC1/Lis1* by two-hybrid analysis. (A) STU2 interacts with SUMO-GG but not SUMO-GA. Two-hybrid reporter strains were generated by transforming either BD-STU2 (pRM7247), empty-BD (pRM1154) and AD-FL-SUMO (pRM4920), AD-SUMO-GG (pRM4382), or SUMO-GA (pRM4383). Transformants were selected on SC media lacking uracil and tryptophan (-ura -trp). Interaction was assayed by yeast growth on media lacking histidine (-his) as previously described (Alonso et al., 2012). Two independent colonies are shown for each interaction. (B) STU2 interacts with multiple enzymes in the sumoylation pathway. BD-STU2 (pRM7247) was tested for interaction with AD-SUMO (pRM4920), AD-UBC9 (pRM4495), and AD-NFI1 (pRM4496). (C) STU2 interacts with PAC1/Lis1. BD-PAC1 (pRM3604) was analyzed for interaction with AD-STU2 (pRM1916). This encodes STU2-aa649-888. AD-BIK1 (pRM2627) serves as a positive control.

Conserved in yeast and mammalian sytems, Pac1p/Lis1 interacts with Bik1p/CLIP-170 (Markus et al., 2011) (Coquelle et al., 2002) (Tai et al., 2002). Bik1p has previously been shown to interact with Stu2p (Wolyniak et al., 2006). We therefore tested whether *STU2* might also interact with *PAC1/Lis1*. As shown in Figure 1C, it does, confirming previous genomics reports (Wong et al., 2007). The *STU2* two-hybrid construct used in this analysis (*STU2*-aa649-888) lacks the two TOG domains, coding for only the dimerization and MAP domains of Stu2p. This finding suggests that the Stu2p-Pac1p interaction does not require the TOG domains of Stu2p. As Pac1p/Lis1 was recently demonstrated to be sumoylated, this represents the fifth sumoylated MAP with which Stu2p interacts (Montpetit et al., 2006) (Meednu et al., 2008) (Alonso et al., 2012).

The interaction of Pac1p/Lis1 with SUMO requires the presence of its binding partner Bik1p (Alonso et al., 2012), and vice versa. To ascertain whether Bik1p or other SUMO-interacting MAPs are necessary for Stu2p's interaction with SUMO, we tested *STU2*'s interaction with SUMO in two-hybrid reporter strains that were deleted for each of these MAPs. The interaction of Stu2p with SUMO was not altered in reporter strains deleted for *BIK1/CLIP-170*, *PAC1/LIS1*, or *BIM1/EB1* (Figure 2A-C). This suggests that Stu2p's interaction with SUMO does not require these MAPs. It also implies that Bik1p/CLIP-170, Bim1p/EB1 or Pac1/Lis1 do not serve a bridging function between Stu2p and SUMO. Kar9p is a cytoskeletal linker protein that orients microtubules for spindle positioning (Miller and Rose, 1998) (Miller et al., 1999) (Bloom, 2000) (Lee et al., 2000) (Liakopoulos et al., 2003) (Gundersen and Bretscher, 2003). Like Stu2p, it also plays a role at the kinetochore (Schweiggert et al., 2016). Kar9p interacts with Stu2p as well (Miller et al., 2000) (Moore and Miller, 2007). Like Pac1p/Lis1 and Bim1p/EB1, Kar9p also was not required for Stu2p's interaction with SUMO. However, in the *kar9*Δ strain, Stu2p displayed reduced interactions with SUMO, with the E2 enzyme Ubc9p, the E3 enzyme Nfi1p, and the protease Wss1p. This suggests that Kar9p may facilitate the interaction of Stu2p with the sumoylation machinery (Figure 2D). Combined, these findings suggest that the interaction of SUMO with Stu2p is largely independent of several of its binding partners.

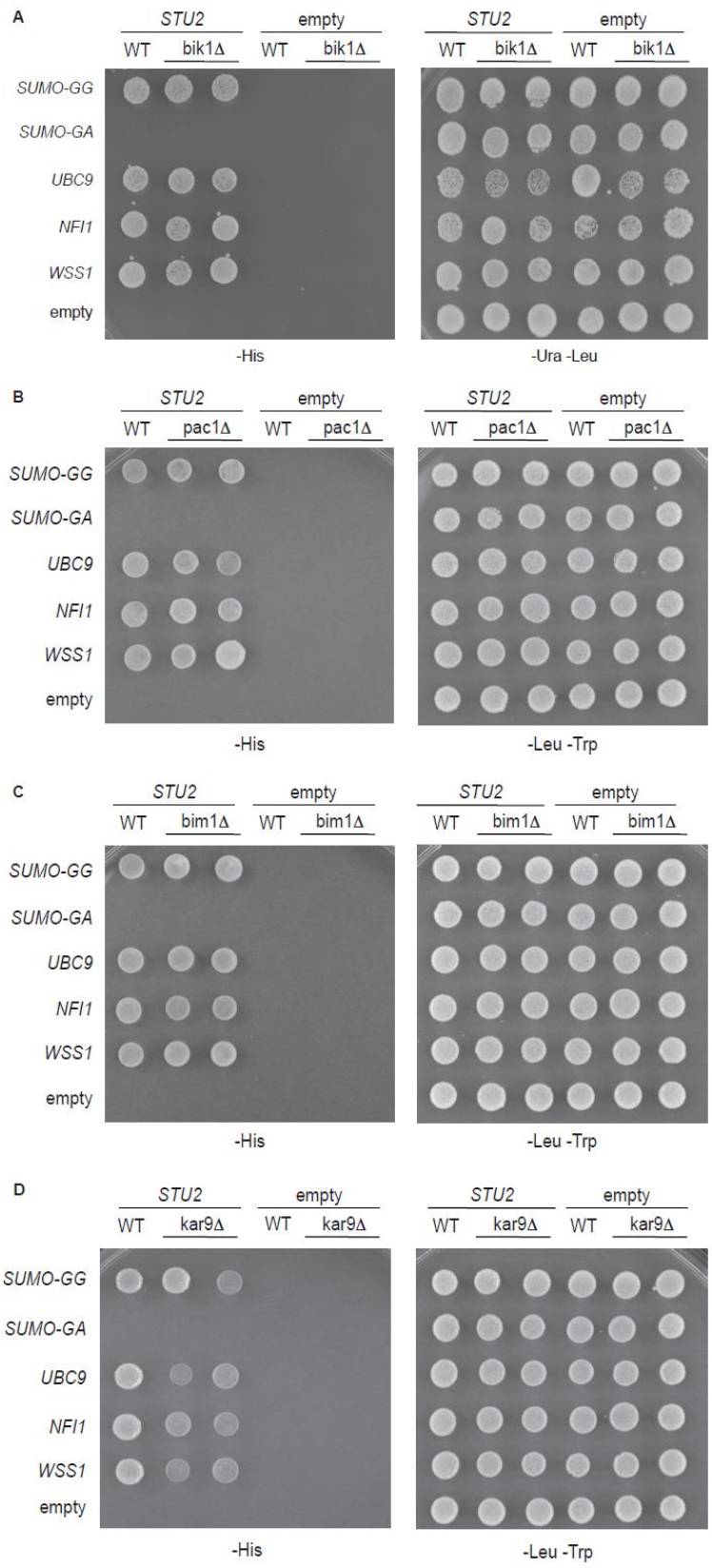

Figure 2 Bik1p/CLIP-170, Pac1p/Lis1, and Bim1p/EB1 are not required for Stu2p's interaction with SUMO, whereas Kar9p facilitates interactions between Stu2p and the sumoylation pathway. AD-SUMO-GG (pRM4382), AD-SUMO-GA (pRM4383), AD-*UBC9* (pRM4495), AD-*NFI1* (pRM4496), AD-*WSS1* (pRM4597), or empty-AD (pRM1151) were transformed into a two-hybrid reporter strain containing BD-*STU2* (pRM7247) or empty-BD (pRM1157). The reporter strains used were wild type (yRM1757), and strains deleted for *KAR9* (yRM6172), *BIM1/EB1* (yRM2057), or *PAC1/Lis1* (yRM6249). For the *bik1*Δ strain (yRM2258), the BD-*STU2* plasmid (pRM9426) and the empty BD (pRM1154) were used to meet auxotrophic selection requirements.

The dimerization domain of Stu2p is necessary and sufficient for interaction with SUMO.

Stu2p is comprised of several well-characterized domains. Its two TOG domains are responsible for binding tubulin dimers (Al-Bassam et al., 2006) (Widlund et al., 2011). The MT domain is involved in interaction with MT polymers (Wang and Huffaker, 1997). The Huffaker lab previously demonstrated that the dimerization domain is necessary and sufficient for Stu2p's interaction with itself (Wolyniak et al., 2006). The C-terminal MAP domain has been shown to be important for interactions with several MAPs (Miller et al., 2000) (Wolyniak et al., 2006). To identify the regions of Stu2p that are required for interaction with SUMO and the sumoylation machinery, we created a series of N- and C- terminal truncations of Stu2p for two-hybrid analysis. When the region encoding the dimerization domain and the MAP- interaction domain was deleted, Stu2p interactions with SUMO and the sumoylation machinery were lost (Figure 3, AA 1-658). In contrast, when the TOG domains were deleted, the interaction with SUMO was retained (Figure 3, AA540-888). The two-hybrid construct lacking a significant portion of the MT binding domain but containing both the dimerization domain and the MAP domain (AA613-888) did interact with SUMO. In contrast, the construct containing the MT binding domain but lacking the Stu2p dimerization domain (AA540-657) did not interact. The construct expressing only the Stu2p dimerization domain (AA613-801) retained interactions with SUMO, Ubc9p, and Nfi1p. These data suggest that the TOG domains are not required for Stu2p's interaction with SUMO. These data also suggest that the dimerization domain is necessary and sufficient for Stu2p's interaction with SUMO and the sumoylation machinery.

Stu2p can be sumoylated *in vitro*.

We next examined the possibility that SUMO could be attached to Stu2p using an *in vitro* sumoylation assay, described previously (Alonso et al., 2012; Meednu et al., 2008). For this, a Stu2-TAP tag fusion was purified from yeast and components of the sumoylation pathway including SUMO, Ubc9p and Aos1/Uba2p were purified from bacteria (Puig et al., 2001). SUMO was used in the processed form,

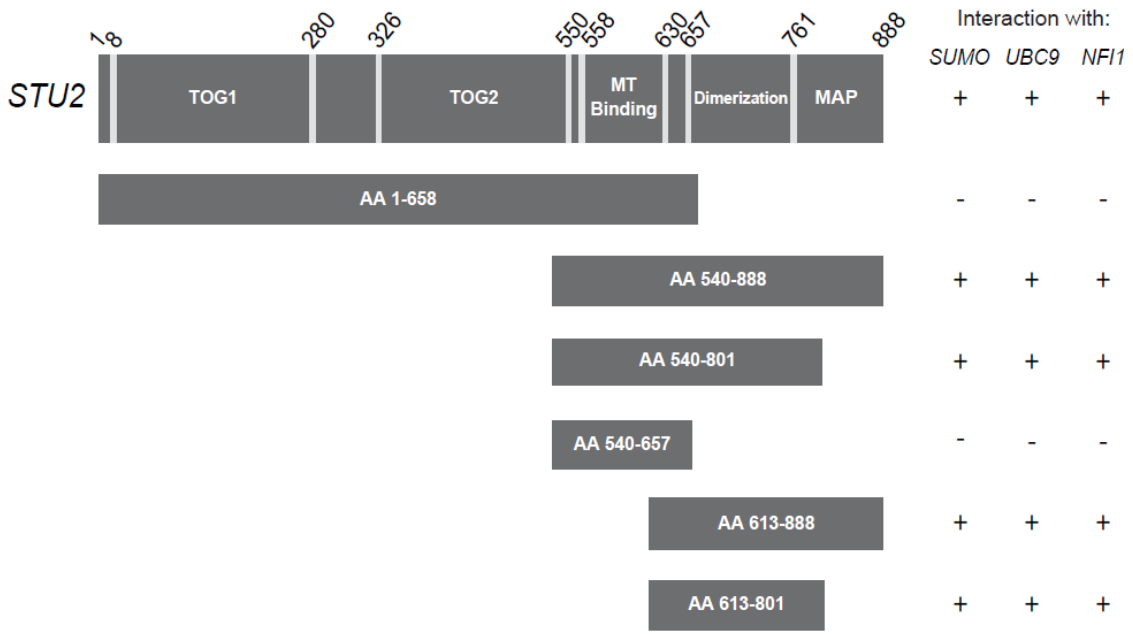

Figure 3 The dimerization domain of Stu2p interacts with SUMO. Two-hybrid interactions with AD-SUMO-GG (pRM4382), AD-*UBC9* (pRM4495) and AD-*NFI1* (pRM4496) were assayed using the indicated amino- and carboxy-terminal truncations of BD-*STU2* in the yeast reporter strain, pJ69-4A/yRM9909. A plus sign represents plasmid combinations that supported yeast growth. The following plasmids were used: pRM9426 encoding full-length *STU2* from amino acids 1-888, pRM7228 encoding amino acids 1-658, pRM10785 encoding amino acids 540-888, pRM10792 encoding amino acids 540-657, pRM10787 encoding amino acids 540-801, pRM9370 encoding amino acids 613-888, and pRM11115 encoding amino acids 613-801. Four independent colonies were tested for each truncation and compared each time to the full-length Stu2p.

SUMO-GG. In the reaction in which all the necessary components of the sumoylation pathway and ATP were included, four shifted bands were observed using anti-HA to detect Stu2-TAP (Figure 4**,** lane 1). When a conjugation-incompetent form of SUMO, SUMO-GA, was used in place of SUMO-GG, the shifted bands were not detected (Lane 7). Therefore, Stu2p can be sumoylated *in vitro* and the terminal glycine residue of SUMO is required for this *in vitro* sumoylation reaction.

Stu2p interacts with the STUbL enzyme Ris1p, and co-purifies with ubiquitin.

STUbL enzymes frequently interact with sumoylated proteins to ubiquitinate them. We previously reported that Pac1p/Lis1 interacts with the STUbL enzyme Ris1p, the bud-neck interacting protein Nis1p, and the SUMO protease Wss1p (Alonso et al., 2012). To determine whether Stu2p displays a similar pattern of interactions, we tested for an interaction between Stu2p and these proteins by two-hybrid analysis. As shown in Figure 5A, they did interact. Because STUbL enzymes ubiquitinate their targets, we next tested for a direct interaction between Stu2p and ubiquitin. We immunoprecipitated ubiquitin and analyzed the precipitate for the presence of Stu2p by western blotting. As shown in Figure 5B, Stu2p co-purified with ubiquitin, but not the vector control.

SUMO and Stu2p co-purify.

To investigate whether the higher molecular weight forms of Stu2p observed *in vitro* are present *in vivo*, whole-cell extracts from a *ulp1*-ts yeast strain expressing Stu2-HA were used in a pull-down using anti-HA agarose beads and blotted for SUMO. At least one higher molecular-weight form of Stu2-HA co-immunoprecipitated with SUMO (Figure 6A). To examine this using the reciprocal approach, we pulled down SUMO using a SUMO antibody and then blotted for Stu2-HA. Stu2p co-immunoprecipitated with SUMO (Figure 6B). These co-immunoprecipitation results could in theory be the result of a co-immunoprecipitation of another SUMO-modified protein that co-migrates at the same molecular weight as Stu2p. To eliminate this possibility, we sought to determine if SUMO would co-isolate with Stu2p under denaturing conditions. Genomic Stu2-his6 solubilized in 8M urea was enriched

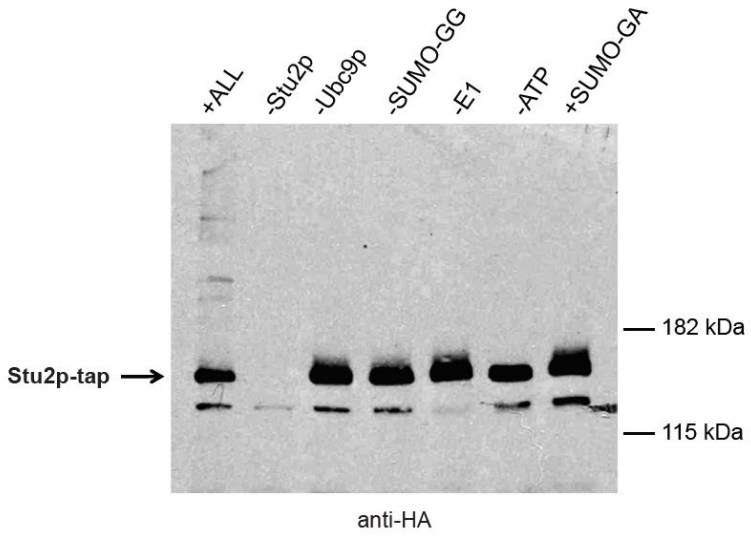

Figure 4 Stu2p can be conjugated by SUMO *in vitro*. Stu2p-TAP (pRM6956) was purified from yeast using nickel column chromatography. The purified protein was incubated with purified components necessary for sumoylation, SUMO-GG (pRM6713), Ubc9p (pRM5169), and Aos1p/Uba2p (pRM6760) in the presence of ATP and an ATP regeneration system (lane 1), as described in Materials and Methods. As controls, each of the required components of the reaction was omitted from the reaction as follows: Stu2p (lane 2), SUMO-GG (lane 3), Ubc9p (lane 4), Aos1/Uba2p (E1) (lane 5) and ATP (lane 6). In the last reaction, SUMO-GG was replaced by SUMO-GA (lane 7), a mutated form of SUMO in which the essential glycine for conjugation is changed to alanine. Anti-HA was used to detect Stu2p. The shifted bands that are recognized by anti-HA (*) are specific to lane 1 when all the essential components are present.

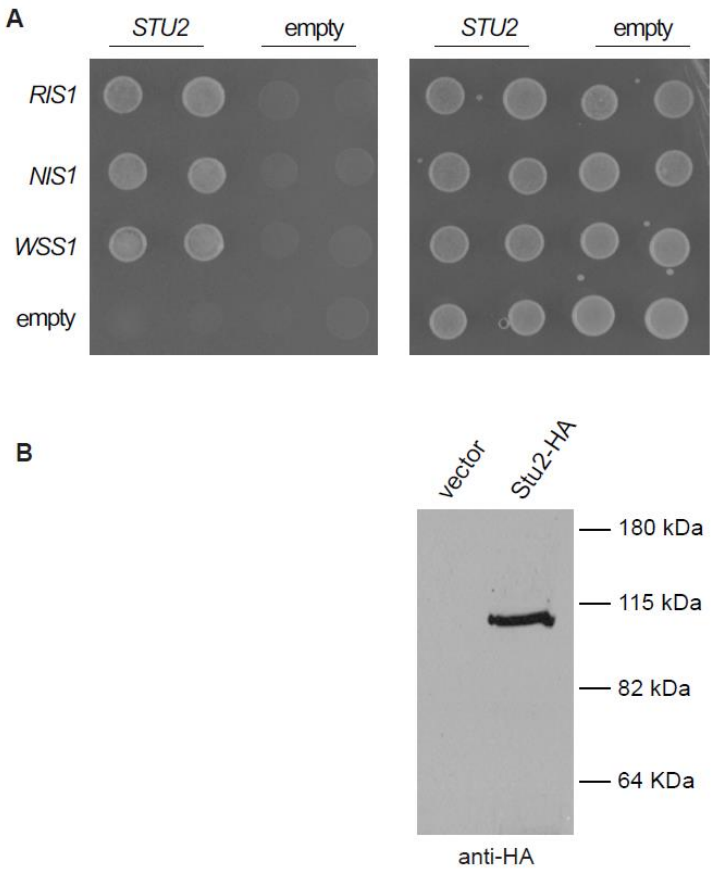

Figure 5 (A) Stu2p interacts with the STUbL enzyme Ris1p, the neck-interacting protein Nis1p, and the SUMO isopeptidase Wss1p by two-hybrid analysis. BD-*STU2* (pRM9426) was tested for interaction against the weak suppressor of SUMO encoded by AD-*WSS1* (pRM4597), AD-*RIS1* (pRM4596), AD-*NIS1* (pRM4595), or empty-AD (pRM4380). Transformants were selected on media lacking uracil and leucine (-ura -leu) and assayed for interactions on media lacking histidine (-his). (B) Stu2p co-IPs with ubiquitin. Plasmids expressing Stu2-HA (pRM2119) or vector (pRM2200) where transformed into a *ulp1-TS* strain (yRM8139). Whole-cell lysates were prepared, as described in Materials and Methods. Ubiquitin was immunoprecipitated with anti-ubiquitin and the precipitate was blotted with anti-Stu2p, as described in Materials and Methods.

Figure 6 (A) SUMO co-IPs with Stu2p. Plasmid expressing Stu2-HA (pRM2119) or vector (pRM2200) where transformed into a *ulp1-TS* strain (yRM8139). Whole-cell lysates were prepared from cultures grown overnight to saturation, as described in Materials and Methods. Stu2-HA was immunoprecipitated using mouse anti-HA agarose beads (Sigma-Aldrich). The western blot was probed with rabbit anti-HA (Sigma-Aldrich). (B) Stu2p co-IPs with SUMO. SUMO was immunoprecipitated with anti-SUMO (Rockland, Inc. Gilbertsville, PA) from a *ulp1-TS* strain (yRM8139) containing Stu2-HA (pRM2119), or an empty vector, as described in Materials and Methods. The blot was probed with mouse anti-HA (Sigma-Aldrich). Saturated overnight cultures were used to prepare whole-cell extracts. (C) Stu2-his6 co-isolates with SUMO under denaturing conditions. Yeast whole-cell extracts containing Stu2-6his (yRM9417) where incubated with Ni-NTA agarose in the presence of 8M urea. To analyze bands for co-reactivity, identical blots where probed with rabbit anti-Stu2p and anti-SUMO.

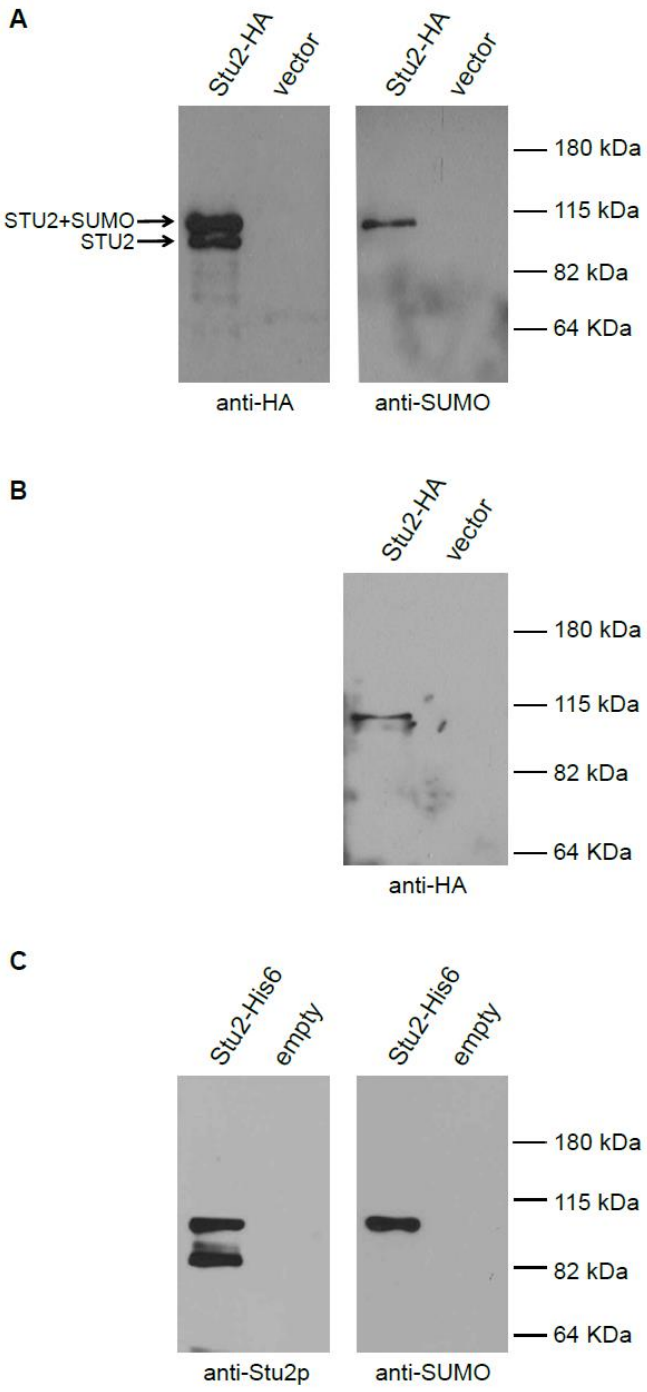

on nickel-NTA agarose, and eluted with sample buffer. Western blot analysis revealed that the slower migrating Stu2 band was immuno-reactive with anti-SUMO (Figure 6C). These findings suggest that SUMO is conjugated to Stu2p.

Stu2p binds non-covalently to SUMO.

It is well known that SUMO can be conjugated to and also bind non-covalently to target proteins. For example, the kinesin CENP-E can interact non-covalently with SUMO and also be conjugated by it (Zhang et al., 2008). To investigate whether Stu2p might bind non-covalently to SUMO, we assayed for an interaction using two forms of SUMO that are incompetent to form an isopeptide bond. In the first construct, GST-SUMO-GA, the terminal glycine of SUMO, glycine 98, was mutated to the conjugation incompetent residue, alanine. In the second construct, SUMO-GST, the terminal glycine of SUMO was fused in frame with the amino terminus of GST in a standard peptide bond, blocking the access of the carboxyl group of the terminal glycine for conjugation. Both constructs were expressed in bacteria and purified on glutathione beads. To test for a non-covalent interaction, yeast extracts were incubated with the two SUMO fusions. As a positive control, Nis1p, a protein known to interact non-covalently with SUMO, was included in the analysis (Uzunova et al., 2007). It was retained on both versions of the SUMO column (Figure 7). In contrast, Stu2-HA was retained on only the GST-SUMO-GA column. These findings suggest that Stu2p interacts non-covalently with SUMO and that this interaction is restricted to one orientation of SUMO.

Tubulin interacts with SUMO non-covalently.

The major binding partner of Stu2p is tubulin. We therefore asked whether tubulin might also bind to SIMs. To answer this question, an identical nitrocellulose membrane was blotted with anti-Tub1p. As shown in Figure 7A, tubulin does bind to the GST-SUMO-GA column. Notably, we observed little or no binding by tubulin to the SUMO-GST or GST alone columns. However, this experiment does not differentiate between a direct or indirect binding of tubulin through a Stu2p bridge. To determine

Figure 7 (A) Stu2p and tubulin bind non-covalently to SUMO. Columns of GST-SUMO-GA (pRM10097), SUMO-GST (pRM10818), or GST alone (pRM2759) were incubated with whole-cell extracts prepared from cells expressing Stu2-HA (yRM10637), Nis1-HA (yRM10782) or empty vector (yRM10641), as described in Material and Methods. Bound proteins were eluted with Laemmli sample buffer and analyzed by immunoblotting. 1/20 of the GST columns are shown in the Coomassie blue stained panel labeled "Columns." To detect the HA epitope of Stu2-HA and Nis1-HA, mouse anti-HA (Santa Cruz Biotechnology, Santa Cruz, CA) was used. To detect tubulin, rat anti-alpha-tubulin (YOL 1/34, Accurate Biochemical, Westbury, NY) was used. To normalize for the different cellular abundance of the two proteins, 1/13th (150 μg) of the column load is shown for Nis1-HA and 1/ 215th (50 μg) of the column load is shown for the Stu2-HA extracts. (B) Stu2 is depleted in the degron shut-off strain. Wild type (yRM2123) and a Stu2-degron strain (yRM2122) were treated with and without 500 μM CuSO4 for 6.5 h as described (Kosco et al., 2001a). Whole-cell extracts were prepared as described in Materials and Methods. Samples were prepared for SDS-PAGE and western blotting with rabbit anti-Stu2p. Anti-tubulin was used as a loading control. (C) Tubulin binds GST-SUMO-GA in the absence of Stu2p. Whole-cell extracts were prepared from the Stu2-degron strain treated with or without copper sulfate as described Materials and Methods. SUMO columns were prepared as described in panel A. Western blots were developed as described in panel A.

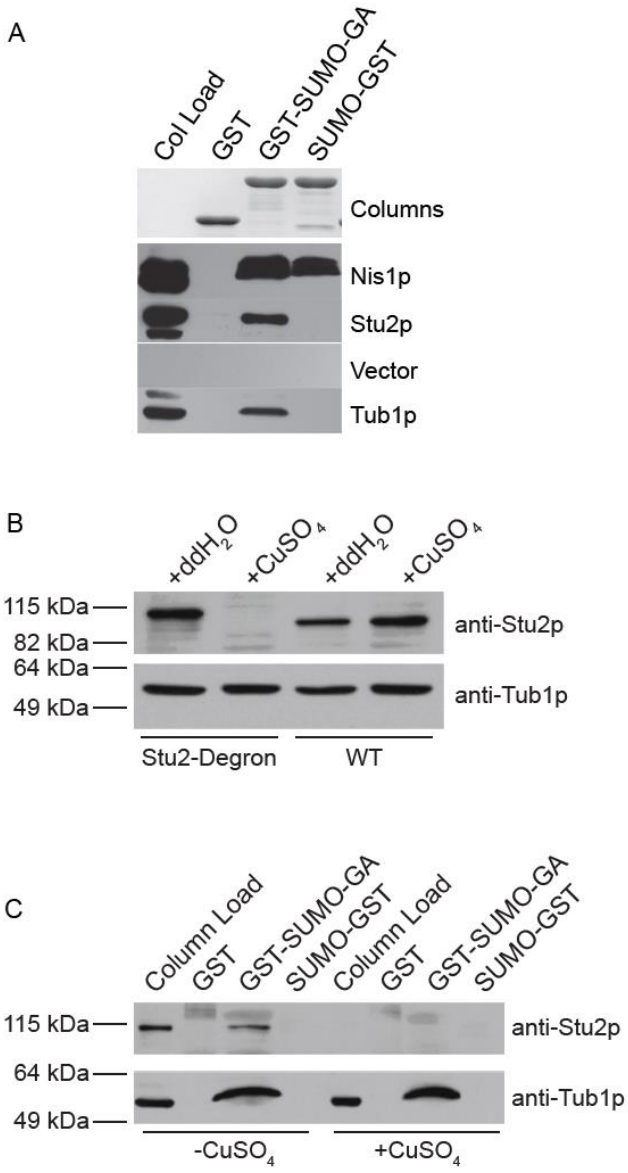

whether tubulin would bind when Stu2p was not present in the extract, we employed the degron-tagged Stu2p previously described by Kosco et al. (Kosco et al., 2001a), and confirmed the "shut-off" of Stu2p (Figure 7B). When Stu2p was "shut off" in the presence of copper sulfate, tubulin still bound to the column (Figure 7C). These findings suggest that Stu2p is not required for the interaction of tubulin with SUMO.

Tubulin interacts with SUMO and a SUMO-targeted ubiquitin ligase by two-hybrid analysis.

Considering that the tubulin dimer is comprised of an alpha and beta subunit, we next wanted to know whether interactions with SUMO could be detected with these tubulin subunits using two-hybrid analysis. Whereas alpha-tubulin two-hybrid constructs are viable, overexpression of beta-tubulin two-hybrid constructs is toxic to the cell. To overcome this limitation, we used a mutated form of beta-tubulin with lower toxicity for these experiments (a kind gift from Kristy Schwartz and David Botstein). Using this construct, we found that the beta-tubulin Tub2p interacted with both SUMO and the E3 enzyme Nfi1p (Figure 8A). The two alpha-tubulins in yeast, Tub1p and Tub3p, also interacted with Nfi1p, but displayed minimal interaction with SUMO. None of the tubulins interacted with the E2 conjugating enzyme Ubc9p (Figure 8A). It is notable that the interaction between beta-tubulin and SUMO was resistant to treatment with the microtubule-destabilizing drug, benomyl (Figure 8B). The interaction between the alpha-tubulins and Nfi1p was greatly decreased by the benomyl treatment but not by the DMSO solvent-alone control (Figure 8B and 8C). In contrast, the interaction of beta-tubulin and Nfi1p was resistant to benomyl treatment.

Because Stu2p interacts with the STUbL enzyme Ris1p (Figure 5), we asked whether the tubulins might also interact with Ris1p. While both alpha-tubulins interacted with the beta-tubulin fusion protein as expected, treatment with benomyl disrupted their interactions, thus serving as a positive control for the functionality of benomyl in this assay. This analysis revealed that Ris1p interacted with all three tubulins, Tub1p, Tub3p, and Tub2p (Figure 9A). Notably, the interactions between the alpha-tubulins and Ris1p

Figure 8 Beta-tubulin interacts with SUMO. (A). Alpha- and beta-tubulins fused to the *GAL4* DNA-binding domain (pRM2095, pRM2096, and pRM10749) were tested for interaction with AD-FL-SUMO, (pRM4920), AD-SUMO-GG (pRM4382), AD-SUMO-GA (pRM4383), AD-*UBC9* (pRM4495), and AD-*NFI1* (pRM4496), and empty-AD (pRM1151), as described above. Haploids were selected on media lacking uracil and tryptophan (-ura -trp) (D), and assayed for interactions on media lacking histidine (-his). Cells were simultaneously transferred to -his plates containing 10 □g/mL of benomyl (B) or an equivalent concentration of the DMSO solvent (C). Two independent colonies of each are shown.

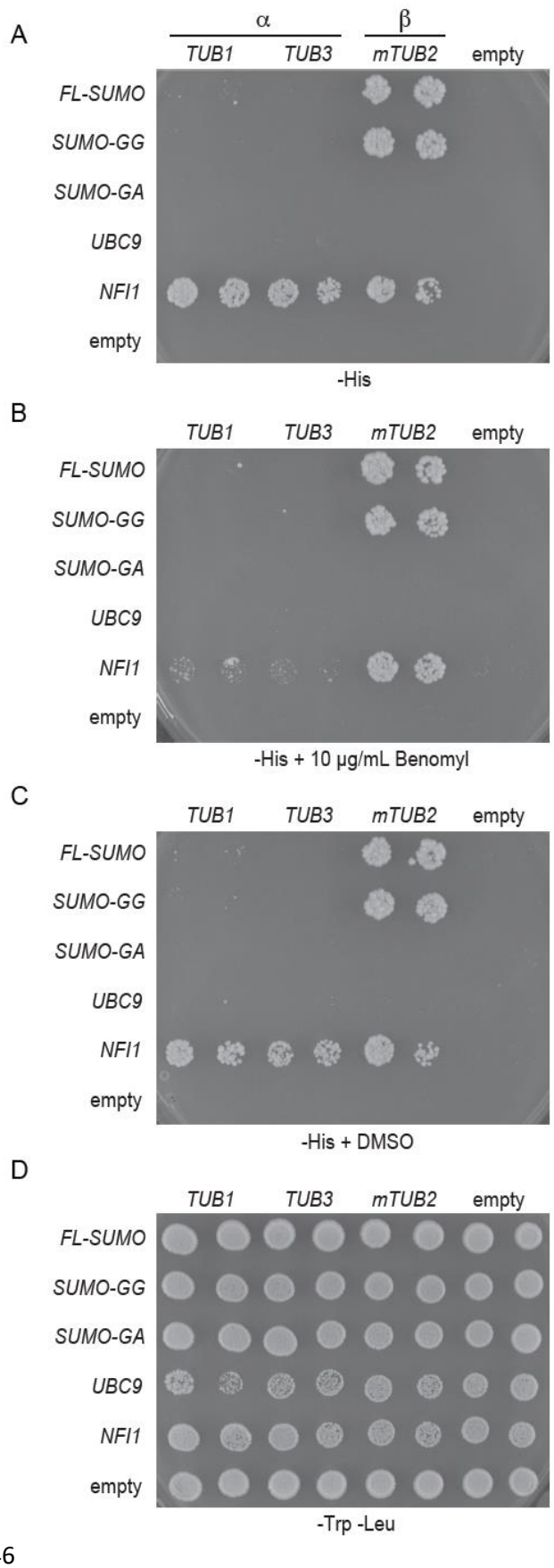

were sensitive to benomyl, whereas the beta-tubulin displayed only a slight sensitivity (Figure 9B). In contrast, the Nis1p protein interacted only with beta-tubulin (Figure 9A). This interaction was eliminated by benomyl treatment. In all of these analyses, the alpha tubulins, Tub1 and Tub3p, displayed concordant results. These findings suggest that beta-tubulin interacts better with SUMO than alpha-tubulins. This raises questions of whether the interactions of alpha-tubulins with SUMO are bridged by their dimer partner, beta-tubulin.

DISCUSSION:

In this report, we present evidence that the microtubule polymerizing protein, Stu2p, interacts with SUMO and several enzymes in the sumoylation pathway. A major function of Stu2p is to promote tubulin-dimer addition onto microtubule plus-ends. Here, we also provide evidence for interactions between tubulin and SUMO.

Our data suggest that Stu2p-SUMO interactions occur by two distinct mechanisms, covalent and non-covalent. The hypothesis that the interaction has a covalent modality is supported by the finding that Stu2p copurifies with SUMO and vice versa. Further, the Stu2p band is reactive with anti-SUMO, even when purified in the presence of a strong denaturant. Stu2p can also be conjugated by SUMO in an *in vitro* assay. However, despite several attempts by mutagenesis and mass spectrometry, we have not yet been able to identify a lysine that is modified. We speculate that this is because of poor ion-mobility of sumoylated peptides in the mass spectrometer. Also, the sumoylated lysine residue may reside outside of the peptide fingerprint generated by the tryptic digestion that we used.

We have previously posited a model for the regulation of the MAP Pac1p/Lis1 by STUbLs and the proteasome (Alonso et al., 2012). Consistent with this model, we show that Stu2p also interacts with the STUbL enzyme Ris1p and ubiquitin. Thus, it is possible that SUMO signals for the rapid degradation of a particular sub-population of Stu2p by the proteasome. Consistent with this, we have seen a higher molecular-weight band of Stu2p that is present in strains with lower levels of SUMO, but disappears with

Figure 9 Alpha- and beta- tubulins interact with the STUbL enzyme, Ris1p. Alpha and beta-tubulins fused to the *GAL4* binding domain (pRM2095, pRM2096, and pRM10749) were tested for interaction with the STUbL enzyme AD-*RIS1* (pRM4596), AD-*NIS1* (pRM4595), AD-*WSS1* (pRM4597) or empty-AD (pRM4380), as described above. Cells were simultaneously transferred to -his plates containing 10 µg/mL of benomyl (B), or an equivalent concentration of the DMSO solvent (C). Two independent colonies of each are shown.

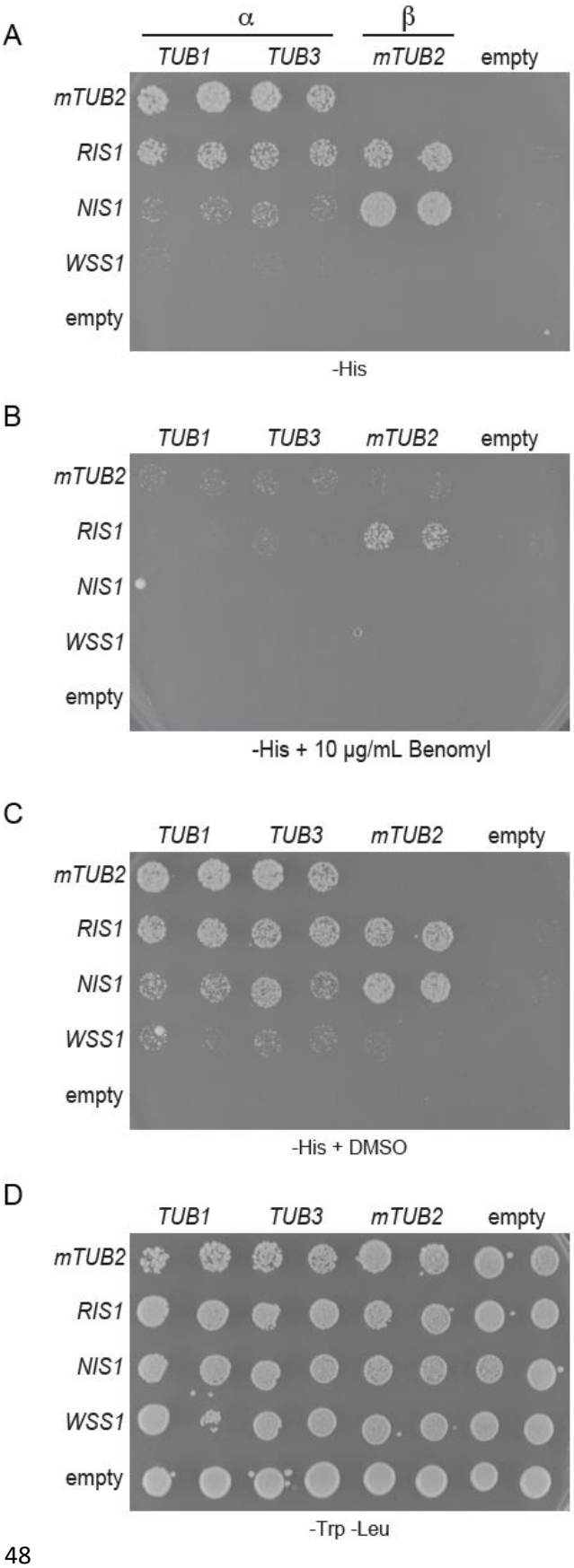

increasing levels of SUMO (data not shown).

In the non-covalent binding experiments, Stu2p bound much better to the SUMO-GA than the SUMO-GST column. This result is informative, since one would expect the SUMO-GST configuration to more accurately model the architecture of a sumoylated substrate than the SUMO-GA. Nevertheless, this differential binding suggests that Stu2p interacts with SUMO in an orientation-specific manner. Although the alpha-helix and beta-sheet in SUMO that are responsible for SIM interactions should be accessible in both constructs, it is likely that steric hindrance imposed by the GST reveals this specificity (Hecker et al., 2006) (Jardin et al., 2015) (Newman et al., 2017). Further, these results demonstrate that Stu2p can bind non-covalently to SUMO.

It should be noted that Stu2p's biochemical non-covalent binding to GST-SUMO-GA represents an inconsistency with our two-hybrid results, in which BD-*STU2* did not interact with an AD-SUMO-GA construct. It should also be noted that the biochemical assays used a C-terminal tag (Stu2-HA) in contrast to the amino-terminal BD fusion (DB-*STU2*) used in the two-hybrid assay. Thus, this difference could reflect an inhibitory effect conferred by the BD fusion to Stu2p.

This work extends previous work suggesting that Stu2p may interact with SUMO. Stu2p was seen to interact with SUMO using a high-throughput bi-fluorescence complementation (BiFC) assay (Sung et al., 2013) and a high throughput proteomics screen (Hendriks et al., 2017). These data suggest a covalent interaction, consistent with our data.

Our domain mapping identified a necessary and sufficient region that supports interactions between Stu2p and SUMO (Figure 3). This domain coincides with the domain responsible for Stu2p dimerization (Wolyniak et al., 2006). This domain of Stu2p also is required for its recruitment to the kinetochore and SPB (Haase et al., 2017). As SUMO is known to regulate the dimerization of several of its targets (Rojas-Fernandez et al., 2014) (Bossis et al., 2005), we are currently working to determine whether SUMO regulates the dimerization of Stu2p. Indeed, the mechanisms regulating Stu2's coiled-

coil formation remain to be elucidated and several highly conserved lysine residues reside within this domain (Haase et al., 2017).

With this work on Stu2p, eight different classes of MAPs have now been shown to interact with SUMO. These are tau (Dorval and Fraser, 2006), Ndc80p (Montpetit et al., 2006), CENP-E (Zhang et al., 2008), Kar9p and Bim1p/EB1 (Meednu et al., 2008) (Leisner et al., 2008), as well as Pac1p/Lis1 and Bik1p/CLIP-170 (Alonso et al., 2012). Interestingly, Stu2p interacts with five of these. Future work will elucidate the extent to which SUMO modulates these interactions, either directly or indirectly.

Future work is also needed to elucidate the function of the interaction of Stu2p with SUMO. Stu2p is a multi-functional protein. In addition to its role in microtubule polymerization and nucleation, it is responsible for microtubule anchorage at MTOCs (Usui et al., 2003) (Wang and Huffaker, 1997) (Podolski et al., 2014). Stu2p also functions at the kinetochore, helping to attach MTs to the outer kinetochore plaque (Miller et al., 2016) (Suzuki et al., 2016) (Haase et al., 2017) (Pearson et al., 2003). The kinetochore contains several sumoylated proteins, including its sumoylated partner, Ndc80p (Aravamudhan et al., 2014) (Montpetit et al., 2006). Stu2p also functions in spindle positioning, interacting with Kar9p, Bim1p/EB1, Bik1p/CLIP-170 and Pac1p/Lis1. While there are myriad potential functions of Stu2p that SUMO could possibly influence, future work will be necessary to precisely define this role in yeast and higher organisms.

Tubulin interactions with SUMO

Tubulin dimers are a major binding partner of Stu2p. Here, we report three lines of evidence suggesting that tubulin interacts with SUMO. Biochemically, tubulin bound to the SUMO-GA column independently of Stu2p. Beta-tubulin also interacted with SUMO by two-hybrid analysis. Both alpha- and beta-tubulin also interacted with two enzymes associated with the SUMO pathway, the E3 enzyme Nfi1p that regulates SUMO conjugation and the STUbL enzyme Ris1p. Work from previous proteomics screens has suggested that tubulin can be conjugated by SUMO (Hendriks et al., 2017). A previous BiFC

bi-fluorescence screen also suggested a covalent interaction (Sung et al., 2013). Combined with our work, this suggests that tubulin can interact with SUMO by both covalent and non-covalent mechanisms.

In the two-hybrid analyses, the alpha- and beta-tubulins displayed different interactions with SUMO. Beta-tubulin interacted with SUMO, whereas the two alpha-tubulins did not. Notably, the beta-tubulin interaction with SUMO was retained under benomyl treatment, as was the Tub2p-Ris1p interaction. In contrast, benomyl eliminated all of the interactions of the alpha-tubulins that we analyzed (Tub2p, the E3 Nfi1, the STUbL Ris1p, and neck protein Nis1p). These findings are consistent with a model in which the alpha-tubulin interactions with SUMO are bridged or facilitated by beta-tubulin.

Our observations that SUMO and the STUbL Ris1p interact preferentially with beta-tubulin are especially relevant in light of the well-documented fact that excess beta-tubulin is toxic to the cell (Burke et al., 1989) (Katz et al., 1990) (Weinstein and Solomon, 1990). Previous work has demonstrated that cells maintain the 1:1 stoichiometry between alpha- and beta-tubulin using a variety of mechanisms, including co-translational regulation of beta-tubulin mRNA degradation and beta-tubulin binding proteins or chaperones (Theodorakis and Cleveland, 1992) (Abruzzi et al., 2002). We speculate that excess beta-tubulin could be degraded through STUbL pathways. This would represent a novel mechanism by which tubulin homeostasis could be regulated by the cell.

MATERIALS AND METHODS:

Two-hybrid analysis.

Two-hybrid analysis was carried out as previously described (Meednu et al., 2008; Moore et al., 2008; Moore and Miller, 2007). All analysis was carried out after 2-3 days of growth at 30 ºC. *STU2*-BD (pRM7247/pCUB495) was a gift from Tim Huffaker.

Table 1 Strains and plasmids used in this study

Yeast Strains	Genotype/comments	Source
yRM1756/PJ69-4α	*MATα trp1-901 leu2-3 leu2-112 ura3-52 his3Δ200 gal4Δ gal80Δ LYS2::GAL1-HIS3 GAL2-ADE2 met2::GAL7-lacZ*	(James et al., 1996)
yRM1757/PJ69-4A	*MAT*a *trp1-901 leu2-3 leu2-112 ura3-52 his3Δ200 gal4Δ gal80Δ LYS2::GAL1-HIS3 GAL2-ADE2 met2::GAL7-lacZ*	(James et al., 1996)
yRM2057	*MAT*a *bim1Δ::KAN trp1-901 leu2-3 leu2-112 ura3-52 his3Δ200 gal4Δ gal80Δ LYS2::GAL1-HIS3 GAL2-ADE2 met2::GAL7-lacZ*	(Miller et al., 2000)
yRM2122/pCUY1147	*MAT*a *PAce1-UBR1 PAce1-ROX1 trp1-Δ1 ade2-101 ura3-52 lys2-801* stu2Δ::*URA3::P$_{Anb1}$UB-R-STU2*	(Kosco et al., 2001b)
yRM2123/pCUY1148	*MAT*a *PAce1-UBR1 PAce1-ROX1 trp1-Δ1 ade2-101 lys2-801 ura3-52::URA3*	(Kosco et al., 2001b)
yRM2146/MS52	*MATα ura3-52 leu2-3 leu2-112 trp1Δ1*	(Miller et al., 1999)
yRM2258	*MAT*a *bik1Δ::TRP1 trp1-901 leu2-3 leu2-112 ura3-52 his3Δ200 gal4Δ gal80Δ LYS2::GAL1-HIS3 GAL2-ADE2 met2::GAL7-lacZ*	(Moore et al., 2006)
yRM6172	*MAT*a *kar9Δ::KAN trp1-901 leu2-3 leu2-112 ura3-52 his3Δ200 gal4Δ gal80Δ LYS2::GAL1-HIS3 GAL2-ADE2 met2::GAL7-lacZ*	(Meednu et al., 2008)
yRM6249	*MAT*a *pac1Δ::KAN trp1-901 leu2-3 leu2-112 ura3-52 his3Δ200 gal4Δ gal80Δ LYS2::GAL1-HIS3 GAL2-ADE2 met2::GAL7-lacZ*	(Alonso et al., 2012)
yRM7230	*MATα ura3-52 leu2-3 leu2-112 trp1Δ* [*pGAL-STU2-TAP (*tag is his6-HA–protein A*) URA3 Amp^R*]	This Study
yRM8011/YOK428	*MAT*a *ulp1*::KAN *his3Δ1* leu2Δ ura3Δ [*ulp1-TS- NAT-TRP1*] [pRS425 GPD- flag-SMT3-GG LEU2 2μ AmpR]	(Elmore et al., 2011)
yRM8012/YOK430	*MAT*a *ulp1*::KAN *his3Δ1 leu2Δ ura3Δ* [*ulp1-TS- NAT-TRP1*] [pRS425 GPD-SMT3-GG LEU2 2l Amp^R]	(Elmore et al., 2011)
yRM8139	*MAT*a *ulp1*::KAN *his3*Δ1 *leu2Δ ura3Δ* [*ulp1-TS-NAT-TRP1*]	(Alonso et al., 2012)
yRM9417	*MAT*a *STU2-his6::HIS3 met15Δ his3Δ leu2Δ ura3Δ*	This study
yRM9909	*MAT*a *trp1-901 leu2-3 leu2-112 ura3-52 his3Δ200 gal4Δ gal80Δ LYS2::GAL1-HIS3 GAL2-ADE2 met2::GAL7-lacZ*	(James et al., 1996)
yRM10637	*MAT*a *his3Δ leu2Δ met15Δ ura3Δ* [pRM2119 *STU2-3xHA* Cen6 *LEU2* Amp^R]	This study
yRM10641	*MATa his3* Δ *met15* Δ *ura3* Δ [pRM2200 *LEU2*+ Amp^R YCP]	This study
yRM10782/yKU5	*MATa NIS1-6HA::TRP1*	(Uzunova et al., 2007)

Plasmids

pRM1151	*pGAD*-empty *LEU2* 2μ Amp^R	(James et al., 1996)
pRM1154	*pGBDU*-empty *URA3* 2μ Amp^R	(James et al., 1996)
pRM1157	*pGBD*-empty *TRP1* 2μ Amp^R	(James et al., 1996)
pRM1493	*GBDU-KAR9 URA3* 2μ Amp^R	(Miller et al., 2000)
pRM1916	*PGAD-STU2-aa649-888 LEU2* 2μ Amp^R	(Miller et al., 2000)
pRM2095	*pGBD-TUB1 CEN* Amp^R *TRP1*	D. Botstein/this study
pRM2096	*pGBD-TUB3 CEN* Amp^R *TRP1*	D. Botstein/this study

pRM2117	*pGAD-TUB2-m CEN* Amp^R *LEU2*	D. Botstein /this study
pRM 2119/WP70	*STU2-3xHA* Cen6 *LEU2* Amp^R	(Wang and Huffaker, 1997)
pRM2200/pRS415	*LEU2 CEN* Amp^R	(Sikorski and Hieter, 1989)
pRM2205/pRS426	*URA3* 2μ Amp^R	(Sikorski and Hieter, 1989)
pRM2627	*GAD-BIK1 LEU2* 2μ Amp^R	(Moore et al., 2006)
pRM2759	*GST* Amp^R	(Moore et al., 2006)
pRM2908	*pGAL URA3* 2μ Amp^R	This study
pRM3595	*KIP2 URA3* 2μ Amp^R	(Meednu et al., 2008)
pRM3604	*GBDU-PAC1 URA3* 2μ Amp^R	This study
pRM4380	*GAD424 LEU2* 2μ Amp^R	(Meednu et al., 2008)
pRM4382/pLAJ20	*GAD-SMT3-GG LEU2* 2μ Amp^R	(Meednu et al., 2008)
pRM4383/pLAJ21	*GAD-SMT3-GA LEU2* 2μ Amp^R	(Meednu et al., 2008)
pRM4495	*GAD-UBC9 LEU2 2μ* Amp^R	(Meednu et al., 2008)
pRM4496	*GAD-NFI1 LEU2* 2μ Amp^R	(Meednu et al., 2008)
pRM4595	*GAD-NIS1 LEU2* 2μ Amp^R	(Meednu et al., 2008)
pRM4596	*GAD-RIS1/ULS1 LEU2* 2μ Amp^R	(Meednu et al., 2008)
pRM4597	*GAD-WSS1 LEU2* 2μ Amp^R	(Meednu et al., 2008)
pRM4920/pLAJ19	*GAD-SMT3 LEU2* 2μ Amp^R	(Meednu et al., 2008)
pRM4924	*GBDU-BIK1 URA3* 2μ Amp^R	This study
pRM5169	*his6-UBC9* Amp^R	(Johnson and Blobel, 1997)
pRM5251	*pGAL-3HA-FLAG-SMT3 HIS3* Amp^R	This study
pRM6713	*his6-S-tag-SMT3-GG* Kan^R	This study
pRM6760	*GST-AOS1/UBA2* 2μ Amp^R	(Bencsath et al., 2002)
pRM6956	*pGAL-STU2-TAP* (tag consists of his6- HA-protein A*) URA3* Amp^R	(Gelperin et al., 2005)
pRM7247/pCUB495	*BD-STU2 TRP*+ 2μ Amp^R	(Wolyniak et al., 2006)
pRM7228	*BD-STU2-aa1-658 URA3* 2μ Amp^R	This study
pRM9370	*BD-STU2-aa613-888 URA3* 2μ Amp^R	This study
pRM9426	*BD-STU2 URA3* 2μ Amp^R	This study

pRM10097	GST-SUMO-GA Amp^R	This study
pRM10749	*GBD-TUB2-m CEN* Amp^R *TRP1*	D. Botstein/this study
pRM10785	*BD-STU2* aa540-888 *URA3* 2μ Amp^R	This study
pRM10787	*BD-STU2* aa540-801 *URA3* 2μ Amp^R	This study
pRM10792	*BD-STU2* aa540-657 *URA3* 2μ Amp^R	This study
pRM10818	SUMO-GST Amp^R	This study
pRM11115	*BD-STU2* aa613-801 *URA3* 2μ Amp^R	This study

***GAL4*-BD m*TUB2* construction.**

Mutant Tub2 was PCR amplified from AD-mTub2 (pRM2117) using primers #1196 5'-ATTAGACTACCCGGGATGAGAGAAATCATTCATATCTCG-3' and #1197 5'-CGCTTATAACTGCAGTTATTCAAAATTCTCAGTGATT-3.' The PCR product was cloned into XmaI and PstI sites of pGBD-C1 vector (pRM1157). This created the Gal4 DBD-mTub2 yeast two-hybrid construct (pRM10749).

His_6-SUMO-GG construction.

SMT3 sequence was amplified from pRM4920 using primer #568 5'-CGGGATCCATGTCGGACTCAGAAGTC-3' and #570 5'-CGCTCGAGCTAACCACCAATCTGTTCTCTG-3.' This generated a SUMO lacking the three terminal amino acids, ATY. A stop codon was added immediately following the glycine 98 residue to generate SUMO in the activated form. The PCR product was cloned into pET-30a(+) (pRM634) at BamHI and XhoI restriction sites. The resulting plasmid was sequenced for verification, generating pRM6711. To express His_6-Smt3p-GG, the plasmid was transformed into BL21-Gold(DE3) (Agilent Technologies, Santa Clara, CA) bacteria, and stored as pRM6713.

His_6-SUMO-GA construction.

Primers 568 5'-CGGGATCCATGTCGGACTCAGAAGTC-3' and 571 5'-CGCTCGAGCTAAGCACCAATCTGTTCTCTG-3' were used to amplify *SMT3* sequence from pRM4920. Primer #571 incorporated mutations that change glycine98 to alanine and a stop codon that follows the mutated alanine residue. The PCR product was cloned into the BamHI and XhoI restriction sites of pET-30(+) (pRM634) to create pRM6720. The accuracy of the construct was confirmed by sequencing. The plasmid was also transformed into BL21-Gold(D3) cells, generating pRM6721.

GST-SUMO-GA construction.

SUMO-GA was PCR amplified using pRM9157 template DNA and primers 854 5'CAACTAATCGTCGACTATGTCGGACTCAGAAGTC-3' and 328 5'-CGTGGAGCTCCCTAATACGTAGCACCACC-3'. SUMO-GA was cloned into the SalI and SacI sites of modified pGEXT-4T-2 vector (pRM2759) in which the NotI site had been replaced with a linker containing the SacI restriction site. This created the GST-SUMO-GA fusion (pRM10097).

SUMO-GST construction.

To engineer a SUMO-GST fusion construct (pRM10815), GST was PCR amplified from pGEX-4T-2 using primers 1191 5'-TTATCGCATGGGCCCGTATTCATGTCCCCTATAC-3' and 1192 5'-GTTCGAGTAGGGCCCCTATTGAACCAGATCCGATTTTG-3' and cloned into the ApaI site of pRS415 to generate pRM10655.

SMT3-GG was then PCR amplified from *S. cerevisiae* genomic DNA using primers 1186 5'-TTATCGCATGGATCCCGATGTCGGACTCAGAAG-3' and 1187 5'-ATAGACACGACTCGTCTCGAGACCACCAATCTGTTCTCTG-3' and ligated into BamHI and XhoI sites upstream of GST in pRM10655 to make pRM10657.

SMT3-GST containing a serine 2 to alanine mutation was PCR amplified from pRM10657 using primers 1233 5'-GATGTACGACCATGGCGGACTCAGAAGTC-3' and 1234 5'-TATCAGCTAGGATCCCTATTTTGGAGGATGGTC-3' and ligated into the NcoI and BamHI restriction sites of pET21d(+) to generate pRM10763. Lastly, the S2A mutation was reverted to the wild-type alanine by site directed mutagenesis using primers 1240 5'-CTTTAAGAAGGAGATATACCATGTCGGACTCAGAAGTCAATCAAG-3' and 1241 5'-CTTGATTGACTTCTGAGTCCGACATGGTATATCTCCTTCTTAAAG-3' to make pRM10818. SUMO-GST was expressed and purified from BL21-Gold(DE3) bacteria (Agilent Technologies, Santa Clara, CA).

***In vitro* sumoylation assay.**

Stu2p was sumoylated using a protocol described previously (Meednu et al., 2008) (Alonso et al., 2012).

Purification of his_6-SUMO-GG, his_6-SUMO-GA and his_6-Ubc9p.

To express and purify his_6-Smt3p-GG (pRM6713), his_6-Smt3-GA (pRM6721), and his_6-Ubc9p (pRM5169), bacteria containing each plasmid were grown overnight in LB plus 50 mg/mL Kanamycin. Saturated cultures were diluted 1:50 into 500 mL of fresh LB plus 50 mg/mL Kanamycin and grown at 37 ºC for approximately 2 h to obtain the OD600 between 0.7-0.8. To induce protein expression, 1 mM IPTG was added to the culture and were grown an additional 2 h at 37 ºC. Cells were harvested by centrifugation at 4,000 rpm. Extracts was prepared by resuspending the cells in 1x binding buffer (20 mM Tris pH 7.9, 300 mM NaCl, 5 mM imidazole) supplemented with bacterial protease inhibitor (Sigma Chemical Co, St. Louis, MO) and 1 mM PMSF before lysing cells by sonication. Extracts were clarified by centrifugation at 13,000 rpm for 30 min at 4 ºC. The supernatant was collected and protein concentration was determined by the Bradford assay using BSA as a standard.

Nickel-NTA resin was used to enrich six histidine-tagged proteins (Novagen, Inc. Madison, WI). Resins were charged according to the manufacturer protocol. Extracts were applied to 2 mL of slurry of the charged nickel resin. Protein was allowed to bind for 30 min on a rotisserie at 4 ºC. The resin was collected by centrifugation at 1,000 rpm for 1 min and the unbound protein was discarded. The resin was then washed as follows: 10 mL of 1x binding buffer with 5 mM imidazole, 10 mL of 1x binding buffer with 50 mM imidazole, and 10 mL of 1x binding buffer with 100 mM imidazole. During each wash, resin was allowed to incubate with the buffer for 10 min on a rotisserie at 4 ºC and collected by centrifugation at 1000 rpm after each wash. To elute bound protein, 1 mL of 1x binding buffer containing 400 mM imidazole was added to the resin and incubated for 10 min at 4 ºC. The eluent was collected by centrifugation at 1,000 rpm for 1 min. The supernatant was transferred to a fresh tube and the resin was

discarded. The protein was aliquoted, flash frozen with liquid nitrogen, and stored at -80 ºC for future use.

For the *in vitro* sumoylation assay, protein was dialyzed with the sumoylation assay buffer (50 mM Tris pH 7.6, 5 mM MgCl2, 15% glycerol) overnight at 4 ºC. The concentration of the protein after dialysis was determined by the Bradford assay (BIO-Rad, Inc. Hercules, CA). After dialysis, Coomassie-blue staining of SDS-PAGE and western blotting using anti-his6 were used to determine the purity of the purified protein.

Purification of GST-Aos1p and Uba2p.

GST-Aos1p and Uba2p (pRM6730) were purified as described (Bencsath et al., 2002) (Meednu et al., 2008). The two proteins were co-expressed from a bi-cistronic vector and co-purified from bacteria using glutathione affinity chromatography. The bacteria were grown overnight to obtain a saturated culture in LB plus 50 mg/mL ampicillin. Saturated cultures were diluted 1:50 into 500 mL fresh LB plus 50 mg/mL ampicillin. The culture was grown to the OD 0.7-0.8 at 37 ºC. To induce the expression of the protein, 1 mM IPTG was added and the culture was grown at 37 ºC for an additional 2 h. Cells were collected by centrifugation at 4,000 rpm and washed once with PBS. Cell pellets were resuspended in PBS containing 1% Triton-X 100, bacteria protease inhibitor, and 1 mM PMSF. Cells were lysed by sonication and centrifuged at 13,000 rpm for 30 min to clarify the protein extract.

Glutathione affinity chromatography was used to purify GST-Aos1p/Uba2p. A 1.5 mL slurry of glutathione beads (Amersham Biosciences, Piscataway, NJ) was equilibrated with PBS. Clarified extracts were applied to the equilibrated glutathione beads and allowed to bind for 1 hour at 4 ºC on a rotisserie. The beads were collected by centrifugation at 1,000 rpm for 1 min and the unbound fraction was discarded. The beads were then washed three times with 10 mL of PBS. Each time, the beads were mixed with the buffer for 10 min on a rotisserie at 4 ºC and collected by centrifugation. To elute the protein from the beads, the fusion protein was cleaved with thrombin overnight on ice. The protein was

then dialyzed into the sumoylation assay buffer (50 mM Tris, pH 7.6, 5 mM MgCl2, 15% glycerol). The concentration of protein after dialysis was determined by Bradford assay. Protein purity was evaluated with anti-GST western blot and Coomassie-blue stained SDS-PAGE. The protein was aliquoted, flash frozen with liquid nitrogen, and stored at -80 ºC for subsequent use.

Stu2p-TAP purification.

TAP-tagged Stu2p was expressed under the *GAL1* inducible promoter (Gelperin et al., 2005). A wild-type yeast strain (yRM7230) containing pGAL-*STU2*-TAP was grown to mid-exponential phase in SC -ura media containing 2% sucrose and induced with 2% galactose for 4 h at 30 ºC. Cell lysates were prepared by breaking open the cell with glass beads in 1x binding buffer supplemented with yeast protease inhibitor cocktail and 1 mM PMSF. After clarification, lysates were applied to charged nickel resin (Novagen, Inc. Madison, WI) and incubated for 1.5 hours at 4 ºC. The beads were first washed with 35 mL 1x binding buffer, followed by washing with 1x binding buffer plus 50 mM imidazole. To elute the bound protein, resin was incubated with 5 mL of 1x binding buffer supplemented with 400 mM imidazole, and 1.5 mL fractions were collected. The fractions were then dialyzed in sumoylation assay buffer (50 mM Tris pH 7.6, 5 mM $MgCl_2$, 15% glycerol) overnight at 4 ºC.

***In vitro* sumoylation of Stu2-TAP.**

To perform the *in vitro* sumoylation assay, one microgram of purified Stu2p-TAP was incubated with 5 µg of His6-Smt3p-GG, His6-Ubc9p, 2 µg Aos1/Uba2p, 4 mM ATP and 7 µl of an ATP regeneration system (3.5 U/mL creatine kinase, 10 mM creatine phosphate and 0.6 U/mL inorganic pyrophosphatase (Sigma Chemical Company, St. Lous, MO). The mixture was incubated for 2h at 30 ºC. To stop the reaction, 3x Laemmli sample buffer plus 5% beta-mercaptoethanol was added and samples were boiled for 5 min. Reaction products were subjected to 6% SDS-PAGE and visualized by western blot analysis. The presence of Stu2p-TAP was confirmed using mouse anti-HA (Santa Cruz Biotechnology, CA).

Preparation of whole-cell extracts.

Ulp1-ts strains expressing Stu2-HA (pRM2119) or vector (pRM2200) were grown to saturation in SC –Leu –Trp liquid media. Cells were collected by low speed centrifugation, washed, and resuspended in cold 1x PBS containing 0.1% Tween buffer and excess fluid was removed. Cells were resuspended in 1x PBS containing 0.1% Tween, 1 mM PMSF, 20 mM N-ethylmaleimide, 40 mM 2-iodoacetamide, and 1% Sigma protease inhibitor cocktail. Cells were lysed by vortexing with glass beads for 10 min. Extracts were clarified by centrifugation at 13,500g for 20 min at 4 °C. Protein concentrations were determined by Bradford Protein Assay (Bio-Rad, Inc. Hercules, CA), using BSA as a standard. Protein samples were analyzed by 10% SDS-PAGE followed by western blotting.

Stu2p pull-down assay.

Yeast whole-cell extracts were prepared as described above by bead beating. Extracts were incubated with agarose anti-HA beads (cat# A2095, Sigma Aldrich, St. Louis, MO,) at 4 °C on a rotisserie for 2 h. Beads were collected and washed twice with ice-cold PBS containing an additional 0.5 M NaCl, for a total of 650 mM NaCl. To elute, beads were boiled with 3x Laemmli sample buffer for 5 min. Stu2-HA was detected using rabbit anti-HA antibody (Sigma Aldrich, St. Louis, MO, Cat #H6908) at 1:1500 in PBS for 2 h at RT. SUMO was detected using rabbit anti-Smt3p (Rockland, Inc. Gilbertsville, PA, Cat #200-401-428) at 1:1000 in PBS for 2 h at RT.

Stu2-his6 enrichment under denaturing conditions.

To prepare yeast whole-cell extracts, strains expressing Stu2-his6 (yRM9417) or non-tagged Stu2p (yRM2146) were grown overnight to saturation. Cells were re-suspended in PBS buffer containing a 2x protease inhibitor cocktail (2 mM PMSF, 86 mM 2-Iodoacetamide, 40 mM NEM, and 1:250 Sigma PIC-P8849) at a ratio of 1 mL of buffer to every 3 grams of cell pellet by weight. The cell suspension was flash frozen by pipetting droplets into liquid nitrogen and stored at -80 °C. Cells were re-chilled in liquid nitrogen and mechanically fractured using a Retsch MM400 cryomill. Frozen-powdered extract

was resuspended to a final concentration of 3.2 mg/mL and 8 M urea in PBS containing 1x protease inhibitor cocktail lacking divalent metal ion chelators (Sigma). To clarify, extracts were centrifuged for 30 min at 16,000 RPM at 4 °C. Ni-NTA agarose resin (100 μL) that was equilibrated in 8M urea/PBS was incubated with approximately 100 mgs of clarified extracts for 2.5 h at 4 °C. Resin was washed five times with 1 mL ice-cold PBS containing 8 M urea. Excess buffer from the final wash was removed using a gel-loading tip. To elute, resin was boiled with 150 μL of 2x Laemmli sample buffer. Proteins were resolved on 10% SDS-PAGE and transferred to nitrocellulose membranes. Following overnight blocking with 0.1% I-block reagent (Applied Biosystems, Bedford, MA) dissolved in PBS containing 0.1% Tween. Proteins were detected with rabbit anti-Stu2p or goat anti-SUMO (SC-11847) and goat anti-rabbit (SC-2004) or donkey anti-goat (SC-2056) conjugated with HRP.

SUMO pull-down assay.

Yeast extracts were prepared as described above. Extracts were incubated overnight with rabbit anti-Smt3p (Rockland, Inc. Gilbertsville, PA Cat #200-401-428). Beads were collected and washed twice with cold PBS containing an additional 0.5 M NaCl, for a total of 637 mM NaCl. To elute, beads were boiled with 3x Laemmli sample buffer for 5 min. Stu2-HA was detected using mouse anti-HA antibody (Sigma Aldrich, St. Louis, MO, #3663) at 1:1500 in PBS for 2 h at RT.

Ubiquitin pull-down assay.

Yeast extracts were prepared as described above. Extracts were incubated overnight with rabbit anti-ubiquitin (Enzo Life Sciences, Inc. Farmingdale, NY Cat #BML-UG9511-0025). Beads were collected and washed twice with ice cold PBS containing an additional 0.5 M NaCl, for a total of 637 mM NaCl. Beads were boiled with 3x sample buffer for 5 min. Stu2p was detected using mouse anti-HA (Sigma Aldrich, St. Louis, MO, Cat #H3663) at 1:1500 dilution in PBS for 2 h at RT.

Non-covalent binding to SUMO affinity columns.

Non-covalent SUMO affinity columns were prepared as follows. Glutathione agarose beads (Pierce Inc, Rockford, IL) were equilibrated in PBS containing 0.1% Triton, 1 mM PMSF. Bacterial cells expressing GST, GST-SUMO-GA, or SUMO-GST were disrupted by sonication in PBS buffer containing 0.1% Triton, 1 mM PMSF. To clarify, extracts were centrifuged at 13,000 RPM for 30 min at 4 °C. Bacterial extracts were incubated with 100 μL of glutathione agarose beads for 2 h with gentle agitation. Resins were then washed two times with 150 column volumes of PBS containing 0.1% Triton. Aliquots of the GST or SUMO-GST affinity matrices were run on SDS-PAGE in triplicate, stained with coomassie blue, analyzed by densitometry, and normalized for subsequent affinity assays. It is interesting to note that for Nis1p, little or no binding was observed when the Nis1p protein was applied to the columns at concentrations higher than 2 mg/mL. This may indicate that complexes can mask the SUMO interaction motif in Nis1p (data not shown).

To prepare yeast whole-cell extracts, cells expressing Stu2-3xHA (pRM10637) or Nis1p-6xHA (pRM10782) from CEN plasmids were grown overnight to saturation. Cells were disrupted by bead beating or by cryomilling in liquid nitrogen in PBS containing 0.1% Triton, 1 mM PMSF, 43 mM 2-Iodoacetamide, 20 mM NEM, and 1:500 dilution of Sigma Protease Inhibitor Cocktail P8215 developed for *S. cerevisiae.* The indicated amounts of extracts containing Nis1p-6xHA (2 mgs), Stu2-3xHA (10.8 mgs), or the empty vector control (10.8 mgs) were incubated with normalized amounts of GST, GST-SUMO-GA, and SUMO-GST on a rotisserie for 3.5 h. Beads were then collected by low-speed centrifugation at 250 RPM for 1 min and washed 5 times with 1 mL PBS. The final wash was removed completely using a gel-loading tip. To elute bound protein, beads were resuspended in 70 μL 2x-Laemmli sample buffer and boiled for 5 min. To confirm the column normalizations, 5% of each pull down was assayed on Coomassie blue stained SDS-PAGE gels. To visualize HA epitope-tagged proteins, pull-downs were immunoblotted with mouse anti-HA (SC-7392, Santa Cruz Biotechnology, Santa Cruz, CA) and goat anti-mouse-HRP (Santa Cruz Biotechnology, Santa Cruz, CA) secondary antibody.

Western blots were stripped and re-probed with anti-alpha-tubulin (YOL1/34 from AbD Serotec, Raleigh, N.D.).

ACKNOWLEGEMENTS:

This work was supported by grants from the Oklahoma Health Research Program of the Oklahoma Center for the Advancement of Science and Technology (OCAST #HR09-150S), NSF (#MCB-0414768 and #MCB-1052174), NIH (R15GM119117-01) and the Oklahoma Agricultural Experiment Station (OKL02961) to RKM. AA was supported in part by a fellowship from the Sloan Foundation. RC and KD were supported in part by the NSF-funded Louis Stokes Alliance for Minority Participation (OK-LSAMP) program at OSU.

CHAPTER IV

STU2 ACETYLATION – A SWITCH BETWEEN SPB AND KINETOCHORE FUNCTIONS?

XMAP215/Stu2 microtubule polymerases perform three important roles at distinct locations during mitosis. However, the underlying mechanisms coordinating Stu2 localization and function remain elusive. Phosphorylation of XMAP215/Stu2 proteins have been shown to regulate interactions with the microtubule lattice (Humphrey et al., 2018; Okada, Toda, Yamamoto, & Sato, 2014; Trogden & Rogers, 2015). Our lab has shown that Stu2 is regulated through SUMO covalently and non-covalently, although the mechanisms and functions of these interactions are still unclear. Acetylation may represent a unified mechanism through which microtubules are regulated since acetylation of several different classes of microtubule associated proteins have been shown over the last decade including Tau (Min et al., 2010), EB1/Bim1 (Xie et al., 2018), CLIP-170/Bik1 (Li et al., 2014), and Hec1/Ndc80 (Zhao et al., 2019). In our efforts to elucidate Stu2's sumoylation sites, we also searched for evidence of Stu2 acetylation. Acetylation of K48 in the human XMAP215 family member, CKAP5/ch-TOG, was detected in proteomics screens but not characterized (Choudhary, et al, 2009). In this chapter, I report that acetylation of the protein Stu2 is important in mitosis and that it regulates microtubule polymerization, chromosome segregation, and γ-tubulin interactions.

SUMMARY OF MANUSCRIPT

Acetylation of Stu2

Stu2 is the *S. cerevisiae* member of the XMAP215 family of microtubule associated proteins. Stu2 is important for microtubule polymerization and is found at the Ndc80 kinetochore complexes which link specialized kinetochore microtubules to sister chromatids during cellular division. Stu2 has also been found at the spindle pole body where it is believed to play a role in microtubule nucleation. Because the regulation of Stu2 is poorly understood, we asked whether Stu2 is acetylated. Acetylation of Stu2 was first detected using western blotting techniques and three different acetylation sites were identified by mass spectrometry. These were located at lysines 252, 469, and 870. When WT-Stu2 and mutants that prevent acetylation at these sites were immunoblotted with AcK antibodies, residual signals were seen. This indicated that there are additional Stu2 acetylation sites yet to be discovered. Nevertheless, we sought to determine their functional significance. To evaluate the likelihood that these acetylation sites control Stu2 function, the amino acid sequence of XMAP215 family members from myriad eukaryotic organisms were aligned to determine the evolutionary conservation of these lysines. This revealed that K469 is conserved across eukarya and K870 is conserved in many fungal organisms. Plasmid shuffling assays demonstrated that mutants mimicking an acetylated and non-acetylated Stu2 were viable at 23 ^{o}C and 30 ^{o}C. No significant phenotypes were detected when mutants were evaluated in microscopy assays for karyogamy. The mutants also displayed little or no significant phenotypes for the majority of the cell cycle except for large budded cells. When large-budded cells characteristic of the mitotic phase of the cell cycle were analyzed, several of these positively identified acetylation site mutants displayed mild to moderate mitotic defects. The TOG2 domain acetyl-mimetic mutant K469Q and the MAP binding domain acetyl-preventative mutant K870R both demonstrated significant resistance to benomyl, a drug that destabilizes microtubules, indicating that these mutants may possess hyper-stable microtubules.

Acetylation inhibitory mutants also reduced Stu2 non-covalent interactions with SUMO, whereas acetylation mimicking mutants did not. Several of the acetylation mutants also caused chromosome segregation defects. Lastly immunoprecipitation assays revealed that Stu2 interactions with γ-tubulin are increased when cells possessed the triple acetylation mimetic mutant Stu2-3KQ. With this work, we demonstrate that a fourth class of microtubule associated protein is regulated by acetylation. As this brings the list of acetylated MAPs to four with CLIP-170/Bik1, EB1/Bim1, and Hec1/Ndc80, it suggests that acetylation may be a common mechanism for MAP regulation. Our assays are the basis for a novel model through which Stu2 may be coordinated to the spindle pole body or kinetochore. Furthermore, our work provides insight to answer questions that have persistently eluded the XMAP215 community, such as how separate pools of Stu2 are targeted to the spindle pole body, microtubule plus ends, and kinetochores.

Acknowledgements

From the subject matter of chapter 4 in this dissertation, a manuscript has been prepared for submission. This article, titled "Stu2 acetylation – A switch between SPB and kinetochore functions?" was co-authored by Matt Greenlee, Jeremy Sabo, Tori Tabb, Braden Witt, Savannah Morris, and Rita K. Miller.

Table	Figure	Contributed by . . .
1	**1a, 1c, 1d, 1e, 2, 3, 4, 5, 7, 8, 9, 10, 11, 12, 13, 14, 15, 16, 18c, 18d**	**Matt Greenlee**
	6	**Savannah Morris**
	1b, 17	**Jeremy Sabo**
2		**Tori Tabb**
	6	**Braden Witt**

Table A The figure, panel, and table contributions of each author for the Greenlee et. al., 2018 manuscript. This manuscript includes figures and panels submitted by the following authors: Matt Greenlee, Jeremy Sabo, Tori Tabb, Braden Witt, Savannah Morris.

Stu2 acetylation: a switch between SPB and kinetochore functions?

Matt Greenlee*, Jeremy Sabo*, Tori Tabb*, Savannah Morris*, and Rita K. Miller*

* Department of Biochemistry and Molecular Biology
Oklahoma State University
Stillwater, OK 74078

Corresponding author:
Rita K. Miller
248A Noble Research Center
Department of Biochemistry and Molecular Biology
Oklahoma State University
Stillwater, Oklahoma 74078

Phone: 405-744-7732
Fax: 405-744-7799

Email: rita.miller@okstate.edu

Key words: *STU2*, XMAP215, acetylation, microtubules, tubulin
Running Head: Stu2 acetylation influences chromosome segregation

Abbreviations:
AcK, acetyl-lysine
MAP, Microtubule associated protein
PBS, Phosphate buffered saline
PFGE, Pulsed field gel electrophoresis
SC, synthetic complete
SIM, SUMO interacting motif
SPB, spindle pole body
WT, wild type
YPD, yeast peptone dextrose
+TIPs, +Tip interacting proteins

ABSTRACT

Stu2 is the *S. cerevisiae* member of the XMAP215/Dis1/ch-TOG family of MAPs that have multiple functions controlling microtubules, including; microtubule polymerization, microtubule depolymerization, linking chromosomes to the kinetochore, and assembly of γ-TuSCs at the SPB. Whereas phosphorylation was shown to be critical for Stu2 localization at the kinetochore, other regulatory mechanisms that control Stu2 function during mitosis are still poorly understood. Here, we show that a novel form of Stu2 regulation occurs through the acetylation of three lysine residues (K252, K469, and K870) located in three distinct domains of Stu2. Alteration of acetylation through acetyl-mimetic and acetyl-blocking mutations did not impact essential functions of Stu2 but lead to both positive and negative changes to chromosome stability, and changes in resistance to the microtubule depolymerization drug, benomyl. Additionally, microscopy experiments indicated mild karyogamy, bi-nucleation, and multi-lobed defects. We also demonstrate that manipulation of Stu2 acetylation regulates Stu2 non-covalent interactions with SUMO and γ-tubulin. This work suggests a novel mechanism by which acetylation regulates chromosome stability through Stu2.

INTRODUCTION

Stu2 is a member of the XMAP215/Dis1/ch-TOG family of MAPs that has multiple microtubule-dependent functions. Stu2 is well known for its role as a microtubule polymerase (Al-Bassam et al., 2006; Ayaz et al., 2014; Brouhard et al., 2008; Podolski et al., 2014; Wang & Huffaker, 1997) (reviewed in Al-Bassam & Chang, 2011). Stu2 promotes microtubule elongation through interactions with tubulin via two TOG domains (Al-Bassam et al., 2007; Al-Bassam et al., 2006; Ayaz et al., 2012, 2014; Slep & Vale, 2007) and interacts with the microtubule lattice through a basic microtubule binding (MT binding) domain (Al-Bassam et al., 2006; Wang & Huffaker, 1997). To carry out microtubule polymerization, Stu2 is also thought to undergo significant conformational changes throughout tubulin binding and microtubule polymerization processes (Al-Bassam & Chang, 2011; Al-Bassam et al., 2006; Ayaz et al., 2014; Nithianantham et al., 2018).

While Stu2 is best known for contributing to microtubule stability and growth, it has also been shown to initiate microtubule depolymerization (Al-Bassam & Chang, 2011; Al-Bassam et al., 2006; Brouhard et al., 2008; Humphrey et al., 2018; Shirasu-Hiza, Coughlin, & Mitchison, 2003; van Breugel, Dreschsel, & Hyman, 2003). Stu2 also functions at the spindle pole body (SPB), where interactions with Spc72 facilitate microtubule nucleation by promoting oligomerization of γ-TuSC assemblies (Chen et al., 1998; Gunzelmann et al., 2018; Thawani et al., 2018; Usui et al., 2003). Additionally, interactions between Stu2 TOG, MT binding, and c-terminal MAP interacting domains and Tub4 (γ-tubulin), Spc97, and Spc72 respectfully all correlate with spontaneous MT nucleation in the presence of Spc72 and tubulin with or without purified γ-TuSC (Gunzelmann et al., 2018). The γ-TuSC complex is thought to have an open form that is inactive and a closed form that actively nucleates microtubules. The differences between the two γ-TuSC states have been investigated and provide a structural basis for actively nucleating and idle MT nucleation (Greenberg et al., 2016).

Stu2 has multiple functions at the kinetochore. It is important for attachment of kinetochore microtubules (K-fibers) to the outer plaque of the kinetochore. It also aids in the selection of correctly oriented kinetochore attachments. Stu2 accomplishes this task by serving as a mechanosensor while bound to the Ndc80 complex (Miller et al., 2016). Levels of tension associated with correct bi-polar microtubule attachments to sister chromatids initiate Stu2 mediated microtubule plus-end depolymerization and subsequent Dam1 complex capture to secure optimal kinetochore K-fiber interactions (Asbury et al., 2006; Humphrey et al., 2018; Miller et al., 2016).

However, many of the regulatory mechanisms that control Stu2 function during mitosis and meiosis are poorly understood. Most recently, a Cdk1 phosphorylation site found in the basic MT binding domain of Stu2 was shown to promote Stu2 localization to the kinetochore (Humphrey et al., 2018). S603 phosphorylation of Stu2 neutralizes the basic MT binding patch and enables Stu2 to more readily concentrate at kinetochores through interactions with other MAPs (Humphrey et al., 2018). While phosphorylation reduced interactions with the MT lattice, the TOG1, the coiled coil Stu2 dimerization, and the C-terminal MAP interacting domains were also important for Stu2 localization to the kinetochore, (Miller et al., 2019). Phosphorylation of other XMAP215 family members has also been reported to control their association with the microtubule lattice; in *S. pombe* CDK mediated phosphorylation was found in Alp14 (Aoki, Nakaseko, Kinoshita, Goshima, & Yanagida, 2006) and Dis1 proteins (Okada et al., 2014), and Msps phosphorylation was found in the *D. melanogaster* (Trogden & Rogers, 2015). While MT binding domain phosphorylation regulates Stu2 association with the microtubule lattice (Humphrey et al., 2018; Okada et al., 2014; Trogden & Rogers, 2015), other mechanisms governing Stu2 localization and functions remain elusive.

In this report, we identify acetylation as a novel post-translational modification of Stu2. We show that acetylation of Stu2 occurs on three lysine residues, K252, K469, and K 870. These

residues are located in the TOG1, TOG2 , and the MAP interacting domains, respectively. The TOG domains bind alpha-beta tubulin heterodimers, whereas the MAP interacting domain is responsible for Stu2 interactions with Bik1, Bim1, and Spc72 (Usui et al., 2003; Wolyniak et al., 2006). Imitation of Stu2 acetylation states with amino acid mimetics resulted in minor rates of bi-nucleation and multibudded defects, changes in resistance to the microtubule depolymerization drug benomyl, as well as positive and negative changes to chromosome stability. We also find that Stu2 acetylation mimetic mutants impact non-covalent interactions between Stu2 and SUMO, as well as interactions between Stu2 and γ-tubulin. This work suggests a novel mechanism by which acetylation regulates chromosome stability through Stu2 and Stu2 interactions at the γ-TuSC.

Acetylation of K212 in the human plus end tracking protein EB1, or BIM1 in yeast, was shown to regulate interactions with CLIP-170, $p150^{glued}$, and APC (Xie et al., 2018). Additionally, K220 acetylation of EB1 plays a role in EB1 localization to mitotic spindle microtubule plus ends and metaphase alignment timing (Xia et al., 2012). Acetylation of CLIP-170, BIK1 in *S. cerevisiae*, was found to influence cellular migration of pancreatic cancer cells (Li et al., 2014). In addition, acetylation of the XMAP215 family member CKAP5/ch-TOG was previously detected using high-throughput proteomics screens (Choudhary et al., 2009). It remains to be seen how or if acetylation regulates many other microtubule associated proteins (MAPs).

RESULTS

Stu2 is acetylated at lysine 252, 469, and 870.

Because EB1 and CLIP-170 can be acetylated, we wondered whether Stu2/XMAP215 proteins, representing another class of MAPs, are also acetylated. For this, we immunoprecipitated HA-tagged or untagged Stu2 from logarithmically growing cultures treated

with the deacetylation inhibitor Trichostatin A (TSA). The precipitate was then immuno-blotted with anti-HA to detect Stu2 and anti-AcK. As shown in Figure 1a, bands with a molecular weight of approximately 115 kDa were observed in both HA and AcK immunoblots. Importantly, the 115 kDa molecular band appeared in extracts containing Stu2-HA but was absent in extracts containing untagged Stu2. These findings suggest that Stu2 is acetylated.

To identify specific acetylated residues, we employed a mass-spectrometry strategy. We first immunoprecipitated Stu2-HA from extracts prepared from logarithmically growing cultures. The precipitate was separated by SDS-PAGE and analyzed by western blotting with anti-HA (Figure 1b). The bands corresponding to Stu2 were excised from a duplicate coomassie blue stained gel and prepared for tandem mass spectrometry (MS/MS) (see Materials and Methods). This analysis identified 7650 spectra corresponding to Stu2. Of these, 59 showed a 42 Da increase in mass characteristic of acetylation with an error of less than 10ppm. Thirty-two of the spectra corresponded to peptides with an acetyl-modification of lysine 252. Nine spectra corresponded to acetylation of lysine 469, and 18 corresponded to acetylation of lysine 870. Nine spectra of AcK 252 and three spectra of AcK 870 had a confidence level of 100%. Eight of the nine spectra obtained for AcK469 had a confidence score of 90% or higher. Many of these putative acetylated peptides also contained immonium reporter ions diagnostic for acetylated lysine (Figure 1 c, d, and e). The confidence scores for these and additional lower-confidence spectra peptides are shown in Table 1. Combined, these data suggest that Stu2 is a bona fide multi-acetylated protein.

Lysine 252, 469, and 870 account for a fraction of Stu2 acetylation

To begin to identify the function of these acetylation sites, we mutated each Stu2 lysine to either arginine to generate an acetylation-inhibitory state or to glutamine to generate an acetylation mimetic state, herein referred to as 3KR and 3KQ. Using cells from logarithmically

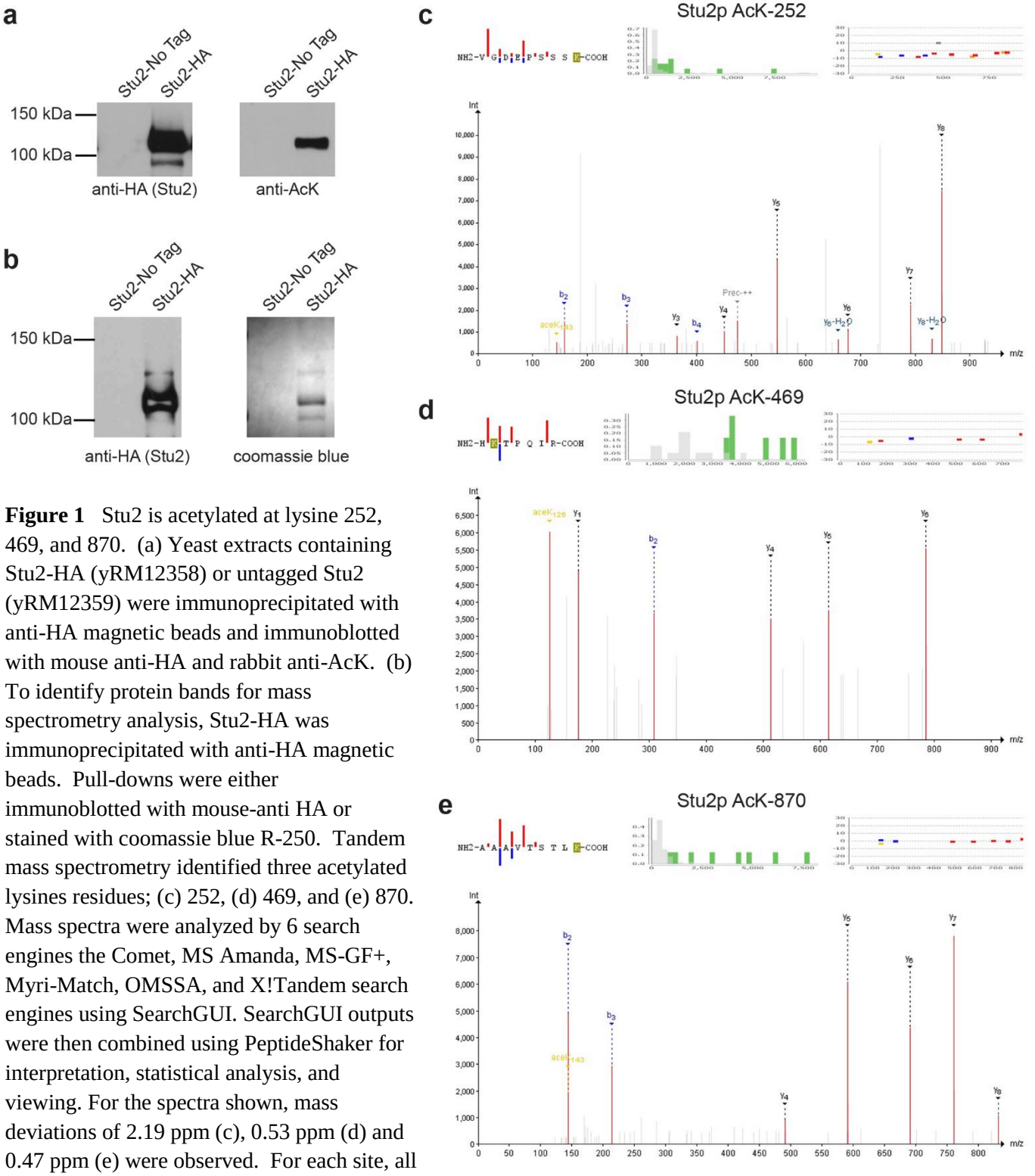

Figure 1 Stu2 is acetylated at lysine 252, 469, and 870. (a) Yeast extracts containing Stu2-HA (yRM12358) or untagged Stu2 (yRM12359) were immunoprecipitated with anti-HA magnetic beads and immunoblotted with mouse anti-HA and rabbit anti-AcK. (b) To identify protein bands for mass spectrometry analysis, Stu2-HA was immunoprecipitated with anti-HA magnetic beads. Pull-downs were either immunoblotted with mouse-anti HA or stained with coomassie blue R-250. Tandem mass spectrometry identified three acetylated lysines residues; (c) 252, (d) 469, and (e) 870. Mass spectra were analyzed by 6 search engines the Comet, MS Amanda, MS-GF+, Myri-Match, OMSSA, and X!Tandem search engines using SearchGUI. SearchGUI outputs were then combined using PeptideShaker for interpretation, statistical analysis, and viewing. For the spectra shown, mass deviations of 2.19 ppm (c), 0.53 ppm (d) and 0.47 ppm (e) were observed. For each site, all 6 search engines presented the acetylated peptide with high certainty.

Stu2 AcK spectra detected from HA immunoprecipitation experiments

AcK site	100% confidence	90-99% confidence	80-89% confidence	<80% confidence	Total spectra
AcK 252	9	20	2	1	*32*
AcK 469	0	8	0	1	9
AcK 870	3	11	4	0	18

.

Table 1 Additional spectra were identified for each acetylated residue. Listed are all of the confidence scores associated with each putative AcK spectra. AcK 252 had a total of 32 spectra with the following confidence scores: 9 with 100%, 5 with 99%, 4 with 97%, 8 with 96%, 2 with 95%, 1 with 94%, 1 with 83%, 1 with 82%, 1 with 32%. AcK 469 had a total of 10 spectra with the following confidence scores: 1 with 97%, 3 with 96%, 1 with 95%, 1 with 94%, 1 with 93%, 1 with 91%, and 1 with 70%. AcK 870 had a total of 18 spectra with the following confidence scores: 3 with 100%, 4 with 99%, 3 with 98%, 3 with 97%, 1 with 96%, 1 with 86%, 1 with 85%, 1 with 82%, and 1 with 80%. All spectra fell well within a 30 ppm mass accuracy with the vast majority of parent ion masses deviating less than 3 ppm.

growing cultures, Stu2 was immunoprecipitated and analyzed by immunoblotting. Comparison of WT cells to 3KR and 3KQ cells (Figure 2a) revealed a moderate reduction in anti-acetyl reactivity of the Stu2 band, indicating that lysine 252, 469 and 870 account for a significant portion of Stu2 acetylation. In addition, the 3KR strain routinely displayed slightly lower Stu2 steady-state abundance of Stu2 (Figure 2b). In contrast, the 3KQ mutant displayed no such reduction in abundance, possibly indicating a role of acetylation in maintaining Stu2 equilibrium. Because acetylation signals were not abolished in the 3KR and 3KQ lanes (Figure 2c), and densitometry experiments showed only a 30% and 10% reduction in 3KR and 3KQ mutant acetylation respectively (Figure 2d), we anticipate that additional acetylation site(s) are present on Stu2. However, additional mass spectrometry experiments will be required to identify them.

When logarithmically growing cell cultures were treated with different concentrations of the pan HDAC inhibitor TSA, we detected different α-AcK signal intensities (Figure 3a & b). Following treatment with 200 ng/mL TSA, band densitometry analysis indicated larger reductions in α-AcK signal of Stu2-3K mutant protein relative to the WT control (Figure 3c). In contrast, when 500 ng/mL TSA was used, significantly more α-AcK signal was observed in the Stu2 band (Figure 3d). This likely indicates the deacetylase is not completely inhibited at lower concentrations of TSA. For each mutant, we quantified the amount of Stu2 protein enriched by magnetic-HA beads relative to their corresponding steady state abundances in WCEs. This analysis made it apparent that 3K acetyl mutations and TSA treatments both influence Stu2 immunoprecipitation, likely through induced conformational changes.

TSA was previously reported to cause G0 and G2/M cell cycle arrest during short treatments and S phase arrest during extended treatments in HeLa cell lines (Tóth et al., 2004; Xu et al., 2006). Therefore, we also evaluated cell cycle progression of our cell cultures following TSA treatments. Before cell collection, aliquots of each culture were sampled, fixed using 25% acetic acid/75% methanol, and evaluated for cell cycle progression defects. As shown in Figure

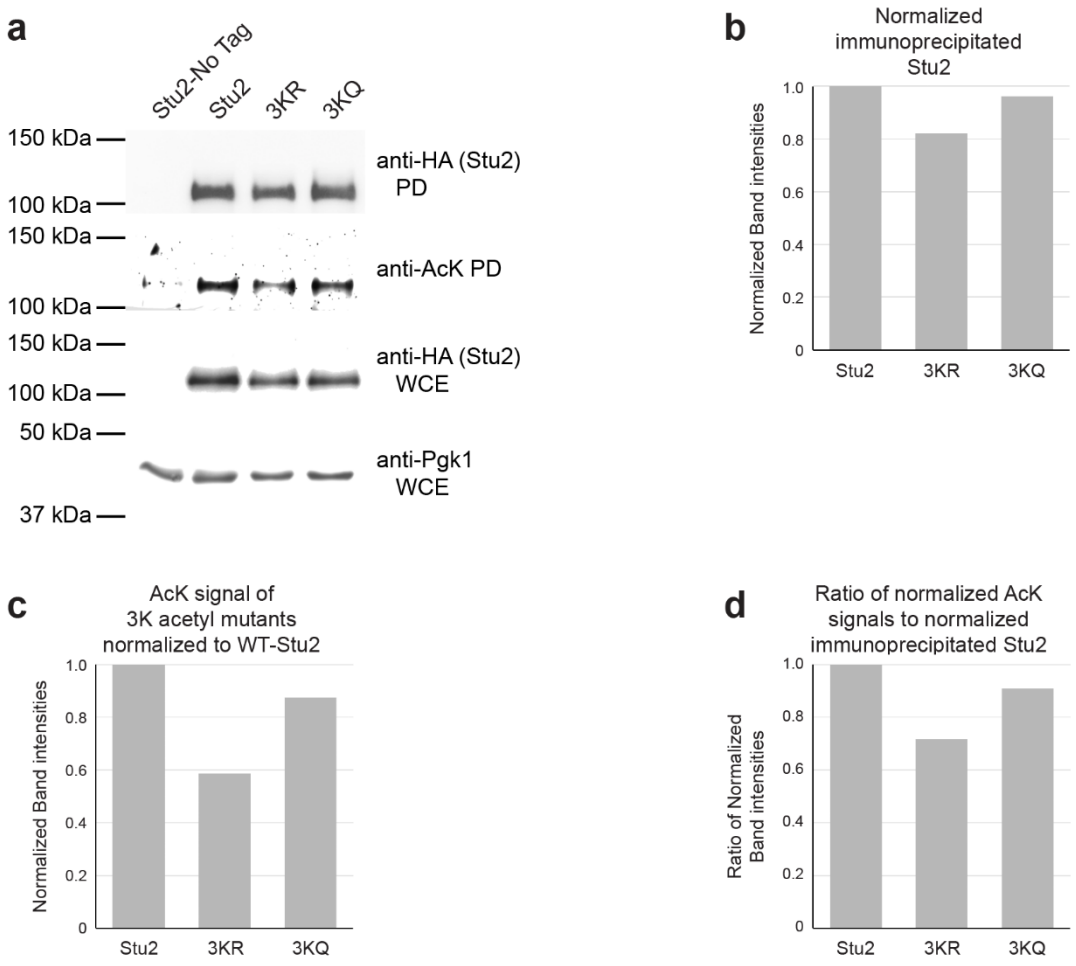

Figure 2 Mutation of lysine 252, 469, and 870 in Stu2-3K mutants leads to reduced detectable Stu2 acetylation. (a) Cells expressing Stu2-HA (yRM12358), untagged Stu2 (yRM12359), Stu2-3KR-HA (yRM12364), or Stu2-3KQ-HA (yRM12369) were immunoprecipitated and western blotted with anti-HA and anti-AcK to evaluate Stu2 enrichment and acetylation. Band densitometry was performed to quantify reductions in Stu2 acetylation. (b) Immunoprecipitated Stu2 from 3KR and 3KQ acetyl mutants was normalized to immunoprecipitated WT-Stu2. (c) Anti-AcK signals from 3KR and 3KQ acetyl mutants were then normalized to anti-AcK signals from WT-Stu2. (d) Lastly, ratios of normalized AcK signals to normalized Stu2 immunoprecipitants were determined for each strain to extrapolate Stu2 acetylation quantities.

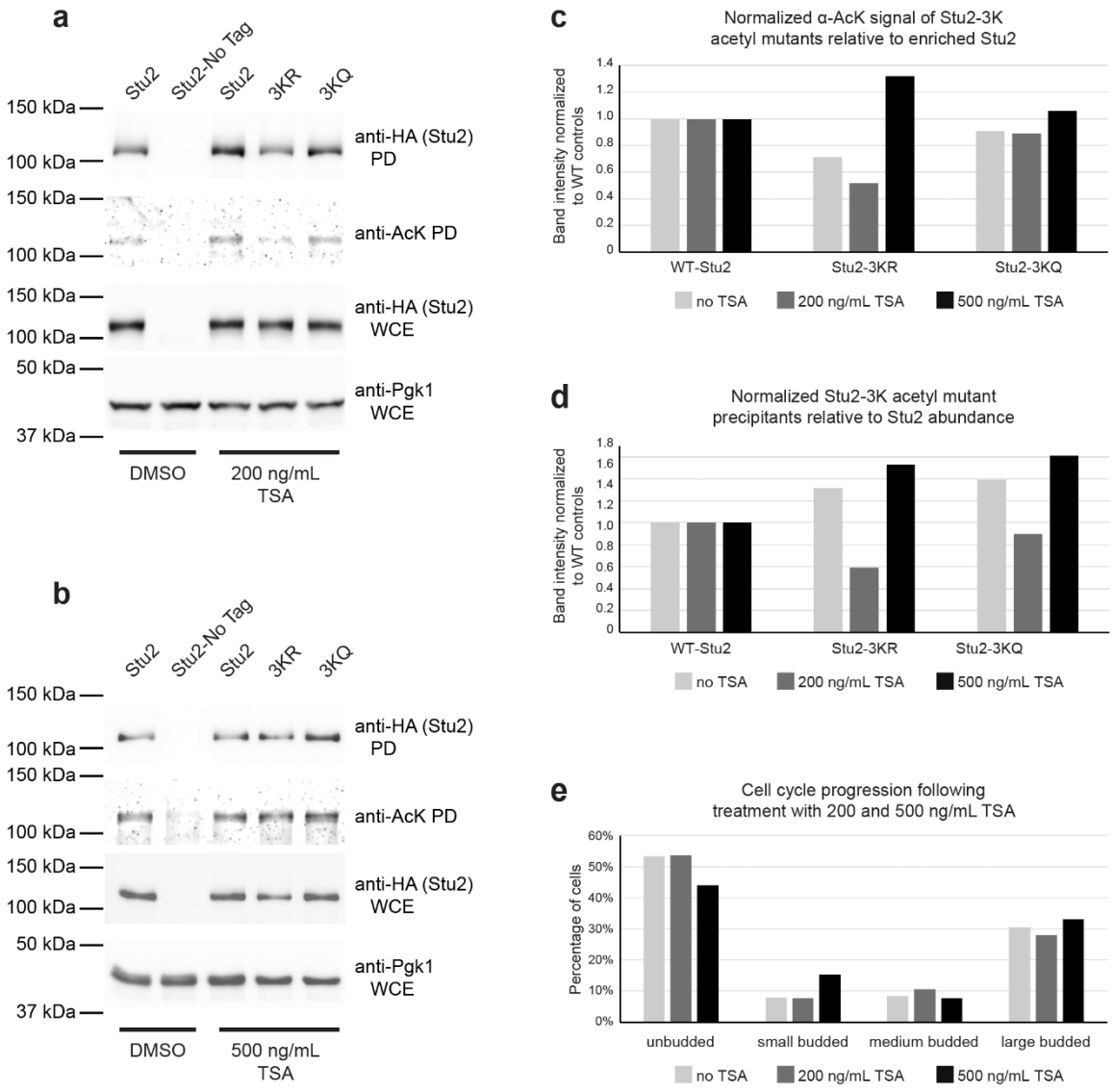

Figure 3 Stu2-3K mutant AcK antibody reactivity and immunoprecipitation responded to treatment with TSA in a dose dependent manner. Logarithmically growing cells expressing Stu2-HA (yRM12358), untagged Stu2 (yRM12359), Stu2-3KR-HA (yRM12364), or Stu2-3KQ-HA (yRM12369) were treated with (a) 200 ng/mL TSA or (b) 500 ng/mL TSA. Cellular extracts were then immunoprecipitated and western blotted with anti-HA and anti-AcK to evaluate Stu2p enrichment and acetylation. Similar to Figure 2d, we used densitometry to determine changes in acetylation between Stu2-3K mutants following TSA treatments. (c) To extrapolate the changes in acetylation of each mutant, we normalized the ratios of each mutants α-AcK signal to enrichment values to corresponding WT controls. (d) We evaluated each mutant's enrichment relative to their corresponding steady state abundance present in western blotted WCEs. (e) We fixed and evaluated a fraction of Stu2-HA cells from each growth condition to determine if TSA treatments lead to cell cycle arrest.

3e, 2 hours of 200 ng/mL TSA treatment did not induce an observable cell-cycle arrest but 500 ng/mL TSA treatments lead to a 2-fold increase in small budded cell populations. Therefore, the lower concentrations of TSA used in these experiments are not likely to be responsible for the phenotypes that we report here.

Acetylated lysine residues are found in multiple domains of Stu2.

To gain insight into how lysine acetylation influences Stu2 function, we mapped each acetylated lysine to a composite of predicted and actual crystal structures of Stu2 using the structural model program I-TASSER. The I-TASSER depiction of the Stu2 TOG domains (Figure 4b) closely resemble published crystal structures of TOG domains bound to αβ-tubulin heterodimers, as the coordinates from the pdb files 4ffb and 4u3j were used (Ayaz et al., 2014; Ayaz et al., 2012). From this model, all acetylated lysines are predicted to be solvent exposed. The first acetyl-lysine, K252, lies between α-helices 14 and 15, a region that comprises a flexible linker connecting TOG1 and TOG2 domains. Lysine 469 lies between α-helices 10 and 11 of the TOG2 domain where it interacts with β-tubulin within the TOG2/tubulin binding pocket. K870 lies in the MAP interacting domain where Stu2 interacts with Bik1, Bim1, Ndc80, and Spc80 (Aravamudhan, Felzer-Kim, Gurunathan, & Joglekar, 2014; Usui et al., 2003; Wolyniak et al., 2006).

To assess if the three acetyl-lysines were evolutionarily conserved amongst the Stu2/XMAP215 family of proteins, we aligned XMAP215 sequences across various eukaryota (Figure 4c) and fungal organisms (Figure 4d). Of the three lysines, lysine 252 was the least conserved. It was found in the budding yeast *S. cerevisiae*, the trypanosome *A. Deanei*, and the protist *P. marinus* but not in the other 25 organisms analyzed. In contrast, lysine 469 was highly conserved across eukaryotes, including all fungal species analyzed. Lysine 870 was conserved in 7 of the 10 fungal XMAP215 proteins, but not in higher order eukaryotes. The lack of

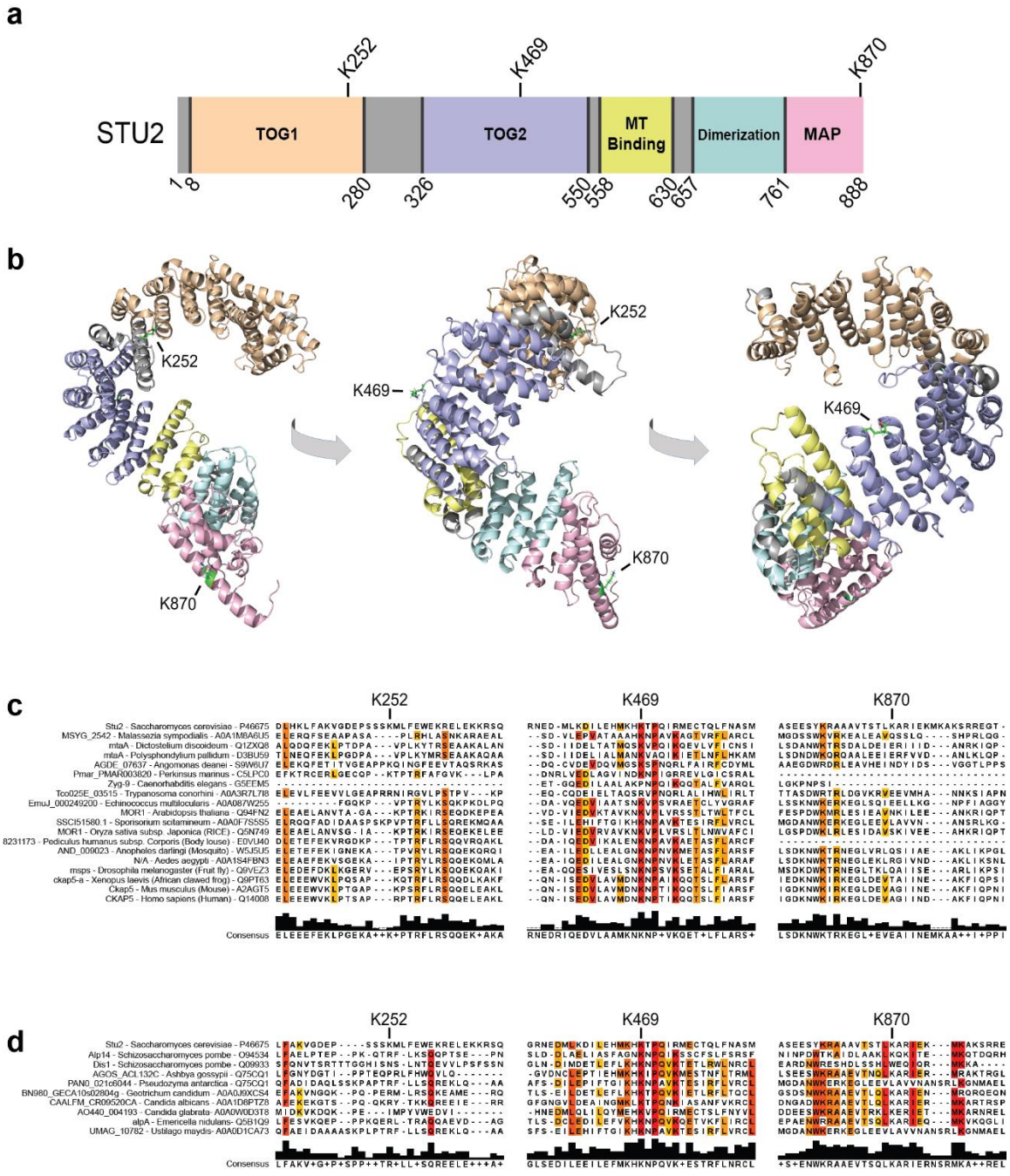

Figure 4 Acetyl-lysines are distributed throughout Stu2 and K469 is evolutionarily conserved. (a) Acetyl lysines are indicated relative to distinct Stu2 domains. (b) The location of acetylated residues are illustrated in a Stu2 structure predicted by I-TASSER. Clustal protein alignments are shown for members of the Stu2/XMAP215 family of microtubule polymerases for members across (c) eukaryota and (d) fungi.

conservation for Stu2's C-terminal acetylation site may reflect diversifying mechanisms through which XMAP215 family members interact with specialized microtubule-based structures.

Mutations in Stu2 acetylation sites are viable and do not disrupt the essential function of Stu2.

To determine if the acetylation impacts the function of Stu2, we mutated lysines 252, 469, and 870 to arginine residues to prevent acetylation while maintaining their positive charge. Substitutions with glutamine were designed to mimic acetylation. Combinations of double and triple mutations were also constructed. For the double mutant, lysines 252 and 469, which both reside in or near the two TOG domains, were mutated as a pair to either arginine or glutamine. This generated the 2KR and the 2KQ mutants. In the triple mutant, lysines 252, 469, and 870 were all mutated to either arginine (3KR) or glutamine (3KQ). As Stu2 is essential for yeast survival, we tested whether these alleles support life as the sole copy of Stu2 in a 5-FOA plasmid shuffle assay. As shown in Figure 5c-e, they did. All of the single, double and triple mutants support life at 23, 30, and 37 °C and displayed little or no observable differences in growth. As *STU2* is an essential gene, these data suggest that these acetylation site mutations do not disrupt the essential function of Stu2.

Acetylation mutants display a mitotic defect in large-budded cells.

The fusion of nuclei during the mating process, known as karyogamy, requires intact microtubule function (Kurihara, Beh, Latterich, Schekman, & Rose, 1994). To ascertain whether the acetylation of Stu2 impacts karyogamy, we employed a bilateral karyogamy mating assay in which both the *MAT*a and *MAT*α partners contained the same stu2 mutation. In comparison to *kar9*Δ, which is known to possess a moderate karyogamy defect (Kurihara et al., 1994; Miller & Rose, 1998) we observed little or no mating defect for K or Q substitutions at the lysines K252, K469 or K870 in Stu2 (Figure 6a). Next, we asked whether acetylation altered the cell-cell

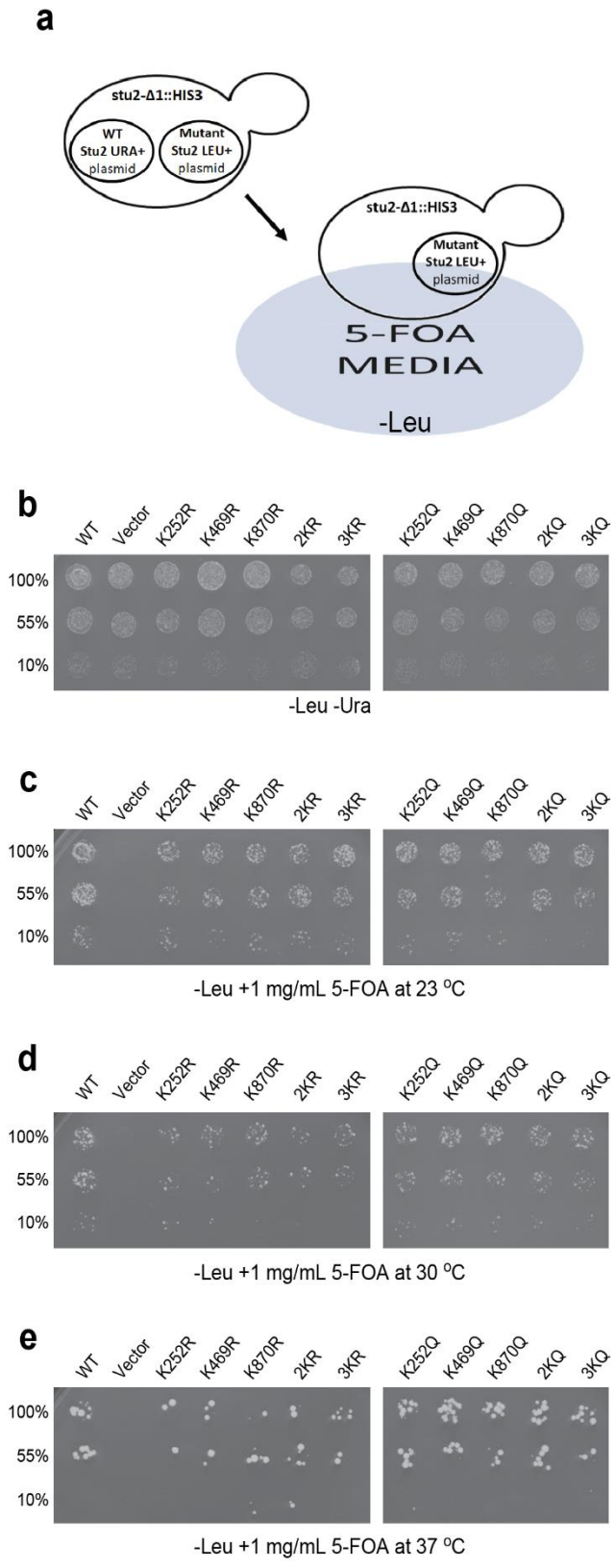

Figure 5 Plasmid shuffle complementation assays demonstrate Stu2 acetyl state mimetic mutants are functional. (a) A plasmid shuffle assay was used to detect phenotypes from acetyl-lysine mimicking (K to R) and inhibitory (K to Q) mutations. Phenotypes are masked using a URA3+ plasmid containing pSTU2-STU2 (pRM10693). Yeast strains also contained LEU2+ plasmids with WT-STU2 (yRM12337), LEU2+ vector (yRM12338), Stu2-K252R (yRM12340), Stu2-K469R (12341), Stu2-K870R (12342), Stu2-2KR (yRM12343), Stu2-3KR (yRM12344), Stu2-K252Q (yRM12345), Stu2-K469Q (yRM12346), Stu2-K870Q (yRM12347), Stu2-2KQ (yRM12348), and Stu2-3KQ (yRM12349). Cells were frogged to (b) plates lacking leucine and uracil and grown at 30 °C or leucine deficient 5-FOA plates and incubated at (c) 23 °C, (d) 30 °C, and (e) 37 °C.

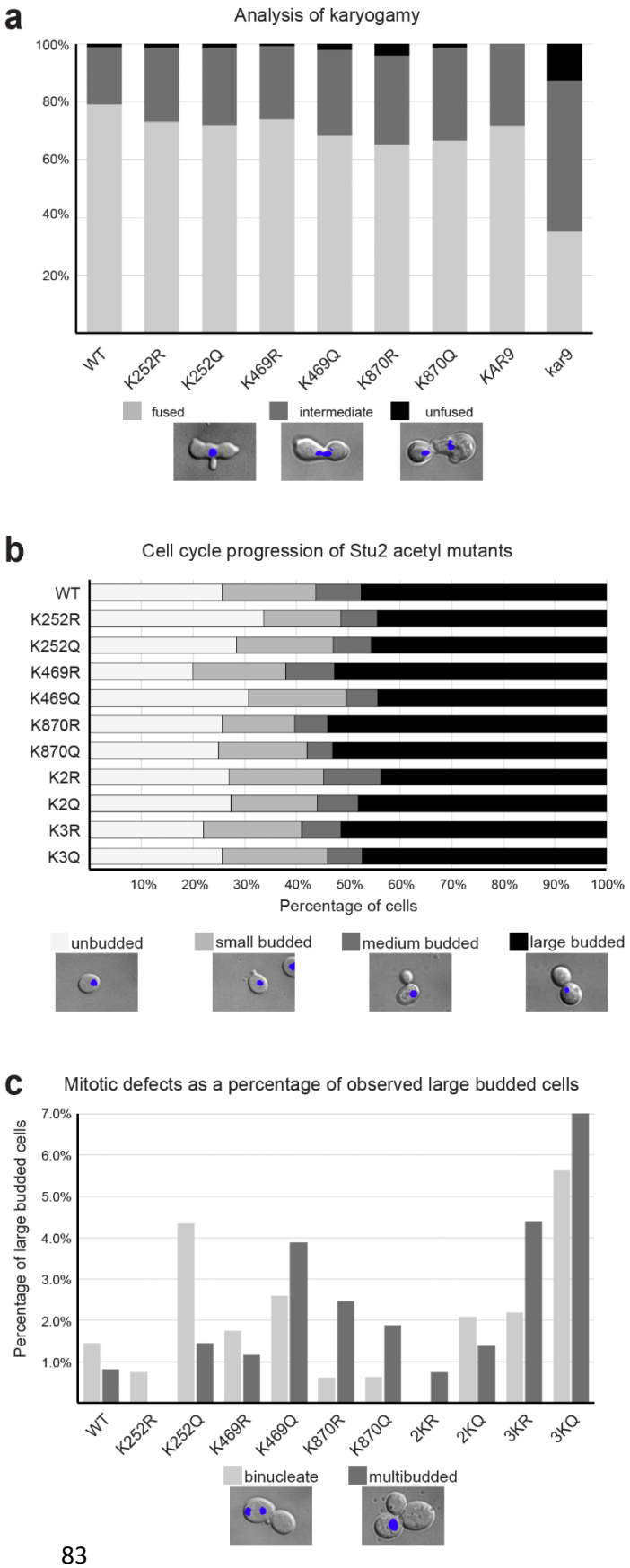

Figure 6 Microscopy assays show mitotic defects in large budded cells of yeast containing Stu2 acetyl mutations. (a) MATa or MATα mating type yeast with plasmids expressing WT-STU2 (yRM11379 and yRM11368), Stu2-K252R (yRM11930 and yRM11892), Stu2-K252Q (yRM11934 and yRM11898), Stu2-K469R (yRM11375 and yRM11362), Stu2-K469Q (yRM11377 and yRM11366), Stu2-K870R (yRM11938 and yRM11912), Stu2-K870Q (yRM11940 and yRM11922) in a stu2Δ background were tested in a karyogamy assay as described in (R. K. Miller & Rose, 1998). In addition, yeast containing a genomic copy of *KAR9* (yRM299 and yRM301) or a disrupted genomic copy of *kar9* (yRM393 and yRM396) were assayed to represent moderate karyogamy defects. (b) Logarithmically growing yeast with plasmids expressing WT-STU2 (yRM12358), K252R (yRM12360), K469R (12361), K870R (12362), 2KR (yRM12363), 3KR (yRM12364), K252Q (yRM12365), K469Q (yRM12366), K870Q (yRM12367), 2KQ (yRM12368), and 3KQ (yRM12369) in a stu2Δ background were evaluated for populations of unbudded, small budded, medium budded and large budded cells. (c) Large budded cells of yeast from panel b were DAPI stained and further examined for binucleate and multibudded phenotypes.

progression by analyzing the distribution of unbudded, small budded, medium budded, or large budded cells in an actively growing culture. As shown in Figure 6b, little or no observable defect was seen. However, in conducting this analysis, we observed that the large-budded cells displayed an increase in nuclei that were aberrantly positioned binucleate cells and apparently multi-budded cells (Figure 6c). Notably, the defects observed for 3KR and 3KQ mutants closely match the additive defects of their corresponding single mutations. This observation supports the hypothesis that Stu2 acetylation sites regulate different Stu2 functions. Strangely, the double TOG domain mutants, 2KR and 2KQ were mild compared to their corresponding single mutations.

During the process of dissecting *STU2*/*stu2*-Δ1::*HIS3* heterozygous delete strains for yeast mating assays, we determined that the Stu2-3KR acetylation preventative mutant possessed a lethal germination defect in the presence of a *STU2* genetic locus. Even with two researchers dissecting the mutant from separate transformations, it was never possible to generate a *STU2* (his-) *pSTU2-STU2-3KR (LEU2)* haploid cell line through dissection (Table 2).

A subset of Stu2 acetylation mutations confer benomyl resistance.

Stu2 promotes microtubule polymerization (Huffaker, Thomas, & Botstein, 1988) and (Podolski et al., 2014). If these mutations were affecting a non-essential function of Stu2, we next theorized that they might be more sensitive to drugs that destabilize microtubules. We first tested the effect of benomyl on the acetyl inhibitory mutants, (K to R). As shown in Figure 7, the K252R, the K469R, and their corresponding double mutant in the TOG domains, 2KR, grew only slightly better than wild type. In contrast, the K870R and the 3KR mutant grew better than wild type. As the triple 3KR mutant also displays benomyl resistance like the single K870R mutant, it suggests that acetylation at K870R is epistatic to acetylation in the TOG domains. Since these mutants were assayed for benomyl resistance in haploid *stu2*-Δ1::*HIS3* background, with the

Total dissections of sporulated yeast tetrads

Strain	Total number of tetrads dissected	Total possible spores	Overall spore viability	Expected HIS+ spores	stu2-Δ1::HIS3+ /LEU2+	Expected his- spores	STU2+ his- /LEU2+
Vector	156	312	91.3%	0	*inviable*	312	**60.1%**
*** WT-HA**	158	632	66.0%	316	39.9%	316	**37.0%**
WT-NT	28	112	53.6%	56	21.4%	56	**26.8%**
K252R	36	144	82.6%	72	69.4%	72	**73.6%**
K469R	48	192	71.9%	96	50.0%	96	**45.8%**
K870R	12	48	81.3%	24	66.7%	24	**58.3%**
2KR	47	188	68.1%	94	42.6%	94	**53.2%**
*** 3KR**	36	144	38.2%	72	37.5%	72	***0.0%***
K252Q	36	144	86.8%	72	79.2%	72	**83.3%**
K469Q	24	96	64.6%	48	47.9%	48	**47.9%**
K870Q	12	48	62.5%	24	29.2%	24	**29.2%**
2KQ	48	192	67.7%	96	41.7%	96	**41.7%**
3KQ	36	144	61.8%	72	51.4%	72	**47.2%**

*Relative to genomic WT/plasmid WT dissected spores, genomic WT/plasmid 3KR spores were completely inviable.

Table 2 STU2/stu2-Δ1::HIS3 heterozygous diploids (yRM11105) were transformed with WT-HA (pRM2119), vector alone (pRM2200), WT-NT (pRM6507), K252R (pRM11481), K469R (pRM11249), K870R (pRM12016), 2KR (pRM11966), 3KR (pRM11976), K252Q (pRM11482), K469Q (pRM11254), K870Q (pRM12015), 2KQ (pRM11969), and 3KQ (pRM11974). Each strain was then sporulated and tetrads were dissected. Genes of interest were auxotrophically marked with *HIS3* (stu2-Δ1::*HIS3*) or *LEU2* yeast centromeric plasmids (YCPs) containing WT-Stu2 or Stu2 AcK mutants for genotypic analysis. Expected HIS3+ spores reflect the 2:2 nature of sister chromatid distribution. Overall spore viability ignores sister chromatid distribution and represents the observed spores relative to the number possible. A stu2-Δ1::HIS3/LEU2+ column reflects each mutants capacity to complement WT-STU2 gene disruption. The STU2+/LEU2+ column indicates the percentage of expected spores carrying genomic STU2 and a LEU2+ Stu2 vector.

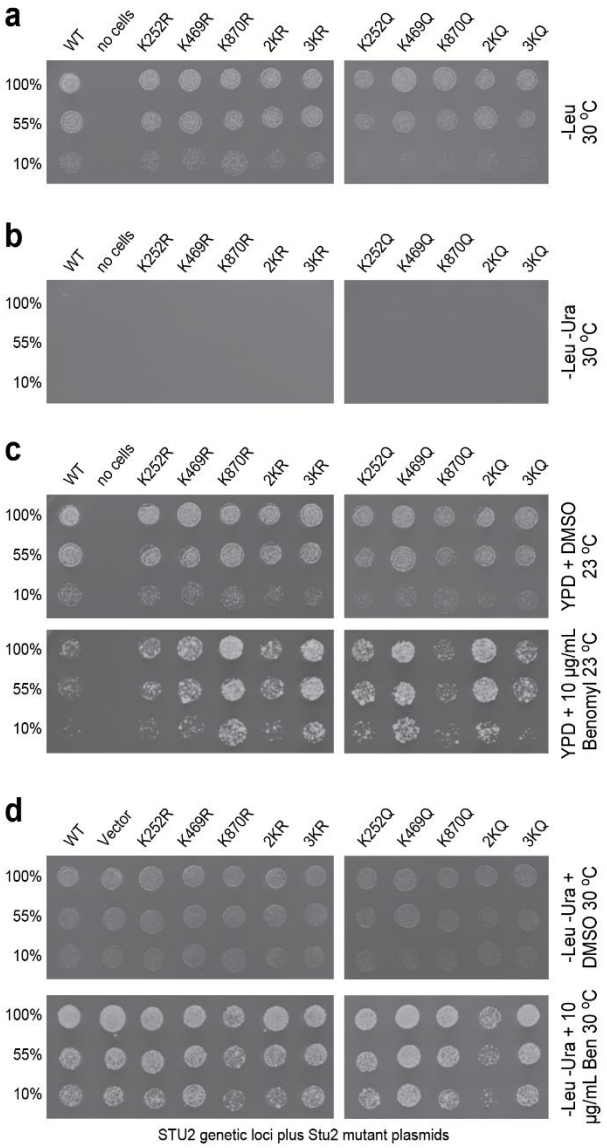

Figure 7 Benomyl resistance assays reveal acetylation site dependent resistance to MT depolymerization stress. Yeast containing LEU2+ plasmids with WT-STU2 (yRM12358), K252R (yRM12360), K469R (yRM12361), K870R (yRM12362), 2KR (yRM12363), 3KR (yRM12364), K252Q (yRM12365), K469Q (yRM12366), K870Q (yRM12367), 2KQ (yRM12368), and 3KQ (yRM12369) were transferred to (a) plates lacking leucine and (b) plates lacking leucine and uracil to confirm removal of pSTU2-STU2 URA+ plasmids. Cells were also transferred to (c) YPD containing DMSO or DMSO + 10 µg/mL Benomyl and grown at 23 °C. (d) Yeast containing LEU2+ plasmids with WT-STU2 (yRM12233), LEU2+ vector (yRM12234), Stu2-K252R (yRM12241), Stu2-K469R (yRM12239), Stu2-K870R (yRM12252), Stu2-2KR (yRM12247), Stu2-3KR (yRM12250), Stu2-K252Q (yRM12242), Stu2-K469Q (yRM12240), Stu2-K870Q (yRM12251), Stu2-2KQ (yRM12248), and Stu2-3KQ (yRM12249) in a heterozygous delete STU2/stu2-Δ1::HIS3 background at the genomic locus were transferred to –Leu –Ura plates containing DMSO or DMSO + 10 µg/mL Benomyl and grown at 30 °C.

mutations present on a YCP plasmid as the cells only source of Stu2, it suggests that the K870R mutation stabilizes microtubules.

To investigate the effect of the presence of a constitutive acetyl moiety, we tested whether acetyl-mimetic mutations would affect Stu2 sensitivity to benomyl. Both the K252Q and K469Q mutations conferred resistance to benomyl and the 2KQ double mutation also conferred benomyl resistance. In contrast to the K870R mutation, the K870Q mutation did not display resistance to benomyl (Figure 7c). To ascertain which phenotype is epistatic, we again compared the 2KQ double TOG mutation to the 3KQ mutant. In this analysis, the 3KQ mutant displayed a similar phenotype to the K870Q single mutant with respect to its level of benomyl resistance. Therefore, we conclude that the K870Q phenotype is epistatic to that of the double Q mutant, K2Q. Notably, both the K870R and the K870Q mutations are epistatic to the corresponding double mutant in the TOG domains. These phenotypes were also visible at 30 °C and to a very limited degree 37 °C (Figure 8). Together, these data suggest that acetylation in the TOG domain at K469 and MAP domain at K870 regulate the ability of Stu2 to stabilize microtubules. Importantly, acetylation at these two domains appear to function in opposition to each other. It remains to be determined whether the on and off cycling of Stu2 acetylation controls microtubule stability.

Because yeast spores with intact *STU2* genomic loci and Stu2-3KR mutant plasmids were inviable following sporulation and germination, we next sought to determine whether benomyl-resistance phenotypes are the result of either dominant or recessive mutations. We assayed for the benomyl sensitivity in strains containing a wild-type *STU2* background at the genomic locus in addition to the Stu2 mutant plasmids. As shown in Figure 7d, the 2KR mutant displayed growth comparable to wild type, whereas the 2KQ mutant grew more slowly, suggesting that the benomyl sensitivity of the 2KQ mutant is dominant. Similarly, the K870R mutant also displayed a dominant benomyl sensitivity, albeit it was a moderate to mild effect

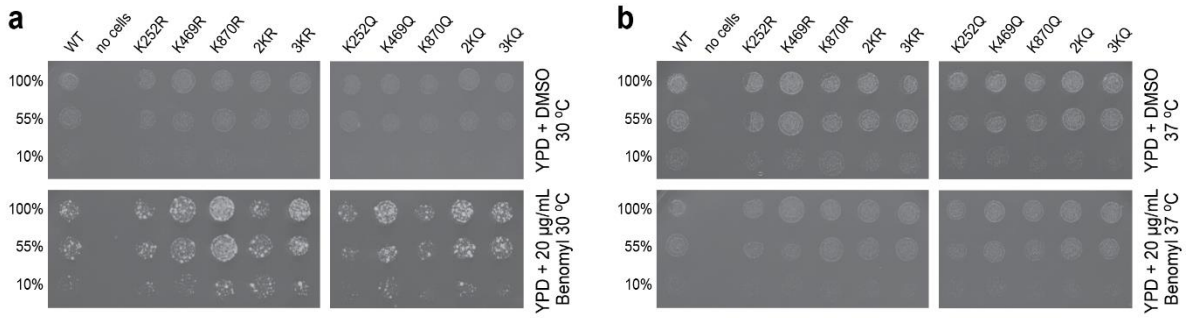

Figure 8 Stu2 acetylation states also confer resistance to MT depolymerization stress at 30 °C and slightly at 37 °C. Yeast containing LEU2+ plasmids with WT-STU2 (yRM12358), K252R (yRM12360), K469R (12361), K870R (12362), 2KR (yRM12363), 3KR (yRM12364), K252Q (yRM12365), K469Q (yRM12366), K870Q (yRM12367), 2KQ (yRM12368), and 3KQ (yRM12369) were transferred to YPD containing DMSO or DMSO + 10 µg/mL Benomyl and grown at 30 °C (a) or 37 °C (b).

compared to the 2KQ. The finding that these benomyl phenotypes are different between the wild type *STU2* and the *stu2-Δ1* delete backgrounds implies that symmetrical acetylation between the two halves of the Stu2p dimer is important.

Acetylation influences Stu2 steady-state levels.

To evaluate steady-state expression levels of these mutants, we examined whole cell extracts from cell cultures expressing each of the acetylation mutants by western blotting with anti-HA. As shown in Figure 9, the K to R (panel a, third row) and the K to Q (panel b, third row) mutants did not display a uniform effect. Notably, the K469R and the 3KR mutations consistently produced levels of Stu2p higher than the wild-type parent (Figure 9a, third panel). It was also notable that only the 2KR and the 2KQ mutants both routinely displayed obviously lower steady-state levels of Stu2. The 3KR and the 3KQ mutants both suppressed the lower expression levels of the corresponding 2K mutations, with the 3KR mutant elevating Stu2 levels to those comparable with K469R. Probing with anti-Pgk1 indicated that protein loading was constant across all samples. Combined, we conclude that acetylation status of the three lysine residues tested can regulate the steady state levels of Stu2p.

The non-covalent interaction of Stu2 with SUMO is regulated by acetylation.

We have previously shown that Stu2 binds noncovalently to SUMO (Greenlee et al., 2018). To determine whether acetylation of Stu2 regulates this interaction, we employed an *in vitro* binding assay using Stu2 expressed in yeast and a SUMO incapable of conjugation. For this, we applied yeast whole cell extracts expressing the varying forms of Stu2 to columns of 5X-SUMO-GST or GST alone. These SUMO columns contained five tandem repeats of SUMO, with the fifth SUMO fused in-frame with GST. This prevented its covalent attachment to substrates as the glycine needed for conjugation is already covalently attached to GST. All of the Stu2 mutants except the 2KR consistently reduced the non-covalent interaction with SUMO

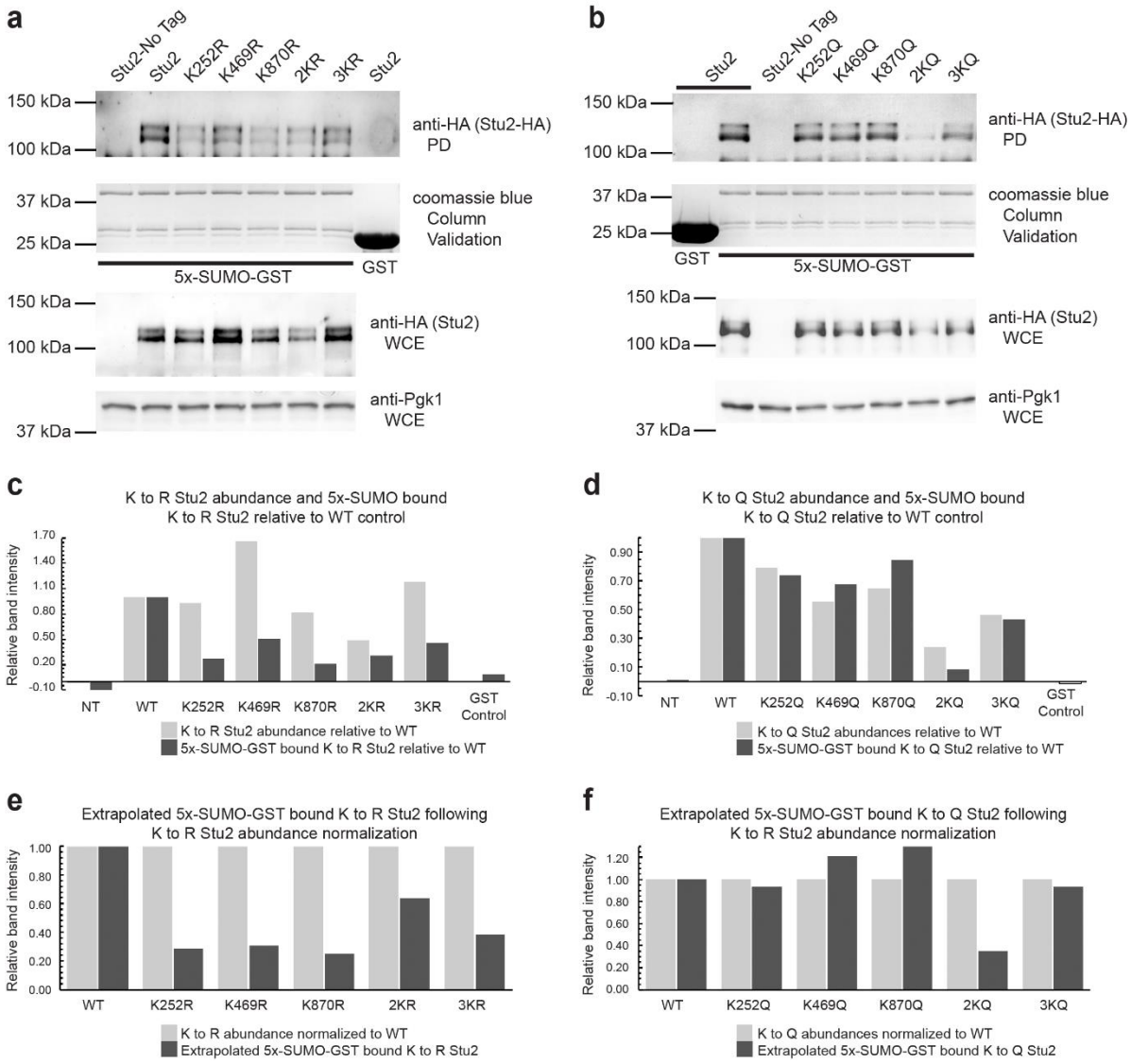

Figure 9 Acetylation regulates steady state levels of Stu2 and its non-covalent interactions with SUMO. Yeast extracts expressing the following mutations of Stu2 as the sole copy were assessed by immunoblot with mouse anti-HA (Santa Cruz Biotechnology, Santa Cruz, CA): (a) WT-Stu2-HA (yRM12358), Stu2-No Tag (yRM12359), Stu2-K252R-HA (yRM12419), Stu2-K469R-HA (yRM12361), Stu2-K870R-HA (yRM12362), Stu2-2KR-HA (yRM12363), and Stu2-3KR-HA (yRM12364) or (b) Yeast extracts containing Stu2-HA (yRM12358), Stu2-No Tag (yRM12359), Stu2-K252Q-HA (yRM12365), Stu2-K469Q-HA (yRM12366), Stu2-K870Q-HA (yRM12367), Stu2-2KQ-HA (yRM12368), and Stu2-3KQ-HA (yRM12369). (first image) To test the binding of each of the acetylation mutants to a non-covalent form of SUMO, each of the WCEs was incubated with glutathione agarose columns enriched with GST (pRM11485) and/or 5x-SUMO-GST (pRM11628) as described in Materials and Methods. (second image) To evaluate whether all affinity columns were uniform, 1/20th of the GST column elutions were stained with Coomassie blue to illustrate equal enrichment of 5x-SUMO-GST columns. (third image) Mutation of acetylated-lysine residues influence Stu2 interactions with SUMO. To assess Stu2 abundance,

Figure 9 continued:. . . Stu2 was visualized in strains grown to saturation, overnight. (fourth image) To evaluate protein concentration in the WCEs, blots were probed with mouse anti-Pgk1 (ThermoFisher Scientific, Waltham, MA) as a loading control. Densitometry analysis of immunoblotted Stu2 K to R (c) and K to Q (d) bands was used to quantify the steady state abundance for the protein of each mutant and 5x-SUMO-GST column enrichment relative to WT controls. Actual amounts of Stu2 K to R (e) and K to Q (f) proteins enriched by 5x-SUMO-GST columns were extrapolated based on each Stu2 mutant's steady state abundance relative to WT-Stu2 controls.

(Figure 9a, first image, and 9c). While the mutations did not eliminate the interaction, the reduction was nevertheless consistently moderate in three independent replicates of this experiment. Single mutations of acetyl-lysines to glutamine did not impact Stu2 protein expression or Stu2 non-covalent interactions with SUMO (Figure 9b, first image, and 9d). In contrast, mutation of both TOG domain sites to glutamine (in the 2KQ mutant) diminished Stu2 interactions with SUMO. Addition of the K870Q mutation partially rescued Stu2 expression and SUMO interactions.

Impaired Stu2 acetylation leads to chromosome instability

We next asked whether sister chromatid segregation is compromised when lysine residues are constitutively acetylated or acetylation is blocked. To test this, we employed the acetylation mimetics and acetylation preventative mutations in an artificial chromosome loss assay using a quantitative 5-FOA counter-selection illustrated in Figure 10a. This standard assay employed yeast containing a 125 kb *URA3* artificial chromosome in a *stu2*-Δ1::*HIS3* background as described in materials and methods. Using these strains, we measured the frequency that cells lost the artificial chromosome by the presence or absence of its *URA3* gene. Orotidine-5'-phosphate (OMP) decarboxylase encoded by the *URA3* gene converts 5-FOA into 5-Fluorouracil, a toxic compound. Only in the absence of the *URA3*-marked artificial chromosome can yeast grow on media containing 5-FOA.

Figure 10b shows that among the acetylation mutants tested, the single acetyl-inhibitory mutants K252R and K469R showed the largest increase in chromosome loss. In comparison, the acetyl-mimetic mutation K252Q showed a mild increase in chromosome loss but K469Q showed no significant increase in chromosome loss when compared to the plasmid-based WT-Stu2 control. Interestingly, we observed antagonistic effects of the acetylation-state mutants that are located in the MAP interacting domain. The acetylated-state mimicking K870Q mutant lead to

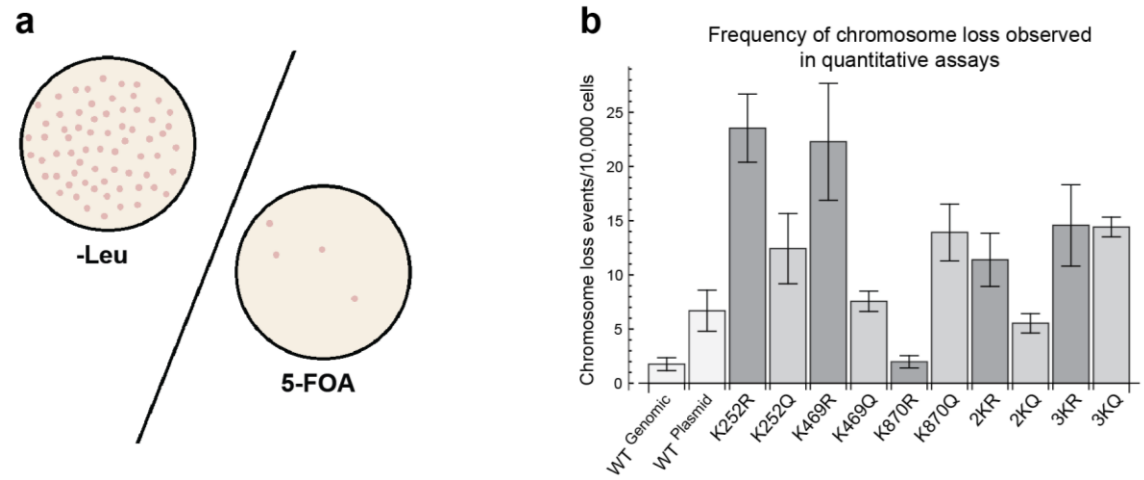

Figure 10 Manipulation of Stu2 acetylation states impacts chromosome segregation. Yeast strains containing a 125 kb artificial chromosome containing the *URA3* gene and plasmids expressing WT-Stu2 (yRM12253), K252R (yRM12261), K252Q (yRM12262), K469R (yRM12301), K469Q (yRM12260), K870R (yRM12271), K870Q (yRM12270), 2KR (yRM12266), 2KQ (yRM12267), 3KR (yRM12269), and 3KQ (yRM12268) in a stu2-Δ1::*HIS3* background, along with a WT-genomic control with an intact *STU2* at its genetic locus and an empty *LEU2* vector (yRM12300) were plated to synthetic deficient media lacking leucine and 5-FOA plates. (a) To quantify frequencies for chromosome loss in Stu2 mutants, concentrated cells were transferred to plates containing 5-FOA or serially diluted and transferred to -Leu synthetically deficient plates. Because 5-FOA is toxic to yeast possessing the *URA3* gene we observe only colonies which have lost the 125 kb artificial chromosome. Colonies growing on leucine deficient plates represent the serially diluted concentration of cells used in the experiment. (b) Quantitative chromosome loss rates reflect the total number of colonies growing on 5-FOA media relative to colonies growing on -Leu synthetic deficient media following serial dilutions. The quantitative chromosomal loss experiments were repeated in triplicate to establish standard deviations for displayed error bars.

mild chromosome loss similar to the K252Q mutant. In contrast, mutating lysine 870 to arginine had an inverse effect and improved chromosome management to the extent that negative impacts associated with Stu2 plasmid expression were masked. Double TOG domain mutants 2KR and 2KQ displayed mild phenotypes relative to their single corresponding TOG domain mutants. Lastly, when all three acetylation sites were mutated to arginine or glutamine, moderate chromosome loss rates were observed. The moderate impacts of double TOG domains and conserved severity of triple mutants indicates Stu2 acetylation may be finely tuned to carry out its multiple roles for MT function. In addition, many of these trends were observed when we performed related qualitative red sector counting assays to determine the impact of acetyl mimetic mutations on chromosome segregation (Figure 11).

Stu2 acetylation regulates interactions with γ-tubulin

In addition to its localization at kinetochores and at MT plus ends, Stu2 also functions at the SPB (Wang & Huffaker, 1997). As Stu2 interacts with the γ-TuSC, of which γ-tubulin is an integral part, and facilitates microtubule nucleation (Gunzelmann et al., 2018), we next asked whether the acetylation state of Stu2 impacts its interactions with γ-tubulin. To answer this, we immunoprecipitated Stu2-HA from the 3KR and 3KQ triple mutants and probed for γ-tubulin in the precipitate. As shown in Figure 12a, γ-tubulin co-precipitated with Stu2 possessing the triple acetylation state mimetic Stu2-3KQ, but not the 3KR mutant. This suggests that acetylation regulates the interaction of Stu2 with gamma tubulin.

Acetylation of Stu2 K469 may differentiate between β- and γ-tubulin interactions.

To gain insight into the molecular basis for the enrichment of γ-tubulin by the Stu2-3KQ mutant, we aligned β- and γ-tubulins from seven eukaryotes across evolution (Figure 13a & b). It has long been recognized that these tubulins overall are highly conserved from fungi to humans. The Rice laboratory previously showed that residues E158-D161 of β-tubulin interacts

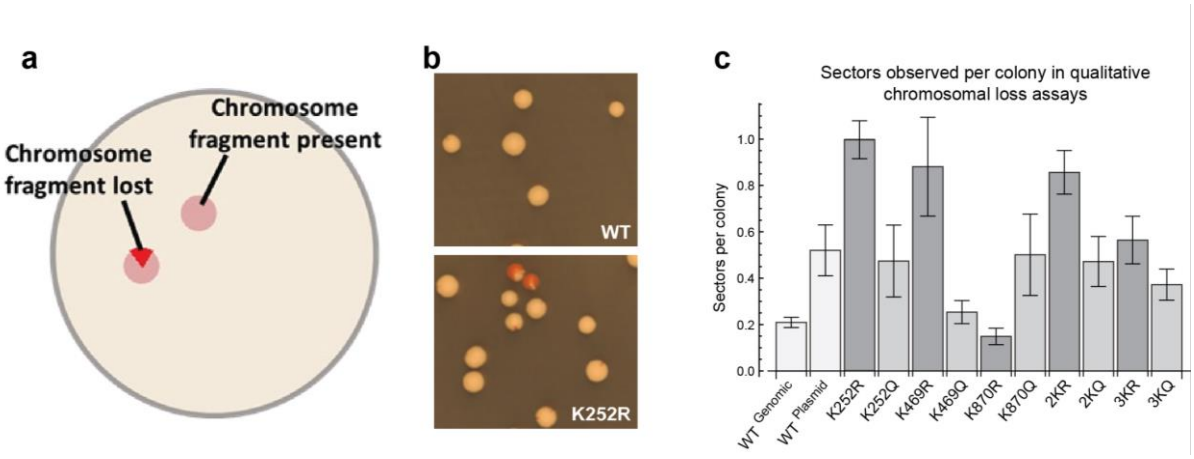

Figure 11 Qualitative chromosome loss assays indicated Stu2 acetylation sites impacted chromosome distribution. (a) Chromosome loss was qualitatively assessed using a red phenotype suppressing 125-kb *SUP11* artificial chromosome (pRM11972/pJS2). (b) Colonies with *STU2* plasmids (pRM2119) form red sectors less frequently than cells containing K252R plasmids (pRM11481). Yeast in this assay contained plasmids with STU2 (yRM12253), K252R (yRM12261), K469R (yRM12301), K870R (yaRM12271), 2KR (yRM12266), 3KR (yRM12269), K252Q (yRM12262), K469Q (yRM12260), K870Q (yRM12270), 2KQ (yRM12267), and 3KQ (yRM12268) in a stu2D::HIS3 background, except for the WT-genomic control which had an intact STU2 at its genetic locus and an empty vector instead of the STU2 on a plasmid (yRM12300). (c) The total number of sectors counted was divided by the total number of colonies present to determine chromosomal loss rates of mutants relative to WT controls.

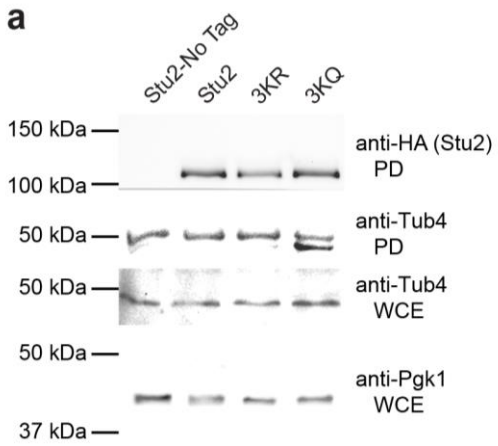

Figure 12 The acetyl-mimetic Stu2-3KQ mutant enriches γ-tubulin better than WT-Stu2 and the Stu2-3KR acetyl preventative mimetic. (a) Yeast expressing Stu2-HA (yRM12358), untagged Stu2 (yRM12359), Stu2-3KR-HA (yRM12364), and Stu2-3KQ-HA (yRM12369) were immunoprecipitated and western blotted for HA tagged Stu2 and γ-tubulin (Tub4). To determine uniform loading of γ-tubulin protein and verify Bradford assays WCEs were western blotted for γ-tubulin and Pgk1.

with lysine 469 of Stu2 (Pelin Ayaz et al., 2014), denoted here as the EFPD loop. Based on this work, we identified the analogous loop within γ-tubulin as residues R166-K169, denoted here as the RYPK loop. We hypothesize that this loop also docks with Stu2. To evaluate conservation of K469 TOG2 interactions with β- and γ-tubulins, we aligned crystal structures of γ-tubulin (pdb:3CB2) with β-tubulin (pdb:4U3J) using Pymol (Figure 13c) (Ayaz et al., 2014; Rice, Montabana, & Agard, 2008). Notably, the EFPD (beta-tubulin) and RYPK (γ-tubulin) loops display a significant difference in their charge. In the case of β-tubulins, the EFPD loop is acidic with a net charge -2 and in the case of γ-tubulins the RYPK loop is basic with net charge +2. We speculate that if γ-tubulin interacts with Stu2 as it does with β-tubulin, then the Stu2 interaction with γ-tubulin will be governed by the acetylation state of lysine 469.

While evaluating K469-TOG2 domain interactions with β- and γ-tubulins, we observed that the K469 side chain was not solved in the crystal structure. Using pymol, we reconstructed the K469 side chain and while screening optimal rotamer confirmations determined it likely forms salt bridges with β-tubulin E158 and D161 residues (Figure 14 f & g). We next paired the TOG2 domain with reconstructed K469 side chains with electrostatic surface maps of β- and γ-tubulins. Figure 13 panels d & e illustrate significant differences in the surface charges of the two tubulins. Similarly to K469 found in TOG2 of Stu2, the side chain of K163 found in γ-tubulin was not solved. Subsequent pymol reconstruction of the γ-tubulin K163 side chain provides a more accurate representation of the region's positively charged surface (Figure 13f). In addition, it became evident that γ-tubulin K163 may form additional contacts with T514 found on an adjacent TOG2 α-helix that is absent in TOG2-αβ-tubulin heterodimer complexes. These reconstructions provide an explanation for how K469Q Stu2 mutants bind γ-tubulin better than WT controls due to reduced electrostatic repulsion with the arginine and lysine residues found in the γ-tubulin RYPK loops. If our hypothesis is true, this model of tubulin selection through Stu2-

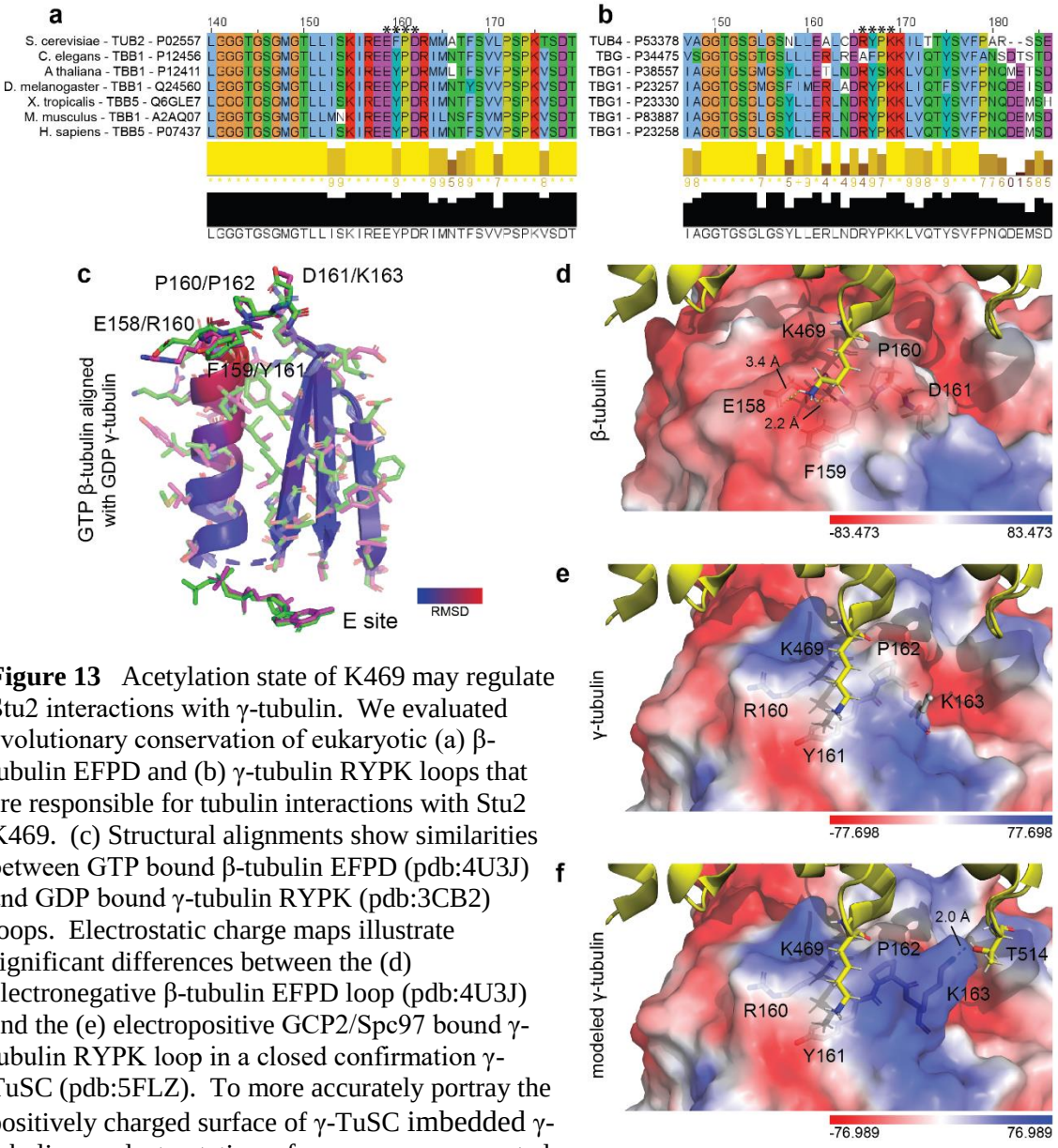

Figure 13 Acetylation state of K469 may regulate Stu2 interactions with γ-tubulin. We evaluated evolutionary conservation of eukaryotic (a) β-tubulin EFPD and (b) γ-tubulin RYPK loops that are responsible for tubulin interactions with Stu2 K469. (c) Structural alignments show similarities between GTP bound β-tubulin EFPD (pdb:4U3J) and GDP bound γ-tubulin RYPK (pdb:3CB2) loops. Electrostatic charge maps illustrate significant differences between the (d) electronegative β-tubulin EFPD loop (pdb:4U3J) and the (e) electropositive GCP2/Spc97 bound γ-tubulin RYPK loop in a closed confirmation γ-TuSC (pdb:5FLZ). To more accurately portray the positively charged surface of γ-TuSC imbedded γ-tubulin, an electrostatic surface map was generated following (f) γ-tubulin K163 side chain reconstruction.

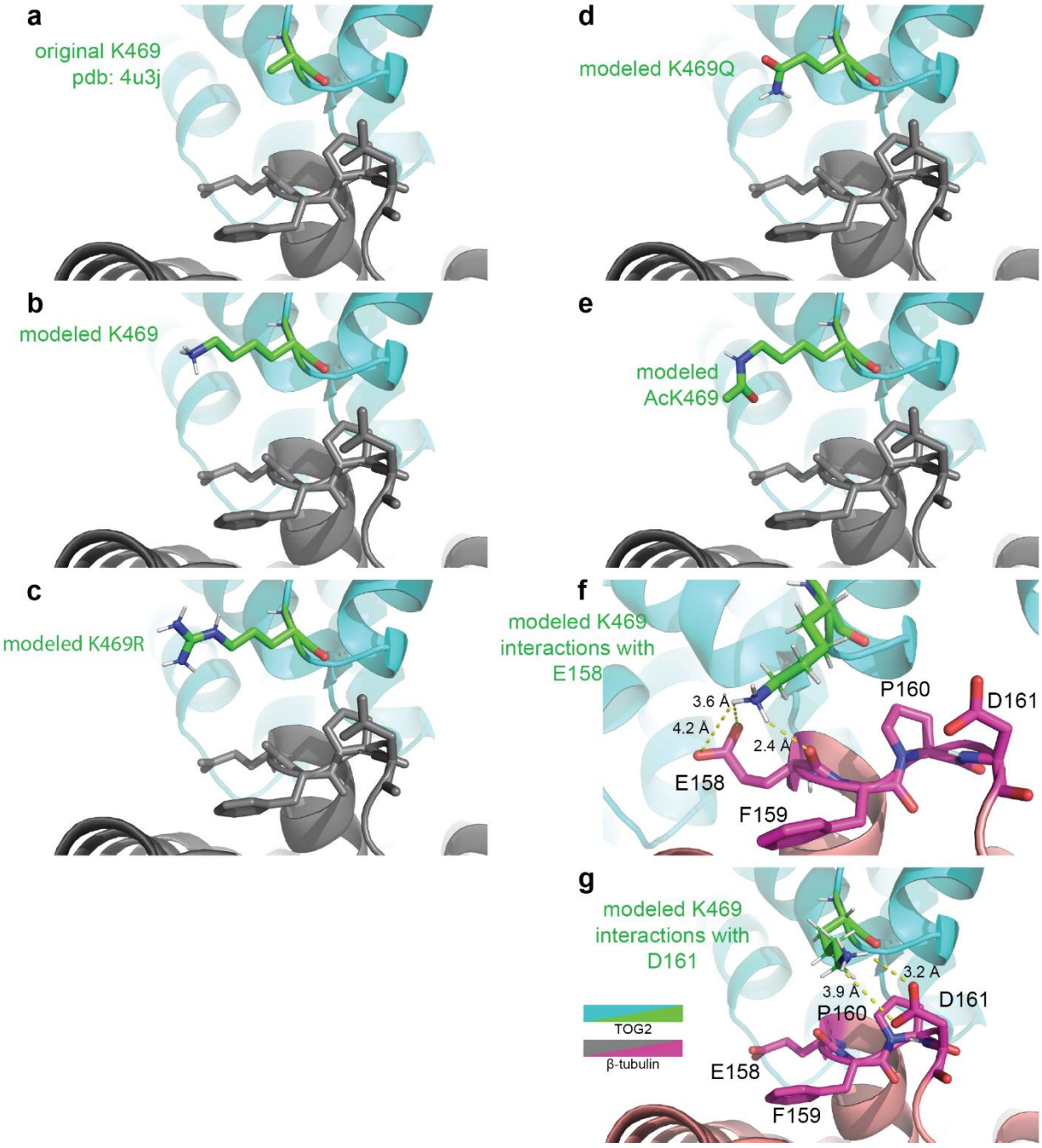

Figure 14 The side chain of K469 was not solved in crystal structures between TOG2 and tubulin heterodimer in pdb: 4U3J (a). Here we modeled K469 using pymol to investigate how K469 may interact with β-tubulin. The TOG2 K469 side chain is reconstructed in panel b. We modeled side chains for the (c) K to R acetylation prevention mutation, the (d) K to Q acetylation mimetic mutation, and (e) acetylated K469. K469 rotamer confirmations were evaluated to mimic the residue interactions with (f) E158 and (g) D161.

TOG2 acetylation should have wide implications for TOG domain interactions with tubulins across the evolutionary spectrum.

Acetylation of K252 may regulate Stu2's intra TOG domain linker

To determine how the K252Q mutation might result in changes within the structure of Stu2, we submitted the Stu2-K252Q sequence to I-TASSER for modeling. Compared to WT-Stu2 (Figure 15c), the K252Q single mutation resulted in a reduction in stability of two nearby alpha-helices (Figure 15d marked with asterisks). As shown in Figure 11d, we noted that the K252Q single mutation resulted in a predicted alteration in two alpha helices. The Q252 is predicted to no longer be salt bridged to D293. If this model is correct, acetylation at K252 should also no longer salt bridge to D293. The resulting loss in structure would result in additional flexibility of the molecule to allow it to interact more freely with tubulins by removing the stress imposed by overlapping tubulin regions displayed in Figure 15b.

DISCUSSION

In this work, we identified multiple acetylation sites on the microtubule polymerase Stu2. Acetylated residues coincide with domains responsible for Stu2 interactions with tubulin and other MAPs. Because of Stu2 functions at the kinetochore, we tested the impact of acetylation sites on microtubule polymerization and chromosome segregation. And as a result of recent findings implicating Stu2 in MT nucleation at γ-TuSCs (Gunzelmann et al., 2018) and XMAP215 from *X. laevis* in MT nucleation at γ-TuRCs (Thawani et al., 2018), we investigated the role of acetylation states on γ-tubulin interactions.

We speculate that multiple aspects of Stu2 functions are regulated through acetylation. Chromosome loss assays demonstrated lysine 252 acetylation is important for faithful segregation of chromosomes. We also observed significant increases in cell binucleation when cells

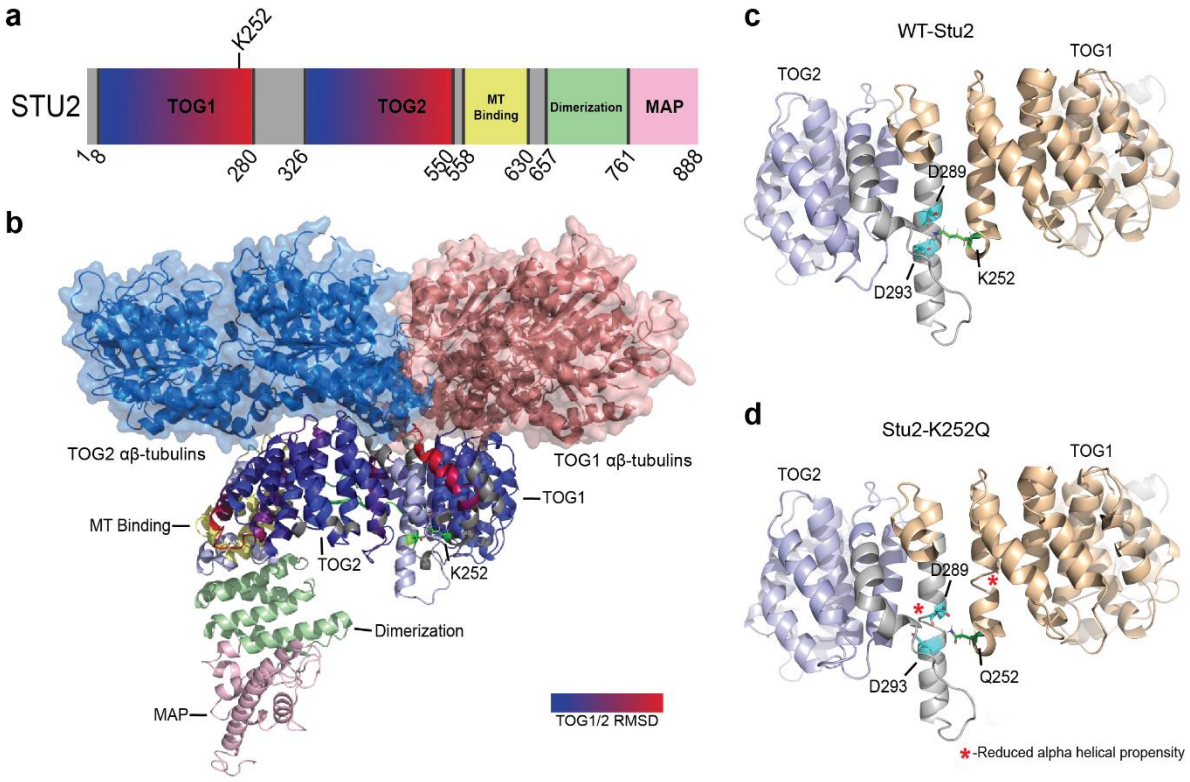

Figure 15 Stu2 lysine 252 acetylation may regulate intra-helical salt bridges between TOG1 and TOG2 domains. (a) Lysine 252 lies at the c-terminal end of TOG1. (b) TOG1/αβ-tubulin heterodimer complexes (pdb:4FFB) and TOG2/αβ-tubulin heterodimer complexes (pdb:4U3J) alignments to an I-TASSER modeled Stu2 structure reveals αβ-tubulin heterodimer overlap. I-TASSER modeling of WT-Stu2 (c) and Stu2-K252Q (d) demonstrated K252 drives salt bridge formation with D289 and D293 to confer stability to the intra-TOG domain linker region by stabilizing α-helices.

possessed only acetylated lysine 252. Meaning the cell simultaneously needs both acetylated and non-acetylated K252.

Several of our assays demonstrated antagonistic roles for K469 and K870 acetylation. A mixture of acetylation states at lysine 469 proved just as important if not more so than the TOG1 site. In addition to its role in chromosome segregation, acetylation of lysine 469 also granted cells significant resistance to the microtubule depolymerization drug benomyl as a sole copy. This trend of microtubule resistance is even faintly detectable in the presence of a wild type *STU2* genetic locus. Cells possessing only Stu2 acetylated at K469 displayed more multi-budded cells than most other strains despite its propensity for polymerization. Additionally, surface charge maps of β- and γ-tubulins indicate a possible role in Stu2-K469 acetylation in tubulin recognition which is supported by γ-tubulin enrichment by our fully acetylated representative Stu2 strain.

Acetylation of lysine 870 appeared to cause more complex phenotypes. This is likely due to the proximity to the MAP binding domain. Acetylation of K870 appeared to increases chromosome instability in the chromosome loss assay, and also compromised basal benomyl resistances conferred to virtually every other acetyl mutant in the benomyl resistance screen. However, mitotic defect screens in microscopy experiments implicated that acetylated and non-acetylated K870 is important for mitosis. Interestingly, in our benomyl microtubule depolymerization assays, the acetylation state of K870 "overwrites" phenotypic states conferred by TOG domain acetylation sites. This may indicate that while TOG1 and TOG2 directly regulate Stu2's role in microtubule polymerization, other functions of Stu2 are directly regulated through the MAP binding domain acetylation state.

Acetylation sites in different domains regulate Stu2 through different mechanisms

K469 and K870 each lie in well characterized domains. K469 lies in a well characterized binding interface where Stu2 forms salt bridges with tubulin heterodimers. The corresponding

lysine in TOG1, lysine 151, forms interactions with β-tubulin, similarly to K469 in TOG2 (Ayaz et al., 2014; Ayaz et al., 2012). Like K469, lysine 151 is evolutionarily conserved. The ε-ammonium group of K151 forms a salt bridge with the carbonyl oxygen of E158 in β-tubulin and given the conserved position of these amino acids, K469 likely forms salt bridges with β-tubulin in the same way (Figure 16) (Ayaz et al., 2012, 2014). Therefore, we speculate that acetylation may also regulate K151 found in TOG1 in addition to K469 found in TOG2. This potentiality is consistent with our findings (Figure 2) that all of Stu2's acetylation sites have not yet been identified. Additional work in this area is ongoing.

Stu2 mutations that impaired TOG interactions with αβ-tubulin heterodimers have thus far only been reported to cause benomyl sensitivity and lead to significant reductions of mitotic spindle lengths (Al-Bassam et al., 2007; Ayaz et al., 2012). Our data showed that when lysine 469 was mutated to glutamine, cells resisted benomyl induced MT stress, indicating that they are likely to display a more robust capacity for microtubule polymerization. The K469 analog present in TOG1, K151 was also shown to reduce interactions between Stu2 and tubulin (Al-Bassam et al., 2007). While we never detected K151 acetylation, potential AcK151 peptides generated through trypsin digestion of Stu2 would either be too small or too large to produce reliable spectra.

Previous work demonstrated the importance of Stu2 MAP binding domains for interactions with Ndc80 and subsequent localization to the kinetochore (Humphrey et al., 2018; Miller et al., 2019). Since Bik1, Bim1, and Spc72 also rely on the MAP binding domain for Stu2 interactions, K870 acetylation may serve as a molecular switch to facilitate molecular specificity among them. We speculate that benomyl resistance observed in our K870R mutants (Figure 7) indicate that non-acetylated Stu2 more readily interacts with microtubule associated proteins that stabilize the microtubule plus end such as Bik1 or Bim1. Spc72 on the other hand, another Stu2 binding partner, localizes to the minus end of MTs as a component of the spindle pole body and

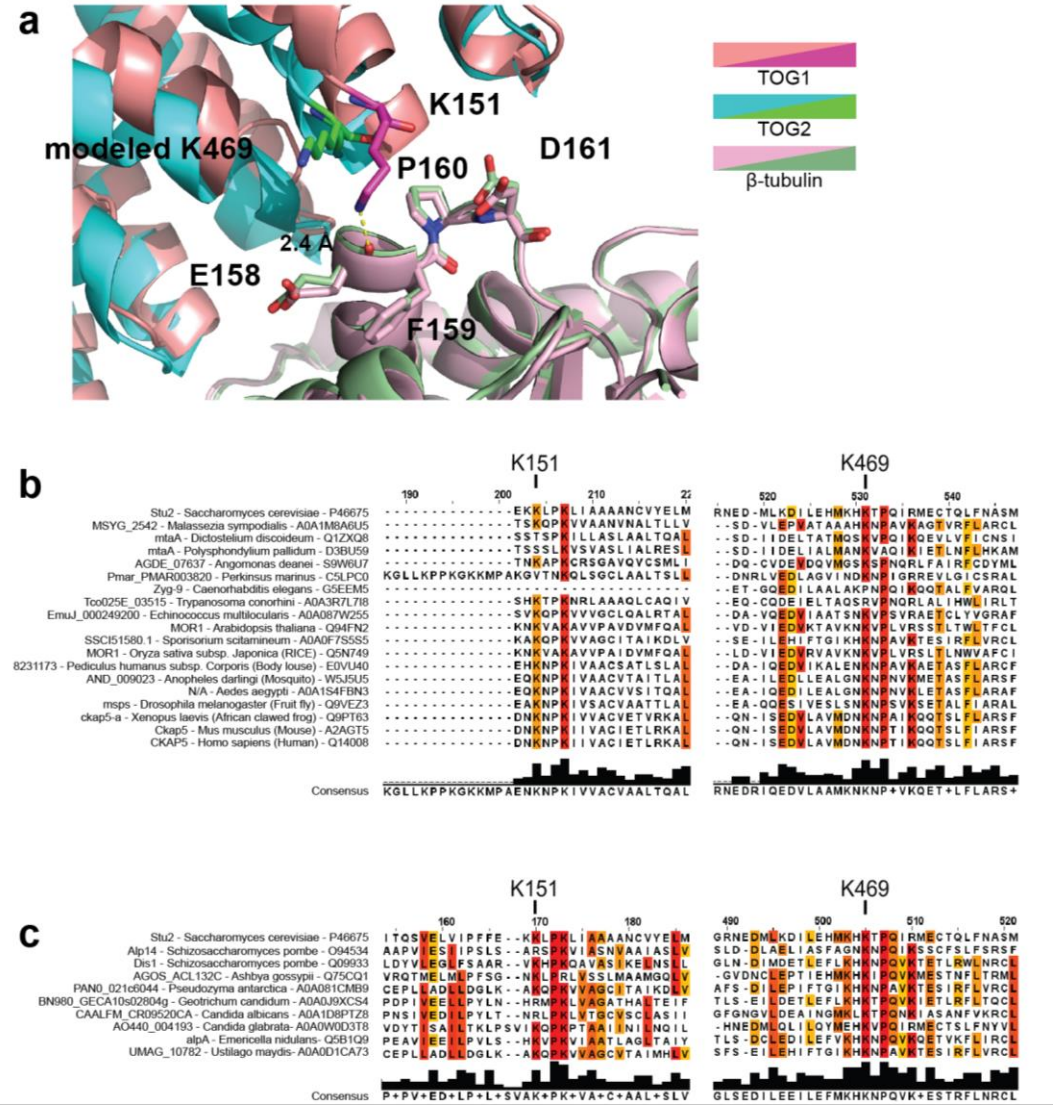

Figure 16 Analogous K151 and K469 residues interact with the same random coil residues of β-tubulin (a) TOG2 K469 and the analogous K151 present on TOG1 are super-imposed to show similar propensities for β-tubulin salt bridge formation. Clustal protein alignments show that K151 is conserved amongst eukaryotic organisms like the acetylated K469 residue. Two separate alignments show members across the eukarya domain (b) and fungi alone (c).

might not facilitate increases in microtubule polymerization. Therefore, it is possible that K870 acetylation states specify the kinetochore, cytoplasmic, and spindle pole body pools of Stu2.

Relative to K469 and K870, the function of K252 acetylation is somewhat elusive. Existing structures indicate that while K252 is solvent exposed, it is far removed from the tubulin binding surface. Because K252 is positioned between TOG1 and TOG2 domains, it is possible it plays a role in the polarized unfurling MT polymerase cycle model proposed by the Al-Bassam lab (Nithianantham et al., 2018). As an addition to this model, K252 may eliminate salt-bridges to facilitate elongation of the intra-TOG domain linker region in microtubule polymerases.

The observation that non-acetylatable Stu2 lost interactions with SUMO implies that Stu2 acetylation promotes interactions with SUMO. While one might speculate that this could have resulted from the activation of latent SIMs containing lysine residues, this seems unlikely as none of the acetylated lysines reside within consensus (I/L/V) X (I/L/V) (I/L/V) SIM motifs (Figure 4) (Song et al., 2004).

Furthermore, while phosphorylation has been shown to regulate SIMs (Anamika & Spyracopoulos, 2016; Chang et al., 2011), acetylation has never been implicated in promoting SIM activity. Whereas the findings reported here are the first to indicate that this non-covalent binding to sumo is likely to be regulated by acetylation, it remains to be determined whether this occurs directly through modulating the SIM motif, either allosterically or via conformational induced changes that exposed SIM binding motifs. Acetylation was previously shown to repress SIM interactions in humans. SUMO1 and SUMO2 acetylation reduces SUMO recognition of SIMs by reducing SUMO affinity for acidic residues that characteristically flank SIMs (Ullmann et al., 2012).

In this work, we describe novel mechanisms for Stu2 regulation through acetylation pathways. As the expression status of Tumor Over expressed Gene protein is important in cancer prognosis (Yu et al., 2016), future work is necessary to determine how the acetylation state of other XMAP215 family members correlate with disease states. Acetylation state mutants of XMAP215 family members will prove powerful tools in ongoing efforts to understand how acetylation of the XMAP215 family protein Stu2 regulates microtubule structure and function. This work reveals that Stu2's various acetylation states cause profound changes in the microtubule associated protein's functionality as evidenced by benomyl sensitivity and chromosome loss assays. These results strongly support the idea that acetylation states of multiple lysine residues coordinate Stu2 activities between the spindle pole body and the kinetochore.

MATERIALS AND METHODS:

Detection of AcK-Stu2 bands

The lysine deacetylase inhibitor Trichostatin A (TSA) was used to preserve Stu2 acetylation for detection with subsequent western blot experiments. Yeast cells were grown as previously described to OD_{600} values of 0.3 and treated with a final concentration of 200 ng/mL TSA in DMSO or DMSO solvent controls for 2 hours at 30 °C. Following TSA treatments, cells were harvested, cryo-milled, and clarified as previously described (Greenlee et al., 2018). Protein concentration was determined by Bradford assay using a BSA standard curve. Extracts containing 91 mgs of whole cell protein with Stu2-HA (yRM12358), untagged Stu2 (yRM12359), Stu2-3KR-HA (yRM12364), or Stu2-3KQ-HA (yRM12369), as described in Table 3, were incubated with anti-HA mag beads, washed, and eluted with 100 uL of 2.5x laemmli sample buffer and boiled for 5 min. 20% of each sample was resolved by SDS-PAGE gels and

Table 3 Yeast strains used in this study

Yeast Strains	Genotype/comments	Source
yRM10637	*MATa his3Δ leu2Δ met15Δ ura3Δ* [pRM2119 = pSTU2-STU2-3xHA *CEN6 ARSH4 LEU2* Amp^R]	(Greenlee et al.)
yRM10641	*MATa his3Δ leu2Δ met15Δ ura3Δ* [pRM2200 = *LEU2 CEN6 ARSH4* Amp^R]	(Greenlee et al.)
yRM11105/ CUY1046	*MATa/MATα STU2/stu2-Δ1::HIS3 ade2-101/ADE2 his3-Δ200/his3-Δ200 leu2-3,112/leu2-3,112 ura3-52/ura3-52*	(P. J. Wang & Huffaker, 1997)
yRM11407	*MATα STU2 ade2-101 his3-Δ200 leu2-3,112 ura3-52* [pRM2119 = pSTU2-STU2-3xHA *CEN6 ARSH4 LEU2* Amp^R]	This study
yRM11408	*MATa stu2-Δ1::HIS3 ade2-101 his3-Δ200 leu2-3,112 ura3-52* [pRM2119 = pSTU2-STU2-3xHA *CEN6 ARSH4 LEU2* Amp^R]	This study
yRM11971/ YCTF58	*MATα his3-Δ200 leu2-Δ1 lys2-801 ura3-52 ade2-101 CFIII (CEN3.L) URA3 SUP11 ctf19-58*	(Kroll, Hyland, Hieter, & Li, 1996)
yRM11988	*MATa/MATα STU2/stu2-Δ1::HIS3 ade2-101/ade2-101 his3-Δ200/his3-Δ200 leu2-3,112/leu2-3,112 ura3-52/ura3-52*	This study
Chromosome loss strains Chromosome loss strains possess a 125-kb pJS2/pRM11972 induced chromosome fragment: CFIII - *SUP11* URA3+ CEN6 D8B Y' amp^r (Figure S3).		
yRM12012	*MATa/MATα STU2/stu2-Δ1::HIS3 ade2-101/ade2-101 his3-Δ200/his3-Δ200 leu2-3,112/leu2-3,112 ura3-52/ura3-52* ChrIII/ChrIII	This study
yRM12233	*MATa/MATα STU2/stu2-Δ1::HIS3 ade2-101/ade2-101 his3-Δ200/his3-Δ200 leu2-3,112/leu2-3,112 ura3-52/ura3-52* ChrIII/ChrIII [pRM2119 = pSTU2-STU2-3xHA *CEN6 ARSH4 LEU2* Amp^R]	This study
yRM12234	*MATa/MATα STU2/stu2-Δ1::HIS3 ade2-101/ade2-101 his3-Δ200/his3-Δ200 leu2-3,112/leu2-3,112 ura3-52/ura3-52* ChrIII/ChrIII [pRM2200 = *LEU2 CEN6 ARSH4* Amp^R]	This study
yRM12239	*MATa/MATα STU2/stu2-Δ1::HIS3 ade2-101/ade2-101 his3-Δ200/his3-Δ200 leu2-3,112/leu2-3,112 ura3-52/ura3-52* ChrIII/ChrIII [pRM11249 = *pSTU2-STU2-K469R-3xHA LEU2+ CEN6 ARSH4 LEU2* Amp^R]	This study
yRM12240	*MATa/MATα STU2/stu2-Δ1::HIS3 ade2-101/ade2-101 his3-Δ200/his3-Δ200 leu2-3,112/leu2-3,112 ura3-52/ura3-52* ChrIII/ChrIII [pRM11254 = *pSTU2-STU2-K469Q-3xHA LEU2+ CEN6 ARSH4 LEU2* Amp^R]	This study
yRM12241	*MATa/MATα STU2/stu2-Δ1::HIS3 ade2-101/ade2-101 his3-Δ200/his3-Δ200 leu2-3,112/leu2-3,112 ura3-52/ura3-52* ChrIII/ChrIII [pRM11481 = *pSTU2-STU2-K252R-3xHA LEU2+ CEN6 ARSH4 LEU2* Amp^R]	This study
yRM12242	*MATa/MATα STU2/stu2-Δ1::HIS3 ade2-101/ade2-101 his3-Δ200/his3-Δ200 leu2-3,112/leu2-3,112 ura3-52/ura3-52* ChrIII/ChrIII [pRM11482 = *pSTU2-STU2-K252Q-3xHA LEU2+ CEN6 ARSH4 LEU2* Amp^R]	This study
yRM12247	*MATa/MATα STU2/stu2-Δ1::HIS3 ade2-101/ade2-101 his3-Δ200/his3-Δ200 leu2-3,112/leu2-3,112 ura3-52/ura3-52* ChrIII/ChrIII [pRM11966 = *pSTU2-STU2-K252R,K469R-3xHA LEU2 YCP* Amp^R]	This study
yRM12248	*MATa/MATα STU2/stu2-Δ1::HIS3 ade2-101/ade2-101 his3-Δ200/his3-Δ200 leu2-3,112/leu2-3,112 ura3-52/ura3-52* ChrIII/ChrIII [pRM11969 = *pSTU2-STU2-K252,469Q-3xHA LEU2+ CEN6 ARSH4 LEU2* Amp^R]	This study
yRM12249	*MATa/MATα STU2/stu2-Δ1::HIS3 ade2-101/ade2-101 his3-Δ200/his3-Δ200 leu2-3,112/leu2-3,112 ura3-52/ura3-52* ChrIII/ChrIII [pRM11974 = *pSTU2-STU2-K252,469,870Q-3xHA LEU2+ CEN6 ARSH4 LEU2* Amp^R]	This study
yRM12250	*MATa/MATα STU2/stu2-Δ1::HIS3 ade2-101/ade2-101 his3-Δ200/his3-Δ200 leu2-3,112/leu2-3,112 ura3-52/ura3-52* ChrIII/ChrIII [pRM11976 = *pSTU2-STU2-K252,469,870R-3xHA LEU2+ CEN6 ARSH4 LEU2* Amp^R]	This study

Table 3 (Continued)

yRM12251	*MATa/MATα STU2/stu2-Δ1::HIS3 ade2-101/ade2-101 his3-Δ200/his3-Δ200 leu2-3,112/leu2-3,112 ura3-52/ura3-52* ChrIII/ChrIII [pRM12015 = *pSTU2-STU2-K870Q-3xHA LEU2+ CEN6 ARSH4 LEU2* Amp^R]	This study
yRM12252	*MATa/MATα STU2/stu2-Δ1::HIS3 ade2-101/ade2-101 his3-Δ200/his3-Δ200 leu2-3,112/leu2-3,112 ura3-52/ura3-52* ChrIII/ChrIII [pRM12016 = *pSTU2-STU2-K870R-3xHA LEU2+ CEN6 ARSH4 LEU2* Amp^R]	This study
yRM12253	*MATα stu2-Δ1::HIS3 ade2-101 his3-Δ200 leu2-3,112 ura3-52* [pRM2119 = pSTU2-STU2-3xHA *CEN6 ARSH4 LEU2* Amp^R]	This study
yRM12260	*MATα stu2-Δ1::HIS3 ade2-101 his3-Δ200 leu2-3,112 ura3-52* [pRM11254 = *pSTU2-STU2-K469Q-3xHA LEU2+ CEN6 ARSH4 LEU2* Amp^R]	This study
yRM12261	*MATα stu2-Δ1::HIS3 ade2-101 his3-Δ200 leu2-3,112 ura3-52* [pRM11481 = *pSTU2-STU2-K252R-3xHA LEU2+ CEN6 ARSH4 LEU2* Amp^R]	This study
yRM12262	*MATα stu2-Δ1::HIS3 ade2-101 his3-Δ200 leu2-3,112 ura3-52* [pRM11482 = *pSTU2-STU2-K252Q-3xHA LEU2+ CEN6 ARSH4 LEU2* Amp^R]	This study
yRM12266	*MATα stu2-Δ1::HIS3 ade2-101 his3-Δ200 leu2-3,112 ura3-52* [pRM11966 = *pSTU2-STU2-K252R,K469R-3xHA LEU2 YCP* Amp^R]	This study
yRM12267	*MATα stu2-Δ1::HIS3 ade2-101 his3-Δ200 leu2-3,112 ura3-52* [pRM11969 = *pSTU2-STU2-K252,469Q-3xHA LEU2+ CEN6 ARSH4 LEU2* Amp^R]	This study
yRM12268	*MATα stu2-Δ1::HIS3 ade2-101 his3-Δ200 leu2-3,112 ura3-52* [pRM11974 = *pSTU2-STU2-K252,469,870Q-3xHA LEU2+ CEN6 ARSH4 LEU2* Amp^R]	This study
yRM12269	*MATα stu2-Δ1::HIS3 ade2-101 his3-Δ200 leu2-3,112 ura3-52* [pRM11976 = *pSTU2-STU2-K252,469,870R-3xHA LEU2+ CEN6 ARSH4 LEU2* Amp^R]	This study
yRM12270	*MATα stu2-Δ1::HIS3 ade2-101 his3-Δ200 leu2-3,112 ura3-52* [pRM12015 = *pSTU2-STU2-K870Q-3xHA LEU2+ CEN6 ARSH4 LEU2* Amp^R]	This study
yRM12271	*MATα stu2-Δ1::HIS3 ade2-101 his3-Δ200 leu2-3,112 ura3-52* [pRM12016 = *pSTU2-STU2-K870R-3xHA LEU2+ CEN6 ARSH4 LEU2* Amp^R]	This study
yRM12300	*MATα STU2 ade2-101 his3-Δ200 leu2-3,112 ura3-52* [pRM2200 = *LEU2 CEN6 ARSH4* Amp^R]	This study
yRM12301	*MATα stu2-Δ1::HIS3 ade2-101 his3-Δ200 leu2-3,112 ura3-52* [pRM11249 = *pSTU2-STU2-K469R-3xHA LEU2+ CEN6 ARSH4 LEU2* Amp^R]	This study
Plasmid shuffle strains		
yRM12337	*MATa stu2-Δ1::HIS3 ADE2 ura3-52 leu2-3,112 his3-Δ200* [pRM10693 = *pSTU2-STU2-HA CEN/ARS URA3* Amp^R] [pRM2119 = *pSTU2-STU2-3xHA CEN6 ARSH4 LEU2* Amp^R]	This study
yRM12338	*MATa stu2-Δ1::HIS3 ADE2 ura3-52 leu2-3,112 his3-Δ200* [pRM10693 = *pSTU2-STU2-HA CEN/ARS URA3* Amp^R] [pRM2200 = *LEU2 CEN6 ARSH4* Amp^R]	This study
yRM12340	*MATa stu2-Δ1::HIS3 ADE2 ura3-52 leu2-3,112 his3-Δ200* [pRM10693 = *pSTU2-STU2-HA CEN/ARS URA3* Amp^R] [pRM11481 = *pSTU2-STU2-K252R-3xHA LEU2+ CEN6 ARSH4 LEU2* Amp^R]	This study
yRM12341	*MATa stu2-Δ1::HIS3 ADE2 ura3-52 leu2-3,112 his3-Δ200* [pRM10693 = *pSTU2-STU2-HA CEN/ARS URA3* Amp^R] [pRM11249 = *pSTU2-STU2-K469R-3xHA LEU2+ CEN6 ARSH4 LEU2* Amp^R]	This study
yRM12342	*MATa stu2-Δ1::HIS3 ADE2 ura3-52 leu2-3,112 his3-Δ200* [pRM10693 = *pSTU2-STU2-HA CEN/ARS URA3* Amp^R] [pRM12016 = *pSTU2-STU2-K870R-3xHA LEU2+ CEN6 ARSH4 LEU2* Amp^R]	This study
yRM12343	*MATa stu2-Δ1::HIS3 ADE2 ura3-52 leu2-3,112 his3-Δ200* [pRM10693 = *pSTU2-STU2-HA CEN/ARS URA3* Amp^R] [pRM11966 = *pSTU2-STU2-K252,469R-3xHA LEU2+ CEN6 ARSH4 LEU2* Amp^R]	This study

Table 3 (Continued)

yRM12344	*MATa stu2-Δ1::HIS3 ADE2 ura3-52 leu2-3,112 his3-Δ200* [pRM10693 = *pSTU2-STU2-HA CEN/ARS URA3* Amp^R] [pRM11976 = *pSTU2-STU2-K252,469,870R-3xHA LEU2+ CEN6 ARSH4 LEU2* Amp^R]	This study
yRM12345	*MATa stu2-Δ1::HIS3 ADE2 ura3-52 leu2-3,112 his3-Δ200* [pRM10693 = *pSTU2-STU2-HA CEN/ARS URA3* Amp^R] [pRM11482 = *pSTU2-STU2-K252Q-3xHA LEU2+ CEN6 ARSH4 LEU2* Amp^R]	This study
yRM12346	*MATa stu2-Δ1::HIS3 ADE2 ura3-52 leu2-3,112 his3-Δ200* [pRM10693 = *pSTU2-STU2-HA CEN/ARS URA3* Amp^R] [pRM11254 = *pSTU2-STU2-K469Q-3xHA LEU2+ CEN6 ARSH4 LEU2* Amp^R]	This study
yRM12347	*MATa stu2-Δ1::HIS3 ADE2 ura3-52 leu2-3,112 his3-Δ200* [pRM10693 = *pSTU2-STU2-HA CEN/ARS URA3* Amp^R] [pRM12015 = *pSTU2-STU2-K870Q-3xHA LEU2+ CEN6 ARSH4 LEU2* Amp^R]	This study
yRM12348	*MATa stu2-Δ1::HIS3 ADE2 ura3-52 leu2-3,112 his3-Δ200* [pRM10693 = *pSTU2-STU2-HA CEN/ARS URA3* Amp^R] [pRM11969 = *pSTU2-STU2-K252,469Q-3xHA LEU2+ CEN6 ARSH4 LEU2* Amp^R]	This study
yRM12349	*MATa stu2-Δ1::HIS3 ADE2 ura3-52 leu2-3,112 his3-Δ200* [pRM10693 = *pSTU2-STU2-HA CEN/ARS URA3* Amp^R] [pRM11974 = *pSTU2-STU2-K252,469,870Q-3xHA LEU2+ CEN6 ARSH4 LEU2* Amp^R]	This study
Plasmid shuffle strains without URA3+ phenotypic masking plasmids		
yRM12358	*MATa stu2-Δ1::HIS3 ADE2 ura3-52 leu2-5,112 his3-Δ200* [pRM2119 = *pSTU2-STU2-3xHA LEU2+ CEN6 ARSH4 LEU2* Amp^R]	This study
yRM12359	*MATa stu2-Δ1::HIS3 ADE2 ura3-52 leu2-5,112 his3-Δ200* [pRM6507 = *pSTU2-STU2 LEU2+ CEN6 ARSH4 LEU2* Amp^R]	This study
yRM 12360	*MATa stu2-Δ1::HIS3 ADE2 ura3-52 leu2-5,112 his3-Δ200* [pRM11481 = *pSTU2-STU2-K252R LEU2+ CEN6 ARSH4 LEU2* Amp^R]	
yRM12361	*MATa stu2-Δ1::HIS3 ADE2 ura3-52 leu2-5,112 his3-Δ200* [pRM11249 = *pSTU2-STU2-K469R-3xHA LEU2+ CEN6 ARSH4 LEU2* Amp^R]	This study
yRM12362	*MATa stu2-Δ1::HIS3 ADE2 ura3-52 leu2-5,112 his3-Δ200* [pRM12016 = *pSTU2-STU2-K870R-3xHA LEU2+ CEN6 ARSH4 LEU2* Amp^R]	This study
yRM12363	*MATa stu2-Δ1::HIS3 ADE2 ura3-52 leu2-5,112 his3-Δ200* [pRM11966 = *pSTU2-STU2-K252,469R-3xHA LEU2+ CEN6 ARSH4 LEU2* Amp^R]	This study
yRM12364	*MATa stu2-Δ1::HIS3 ADE2 ura3-52 leu2-5,112 his3-Δ200* [pRM11976 = *pSTU2-STU2-K252,469,870R-3xHA LEU2+ CEN6 ARSH4 LEU2* Amp^R]	This study
yRM12365	*MATa stu2-Δ1::HIS3 ADE2 ura3-52 leu2-5,112 his3-Δ200* [pRM11482 = *pSTU2-STU2-K252Q-3xHA LEU2+ CEN6 ARSH4 LEU2* Amp^R]	This study
yRM12366	*MATa stu2-Δ1::HIS3 ADE2 ura3-52 leu2-5,112 his3-Δ200* [pRM11254 = *pSTU2-STU2-K469Q-3xHA LEU2+ CEN6 ARSH4 LEU2* Amp^R]	This study
yRM12367	*MATa stu2-Δ1::HIS3 ADE2 ura3-52 leu2-5,112 his3-Δ200* [pRM12015 = *pSTU2-STU2-K870Q-3xHA LEU2+ CEN6 ARSH4 LEU2* Amp^R]	This study
yRM12368	*MATa stu2-Δ1::HIS3 ADE2 ura3-52 leu2-5,112 his3-Δ200* [pRM11969 = *pSTU2-STU2-K252,469Q-3xHA LEU2+ CEN6 ARSH4 LEU2* Amp^R]	This study
yRM12369	*MATa stu2-Δ1::HIS3 ADE2 ura3-52 leu2-5,112 his3-Δ200* [pRM11974 = *pSTU2-STU2-K252,469,870Q-3xHA LEU2+ CEN6 ARSH4 LEU2* Amp^R]	This study
yRM12419	*MATa stu2-Δ1::HIS3 ADE2 ura3-52 leu2-5,112 his3-Δ200* [pRM11481 = *pSTU2-STU2-K252R-3xHA LEU2+ CEN6 ARSH4 LEU2* Amp^R]	This study

Table 4 Plasmids used in this study.

Bacterial Strains	Genotype/comments	Source
pRM2119/pWP70	pSTU2-STU2-3xHA *CEN6 ARSH4 LEU2* Amp^R	(P. J. Wang & Huffaker, 1997)
pRM2200/pRS415	*LEU2 CEN6 ARSH4* Amp^R	(Sikorski & Hieter, 1989)
pRM6507/pWP45	*pSTU2-STU2*-No Tag *CEN6 ARSH4 LEU2* Amp^R	(P. J. Wang & Huffaker, 1997)
pRM10693/ pCUB1179	*pSTU2-STU2-HA CEN/ARS URA3* Amp^R	A gift from Tim Huffaker
pRM10762	SUMO-S2A-*GST* Amp^R	This study
pRM11249	*pSTU2-Stu2-K469R-3xHA LEU2+ CEN6 ARSH4 LEU2* Amp^R	This study
pRM11254	*pSTU2-Stu2-K469Q-3xHA LEU2+ CEN6 ARSH4 LEU2* Amp^R	This study
pRM11481	*pSTU2-Stu2-K252R-3xHA LEU2+ CEN6 ARSH4 LEU2* Amp^R	This study
pRM11482	*pSTU2-Stu2-K252Q-3xHA LEU2+ CEN6 ARSH4 LEU2* Amp^R	This study
pRM11485	*GST* Amp^R	(Greenlee et al.)
pRM11628	5x-SUMO-*GST* Amp^R	This study
pRM11966	pSTU2-Stu2-K252,469R-3xHA *LEU2+ CEN6 ARSH4 LEU2* Amp^R	This study
pRM11969	*pSTU2-Stu2-K252,469Q-3xHA LEU2+ CEN6 ARSH4 LEU2* Amp^R	This study
pRM11974	*pSTU2-Stu2-K252,469,870Q-3xHA LEU2+ CEN6 ARSH4 LEU2* Amp^R	This study
pRM11976	*pSTU2-Stu2-K252,469,870R-3xHA LEU2+ CEN6 ARSH4 LEU2* Amp^R	This study
pRm12015	*pSTU2-Stu2-K870Q-3xHA LEU2+ CEN6 ARSH4 LEU2* Amp^R	This study
pRM12016	*pSTU2-Stu2-K870R-3xHA LEU2+ CEN6 ARSH4 LEU2* Amp^R	This study
pRM11972/ pJS2	*SUP11 URA3+ CEN6 D8B Y'* Amp^R. linearized with NotI or EcoRI to integrate	(Shero et al., 1991)

transferred to nitrocellulose membranes for immunoblotting with anti-HA (Santa Cruz, clone F-7) to detect Stu2 or anti-AcK (Genetex, Acetyl Lysine antibody clone 1C6) to detect acetylation.

Detection of Stu2 acetyl-lysines using mass spectrometry.

Yeast cells containing Stu2-HA (yRM10637) or a vector control (yRM10641) were grown to mid-log and disrupted using cryo-milling as described in Greenlee et. al., 2018. 75 mgs of logarithmic Extracts in 1x PBS containing 0.1% Tween were incubated with anti-HA magnetic beads for 1 hour at 4 °C and washed 3 times with 1x PBS containing 0.1% Tween. To elute, pull-downs were boiled in 100 uL of 2.5X sample buffer for 5 minutes. Proteins were resolved on 10% SDS PAGE until 50 kDa markers were run off the gel to ensure optimal band separation. The SDS-PAGE gel was then fixed in 50% methanol, 10% acetic acid for 1 hour and stained for 15 minutes using Coomassie blue. To confirm the presence of Stu2 in bands, a small amount of each pull-down was run on SDS-PAGE and transferred to a nitrocellulose membrane and blocked overnight in 0.1% I-block reagent (Applied Biosystems, Bedford, MA) dissolved in PBS containing 0.1% Tween. The Membrane was immunoblotted with mouse anti-HA to identify HA tagged Stu2. SDS PAGE bands containing Stu2 were cut from the gel, extracted with acetonitrile, and digested with trypsin in 2M Urea.

Peptides from the digested samples were dissolved in 0.1% aqueous formic acid, and injected onto a 0.075 x 400 mm nano HPLC column packed with 3-um Magic AQ C18 particles. Peptides were separated using a 120-min gradient of 3-30% acetonitrile/0.1%formic acid and eluted through a stainless-steel emitter for ionization in a Proxeon ion source. Peptide ions were analyzed by a high/high mass accuracy approach. Parent ions were measured using the Orbitrap sector of a Fusion mass spectrometer (Thermo), followed by data-dependent quadrupole selection of individual precursors and fragmentation in both the ion trap (CID at 35% energy) and in the

HCD cell (25% or 35% energy). Lastly, fragmented ions were measured again in the Orbitrap sector at 30,000 resolution.

Raw mass spectra files were converted to .mgf files using msconvert from Proteowizard (Chambers et al., 2012). SearchGUI was then used to analyze .mgf files with the proteomics search engines Comet, MS Amanda, MS-GF+, MyriMatch, OMSSA, and X!Tandem simultaneously (Barsnes & Vaudel, 2018). Fixed modifications in the searches included methionine oxidation, cysteine carbamidomethylation, and lysine carbamylation and variable modifications included lysine and N-terminal acetylation and phosphorylation of serine, threonine, and tyrosine. All searches omitted matches outside of a +/- 10 ppm mass accuracy window. SearchGUI outputs were then combined using PeptideShaker to compare peptide identifications from each independent search engine.

Stu2 structure prediction and residue conservation analysis

The structural prediction of Stu2 was generated with I-TASSER (Yang et al., 2015) (Roy, Kucukural, & Zhang, 2010; Zhang, 2008) using the full Stu2 sequence as a template (uniprot:P46675, SGD:S000004035). To determine the impact of K252Q mutations on Stu2 structure, the full amino acid sequence was submitted to I-TASSER with the lysine 252 to glutamine amino acid substitution.

To determine amino acid conservation of acetyl lysines, we compiled a list of 28 XMAP215 family MT polymerases from 27 different organisms of ranging cellular complexity across Eukarya including: *S. cerevisiae* (P46675), *M. sympodialis* (A0A1M8A6U5), *D. discoideum* (Q1ZXQ8), *P. pallidum* (D3BU59), *A. deanei* (S9W6U7), *P. marinus* (C5LPC0), *C. elegans* (G5EEM5), *T. conorhini* (A0A3R7L7I8), *E. multilocularis* (A0A087W255), *A. thaliana* (Q94FN2), *S. scitamineum* (A0A0F7S5S5), *O. sativa subsp. Japonica* (Q5N749), *P. humanus subsp. Corporis* (E0VU40), *A. darlingi* (W5J5U5), *A. aegypti* (A0A1S4FBN3), *D. melanogaster*

(Q9VEZ3), *X. laevis* (Q9PT63), *M. musculus* (A2AGT5), *H. sapiens* (Q14008), *S. pombe* (Q94534, Q09933), *A. gossypii* (Q75CQ1), *P. antarctica* (A0A081CMB9), *G. candidum* (A0A0J9XCS4), *C. albicans* (A0A1D8PTZ8), *C. glabrata* (A0A0W0D3T8), *E. nidulans* (Q5B1Q9), and *U. maydis* (A0A0D1CA73). These MT polymerases were grouped as either fungal organisms or broadly as eukaryotes and aligned using Clustal Omega (Sievers & Higgins, 2018).

Conservation analysis of β- and γ-tubulins was carried out using Clustal Omega as previously described using β-tubulins from *S. cerevisiae* (P02557), *C. elegans* (P12456), *A. thaliana* (P12411), *D. melanogaster* (Q24560), *X. tropicalis* (Q6GLE7), *M. musculus* (A2AQ07), and *H. sapiens* (P07437) and γ-tubulins from *S. cerevisiae* (P53378), *C. elegans* (P34475), *A. thaliana* (P38557), *D. melanogaster* (P23257), *X. tropicalis* (P23330), *M. musculus* (P83887), and *H. sapiens* (P23258).

Structural modeling of β- and γ-tubulin interactions with the Stu2 TOG2 domain

Pymol was used to visualize atomic coordinate data from the following pdb files; TOG/GTP β-tubulin complex: 4u3j, GDP β-tubulin polymerized in MTs: 5w3f, and GDP hydrolyzed γ-tubulin: 3cb2. We used the ColorByRMSD Python Module (Shandilya, Vertrees, & T., 2016) to align and color code positional conservation for a small highly structured region of β- and γ-tubulins that includes the K469 interacting residues (β-EFPD/γ-RYPK) and the GTP hydrolyzing E-site (exchange site) (Ayaz et al., 2014; Howes et al., 2017; Rice, Montabana, & Agard, 2008).

Complementation of *STU2* deletion

5 mL cultures of yeast containing a phenotype masking *URA3*+ plasmid expressing *STU2* (pRM10693) and a *LEU2*+ plasmids expressing *STU2* (yRM12337), vector (yRM12338), K252R (yRM12340), K469R (yRM2341), K870R (yRM12342), 2KR (yRM12343), 3KR (yRM12344),

K252Q (yRM12345), K469Q (yRM12346), K870Q (yRM12347), 2KQ (yRM12348), and 3KQ (yRM12349) were grown overnight. OD_{600} values were determined for each culture and normalized to 0.100 each. Normalized cultures were further diluted in 96 well plates to prepare 0.100, 0.055, and 0.010 dilutions. 96 well plates were used to frog synthetic deficient media lacking histidine, leucine, and uracil to confirm equal loading of cells. 5-FOA plates lacking leucine were used to test functionality of Stu2 mutants by depleting *URA3*+ plasmid expressed *STU2*. Vector controls in plates containing 5-FOA demonstrated complete removal of URA3+ plasmid amongst actively growing cells.

Benomyl resistance of Stu2 mutants

Cultures of yeast containing *STU2* (yRM12358), K252R (yRM12360), K469R (12361), K870R (12362), 2KR (yRM12363), 3KR (yRM12364), K252Q (yRM12365), K469Q (yRM12366), K870Q (yRM12367), 2KQ (yRM12368), or 3KQ (yRM12369) were normalized to OD_{600} values of 0.100 and diluted as described above. Cells were transferred to leucine deficient media to confirm equal loading and plates lacking histidine, leucine, and uracil to confirm the absence of the URA3+ WT-STU2 plasmid. To test mutant Stu2 resistance to microtubule stress, cells were transferred to DMSO, DMSO + 10 μg/mL of benomyl, and 20 μg/mL of benomyl and grown at 23, 30, and 37 °C. Stu2 acetyl-lysine mutants were also tested on benomyl in a WT background using a pSTU2-STU2 URA3+ plasmid to detect whether observed phenotypes are dominant.

5x-SUMO-GST construction

A chain of five tandem SUMO proteins attached to GST was engineered and expressed in bacteria as follows. An initial full length SUMO was followed by four subsequent truncated SUMOs consisting of amino acids 11-98. This construct approximated a K11 chain of SUMO (Ulrich, 2008). Glycine 98 was fused in-frame with the amino-terminus of GST, preventing

conjugation to substrate proteins. To prevent the formation of adverse secondary structure associated with repeating *SMT3* genes that can complicate cloning, we randomized the codons coding for SUMOs while preserving amino acid sequence and composition of SUMO. This codon randomization was carried out using the Python program, NulSeq (Liu, Hockenberry, Lancichinetti, Jewett, & Amaral, 2016). The randomized codons were additionally processed using Integrated DNA Technologies' codon optimization tool using *E. coli* codon preferences. Because of the number of tandem repeats, this process was repeated two additional times to generate a suitable gene. A gene block of this construct was ordered (see Figure 17, gBlocks, Integrated DNA Technologies, Coralville, IA). The vector backbone used for this construct was gel purified from pRM10762 following restriction digest with NcoI and MscI. NcoI and MscI digested 5x-SUMO was ligated into the pRM10762 backbone in frame at the amino-terminus of the GST gene to create the 5x-SUMO-GST construct, pRM11577. Its identity was confirmed by sequencing. For inducible protein expression, pRM11577 was transformed into BL21-Gold(DE3) (Agilent Technologies, Santa Clara, CA) (pRM10694) to produce pRM11628.

Stu2 enrichment with 5x-SUMO-GST columns

Noncovalent SUMO affinity columns were prepared as follows. Bacterial cells expressing GST (pRM11485), GST-SUMO-GA (pRM11487), or 5x-SUMO-GST (pRM11628) were lysed in PBS containing 0.1% Triton, 1 mg/mL lysozyme, 10 µg/mL DNaseI, 40 mM 2-Iodoacetamide (2-IAA), 20 mM N-Ethylmaleimide (NEM), 1:500 dilution of Sigma PIC (#P8849), and 1 mM PMSF at 4 degrees while rotating approximately 15 times per minute for 2 hours. To clarify, extracts were centrifuged at 13,000 RPM for 30 minutes at 4 °C. Glutathione agarose beads (Pierce, Rockford, IL) were equilibrated in PBS containing 0.1% Triton. Clarified extracts were incubated with 32 uL/column of equilibrated glutathione agarose beads at 4 degrees while rotating approximately 15 times per minute for 2 hours. Resins were then washed twice

5x-SUMO-GST gene block sequence

NcoI Restriction Endonuclease site - CCATGG

TATCTAGTA**CCATGG**CGGACTCAGAAGTCAATCAAGAAGCTAAGCCCGAAGTCAAGCCTGAGGTTA
AACCAGAAACACATATTAACTTAAAAGTCAGCGATGGGAGCTCTGAGATTTTCTTCAAAATCAAGA
AAACCACACCCTTGCGTCGCTTAATGGAAGCATTCGCCAAACGCCAAGGAAAGGAAATGGATTCTT
TACGTTTTCTGTACGATGGTATCCGTATCCAAGCAGATCAAACCCCAGAGGATTTAGACATGGAAG
ACAACGACATCATCGAAGCCCACCGTGAGCAGATCGGAGGGAAACCTGAGGTCAAACCGGAAGTCA
AGCCCGAGACCCACATCAACCTTAAAGTCAGTGATGGCAGCAGTGAAATCTTCTTTAAGATTAAGA
AAACTACGCCTCTGCGCCGTTTGATGGAGGCATTCGCCAAGCGTCAGGGAAAAGAGATGGACTCAC
TGCGCTTCCTGTACGACGGGATTCGTATTCAAGCGGATCAGACACCTGAGGACCTGGACATGGAGG
ACAACGACATCATTGAAGCGCACCGCGAACAGATCGGTGGGAAGCCCGAAGTGAAGCCAGAAGTGA
AACCTGAAACTCATATTAATCTTAAGGTCTCAGATGGATCGAGTGAAATTTTTTTCAAAATTAAAA
AGACTACACCCTTGCGTCGTCTGATGGAAGCATTTGCGAAACGCCAAGGCAAGGAGATGGACTCTT
TACGCTTTTTTATATGATGGAATTCGTATCCAAGCTGACCAAACACCAGAGGACTTAGATATGGAAG
ACAACGATATTATTGAGGCCCACCGCGAACAAATTGGCGGAAAGCCTGAAGTTAAACCCGAGGTAA
AGCCGGAGACGCACATCAACCTGAAGGTTTCGGATGGTAGCAGCGAAATCTTCTTCAAGATCAAAA
AAACTACTCCTCTTCGCCGTCTTATGGAAGCCTTCGCAAAACGTCAAGGTAAGGAGATGGACAGTC
TTCGTTTTTTTATATGATGGAATCCGTATCCAGGCCGATCAAACACCTGAGGATTTAGACATGGAGG
ATAATGACATCATTGAAGCACATCGCGAACAAATTGGGGGGAAACCTGAGGTTAAACCTGAGGTTA
AGCCTGAGACACACATCAACTTGAAGGTGTCGGACGGATCATCCGAGATTTTTTTCAAGATCAAGA
AGACTACCCCGCTGCGCCGCCTGATGGAGGCCTTCGCGAAACGCCAGGGAAAGGAGATGGACAGTT
TACGTTTTTTGTACGATGGCATTCGTATCCAAGCAGACCAGACACCAGAGGATCTGGACATGGAAG
ACAACGATATCATTGAGGCACATCGTGAGCAGATCGGTGGCCTTGAAGGTGGCCCCGTGTTTATGT
CCCCAATCCTTGGTTACTGGAAGATTAAGGGGCTTGTGCAGCCTACCCGTTTATTGTTAGAGTACC
TGGAGGAGAAGTACGAAGAGCATTTGTACGAACGCGATGAGGGCGACAAATGGCGCAACAAGAAGT
TTGAGCTGGGGCTGGAATTTCCTAACCTTCCCTATTACATCGATGGGGATGTCAAGTTAACCCAGA
GTA**TGGCCA**GGATACATT

MscI Restriction Endonuclease site - TGGCCA

ORF - 5x-SUMO for ligation into GST backbone.

Restriction sites

CUTTING NUCLEOTIDES 5’(TATCTAGTA) 3’(GGATACATT)

Figure 17 The complete gene block sequence of the K11 5X-SUMO-GST construct. Restriction sites NcoI 5’ and MscI 3’ are underlined and cutting nucleotides were included to facilitate digestion by restriction endonucleases.

with 50 column volumes of PBS containing 0.1% Triton. Resins were then divided evenly amongst 1.7 mL eppendorf tubes to be used in subsequent pull-downs.

To prepare yeast whole-cell extracts, cells expressing Stu2-HA (yRM12358), Stu2-No Tag (yRM12359), Stu2-K252R-HA (yRM12419), Stu2-K469R-HA (yRM12361), Stu2-K870R-HA (yRM12362), Stu2-2KR-HA (yRM12363), Stu2-3KR-HA (yRM12364), Stu2-K252Q-HA (yRM12365), Stu2-K469Q-HA (yRM12366), Stu2-K870Q-HA (yRM12367), Stu2-2KQ-HA (yRM12368), or Stu2-3KQ-HA (yRM12369) were grown overnight to saturation. Cells were collected by centrifugation at 30 °C for 5 minutes, transferred to pre-weighed 50 mL tubes, and immediately flash frozen in liquid nitrogen. A 4x protease inhibitor cocktail cap consisting of 0.1% Triton PBS, 160 mM 2-IAA, 80 mM NEM, 1:125 dilution of Sigma PIC, and 4 mM PMSF equal to one-third the pellets mass was then pipetted on-top of the yeast pellet and flash frozen. Yeast cell pellets were cryomilled in liquid nitrogen. To clarify, cryomilled powder was resuspended to a final volume of 7-8 mLs in 15 mL falcon tubes and centrifuged at 3000 RPM for 3 minutes. Supernatant from the pre-clarification was then transferred to 1.7 mL eppendorf tubes and centrifuged for 25 minutes at 14,000 RPM.

Protein concentrations were determined by Bradford assay using a BSA standard curve. Clarified extracts were incubated with GST or 5x-SUMO-GST enriched agarose at 5.3mg/mL (9 mgs in 1.7 mLs) for 1 hour. Resins were collected at 500 xg for 1 minute and washed 2 times with 50 column volumes of 0.1% Triton PBS. Following the second wash, resins were transferred to lightly perforated PCR tubes and spun to completely remove residual buffer. To elute, PCR tubes containing dried resins were transferred to fresh 1.7 mL tubes, 100 uL of 2.5x Laemmli sample buffer was added to each resin, and samples were boiled for 5 minutes. After boiling, samples were centrifuged at 800 xg for 2 minutes to remove buffer

soluble protein from agarose resins. Pull-downs were run on 10% SDS PAGE gels and transferred to nitrocellulose using a tank transfers for western blot analysis.

To visualize HA epitope tagged Stu2, membranes were immunoblotted with mouse anti-HA (SC-7392, Santa Cruz Biotechnology, Santa Cruz, CA) and goat anti-mouse-HRP (#115-036-146, Jackson Immuno Research Labs, West Grove, PA) secondary antibody. To visualize tubulin, membranes were immunoblotted with rat anti-α-tubulin MCAB (YSRTMCA78G) and goat anti-rat (SC-7392, Santa Cruz Biotechnology). To visualize Act1p and Pgk1p, membranes were immunoblotted with mouse anti-Act1p or -Pgk1p (#MA1-744, or #459250 respectively, ThermoFisher Scientific).

Chromosome III fragmentation

We generated a diploid yeast strain containing a 125-kb chromosome fragment specifically to study the essential protein STU2 as described in (Shero et al., 1991). The heterozygous diploid yRM11988 homozygous for the ade2-101 mutant and heterozygous STU2 knockout was generated by mixing lightly grown (OD_{600} < 0.100) overnight cultures of the *MAT*a strain yRM11408 and the *MAT*α strain yRM11407 were mixed for 1 hour. 10 µL of mating cells were transferred to leucine deficient media, scanned for mating cellular morphology, and isolated using an Olympus BX41 dissection microscope. Putative diploids were confirmed through sporulation and leu- isolates were obtained through replica plating to leucine and histidine deficient plates. Chromosome III fragmentation events were induced through the integration of NotI linearized pJS2/pRM11972 plasmid. (Figure 18a & b)

Following artificial chromosome induction, colonies were selected based on a pink color phenotype associated with presence of single chromosome fragments. Whole chromosome samples were prepared and visualized using methods adapted from (Carle & Olson, 1985) and (Warren et al., 2002). To create yeast protoplasts, 5 mLs of uracil deficient media were

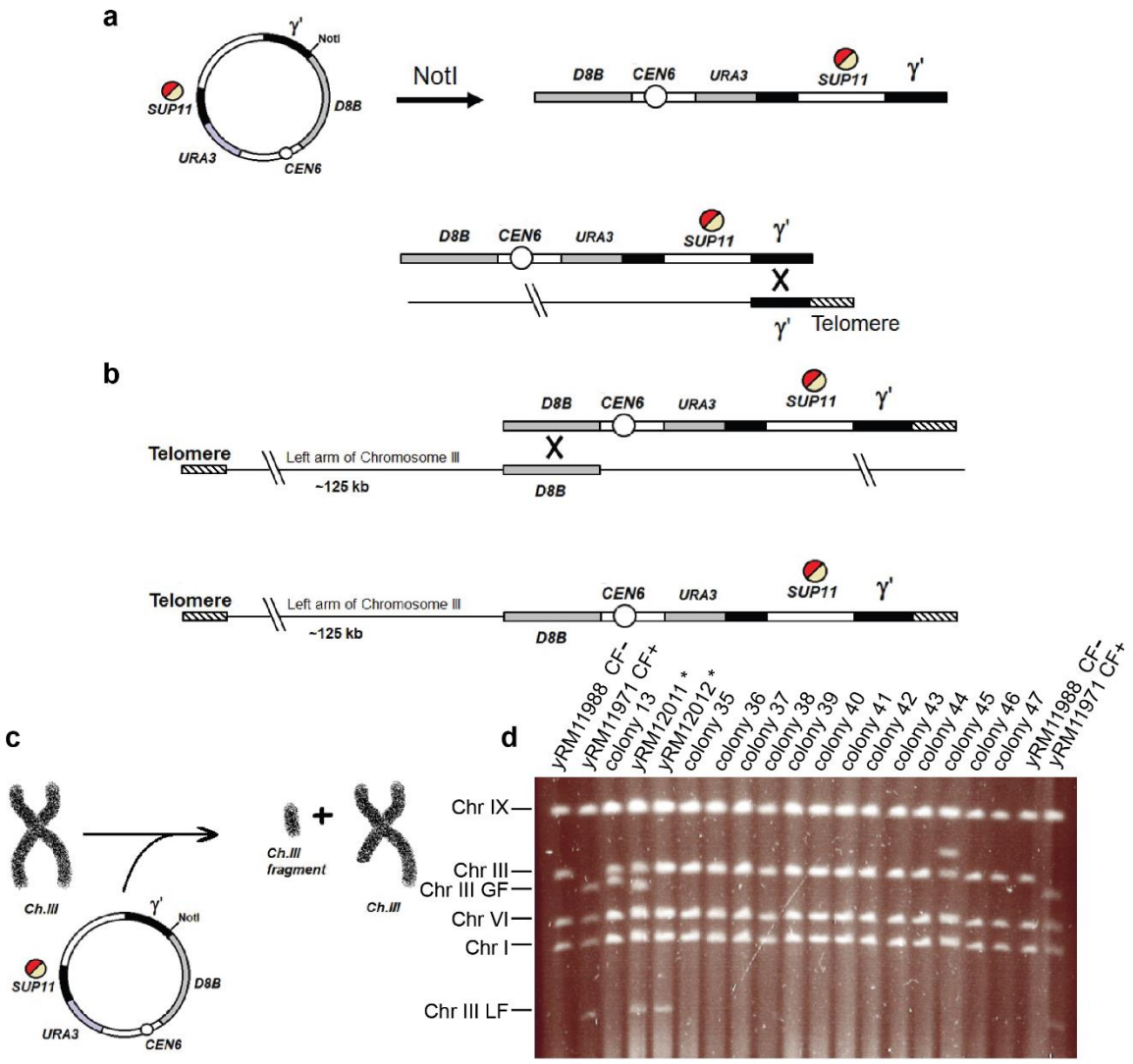

Figure 18 Fragmentation of Chromosome III adapted from (Shero et al., 1991). (a) Linearization and cross 1 during pJS2/pRM11972 integration yields one sided telomeric linearized precursor to a Chromosome III fragment. (b) The second cross occurs in the D8B genetic sequence specific to the left arm of chromosome III to yield the 125-kb Chromosome III fragment. (c) A simplified model regarding the aim of chromosome fragmentation. (d) PFGE electrophoretic karyotyping of the four smallest chromosomes of *S. cerevisiae*, the generated Chromosome III greater fragment, and the 125-kb Chromosome III lesser fragment.

inoculated with a no chromosome fragment control (yRM11988), a haploid cell line possessing the 125-kb chromosome III fragment (yRM11971), or fresh pJS2/pRM11972 integrations into yRM11988. Saturated overnight cultures were collected at 3000 RPM for 3 minutes using an Allegra X-15R Beckman Coulter tabletop centrifuge. Growth media was discarded, cell pellets were washed 3 times with 1.6 mLs of 50 mM EDTA, pH 7.5, and resuspended in 300 µL of 50 mM EDTA, pH 7.5. 500 µL of 1% low-gelling-temperature agarose and 100 µL of pH 8.0 SCE buffer containing 1M sorbitol, 100 mM sodium citrate, 10 mM EDTA, 5% β-mercaptoethanol, and 1 mg/mL zymolyase were added to each cell suspension at 37 °C. Protoplast mixes were transferred to 24 well plates to solidify at room temperature. When solid, 500 µL of a liquid overlay layer containing 270 mM EDTA –pH 9.0, 10 mM Tris –pH 8.0, 7.5% β-mercaptoethanol was added to each cell suspension and incubated overnight at 37 °C in a sealed plastic bag.

For protoplast proteolysis, the previous liquid overlay was removed and replaced with a new solution containing 270 mM EDTA and 10 mg/mL N-Lauroylsarcosine at a pH of 9.0, 10 mM pH 8.0 Tris, and 1 mg/mL proteinase K. Protoplasts with proteolysis buffer were incubated overnight at 50 °C in a sealed plastic bag. To store digested cells, the proteolysis liquid overlay was removed and replaced with 500 µLs of pH 9.0 0.5 M EDTA.

Successful chromosome III fragmentation events, illustrated in Figure 18c, were screened using PFGE in a BIORAD CHEF-DR III system. Gel slices of each digestion were transferred to 1.7 mM wells of a 1% agarose gel made with pH 8.0 0.5x TBE buffer containing 45 mM Tris-borate and 1 mM EDTA. PFGE was carried out in 0.5x TBE buffer at 200 V and 14 °C for 30 hours using continuous ramp switch times of 24 to 54 seconds. To visualize bands, the gel was stained in 0.5 µg/mL ethidium bromide in ddH_2O for 1 hour and destained in ddH_2O for 1.5 hours. Using electrophoretic mobility to separate the 4 smallest chromosomes in *S. cerevisiae*, we identified two strains with Chromosome III fragmentation (Figure S3d.) One of the strains was heterozygous for Chr III fragmentation and possessed an unaltered Chr III along with greater (Chr

III GF) and lesser fragments (Chr III LF) from sister Chr III fragmentation (yRM12011). The second strain was homozygous for full length Chr III but still possessed a band at the molecular weight range diagnostic of a Chr III fragment but lacked the Chr III greater fragment (yRM12012).

Quantitative chromosome loss assay

To quantitatively determine the rates of chromosome loss for the strains previously described, cells were initially grown over night to OD_{600} values of 0.100 to 0.200. Cells were further diluted to OD_{600} values of 0.010 in chilled water or chilled water containing 1 mg/mL 5-FOA and stored at 4 °C for 4 hours. To quantify cells present in the assay, yeast from the 4 hour 4 °C water sample were diluted 100 fold to an expected OD_{600} value of 0.0001. 125 µL of this was then transferred to 3 uracil and leucine deficient plates. Approximately 17,000 Cells from the 5-FOA treated cells were plated to 3 1 mg/mL 5-FOA plates lacking leucine and grown for 4 days at 30 °C. To quantify chromosomal loss, initial cellular densities were back calculated using the uracil leucine deficient plates. Colonies growing on 5-FOA plates were quantified as individual chromosomal loss events. The total number of 5-FOA colonies was then divided by the total number of colonies predicted to determine a quantitative value for chromosomal loss.

Qualitative chromosomal loss assay

To determine relative rates of chromosome loss between mutants and WT-Stu2, yeast strains containing *SUP11* artificial chromosomes and plasmids expressing WT-Stu2 (yRM12253), vector with endogenous Stu2 (yRM12300), K252R (yRM12261), K469R (yRM12301), K870R (yRM12271), 2KR (yRM12266), 3KR (yRM12269), K252Q (yRM12262), K469Q (yRM12260), K870Q (yRM12270), 2KQ (yRM12267), and 3KQ (yRM12268) were initially grown overnight to OD_{600} values between 0.100 and 0.200. Overnight cultures were further diluted to approximately 0.0001 OD_{600} values. 25 or 50 cells of each strain were plated

onto SC deficient for leucine with either 4 µg/mL (20%) or 8 µg/mL (40%) of normal adenine concentrations. Each set of conditions was repeated 3 times to generate error bars. Yeast were then grown at 30 °C for 5 days and stored for 1 day at 4 °C. Because sectors slowly become more apparent at low temperatures, all visible red sectors were counted within 8 hours. For each plate, the total number of sectors relative to colonies was determined as qualitative values.

ACKNOWLEDGEMENTS:

This work was supported by grants from the NIH (R15GM119117-01) and the Oklahoma Agricultural Experiment Station (OKL02961) to RKM. SM was supported in part by an CASNR/OAES Scholarship and a Niblack Research Scholar, both at OSU.

REFERENCES

Abruzzi, K. C., Smith, A., Chen, W., & Solomon, F. (2002). Protection from free beta-tubulin by the beta-tubulin binding protein Rbl2p. *Mol Cell Biol, 22*(1), 138-147. Retrieved from https://www.ncbi.nlm.nih.gov/pubmed/11739729

Acconcia, F., Sigismund, S., & Polo, S. (2009). Ubiquitin in trafficking: The network at work. *Exp Cell Res, 315*(9), 1610-1618. doi:https://doi.org/10.1016/j.yexcr.2008.10.014

Adkins, M. W., Carson, J. J., English, C. M., Ramey, C. J., & Tyler, J. K. (2007). The histone chaperone anti-silencing function 1 stimulates the acetylation of newly synthesized histone H3 in S-phase. *Journal of Biological Chemistry, 282*(2), 1334-1340.

Agarwal, S., & Roeder, G. S. (2000). Zip3 provides a link between recombination enzymes and synaptonemal complex proteins. *Cell, 102*(2), 245-255.

Aguilar, A., Becker, L., Tedeschi, T., Heller, S., Iomini, C., & Nachury, M. V. (2014). α-Tubulin K40 acetylation is required for contact inhibition of proliferation and cell–substrate adhesion. *Mol Biol Cell, 25*(12), 1854-1866.

Akiyoshi, B., Sarangapani, K. K., Powers, A. F., Nelson, C. R., Reichow, S. L., Arellano-Santoyo, H., . . . Biggins, S. (2010). Tension directly stabilizes reconstituted kinetochore-microtubule attachments. *Nature, 468*(7323), 576-579.

Akutsu, M., Dikic, I., & Bremm, A. (2016). Ubiquitin chain diversity at a glance. *Journal of Cell Science, 129*(5), 875-880.

Al-Bassam, J., & Chang, F. (2011). Regulation of microtubule dynamics by TOG-domain proteins XMAP215/Dis1 and CLASP. *Trends in Cell Biology, 21*(10), 604-614.

Al-Bassam, J., Larsen, N. A., Hyman, A. A., & Harrison, S. C. (2007). Crystal structure of a TOG domain: conserved features of XMAP215/Dis1-family TOG domains and implications for tubulin binding. *Structure, 15*, 355-362.

Al-Bassam, J., van Breugel, M., Harrison, S. C., & Hyman, A. A. (2006). Stu2p binds tubulin and undergoes an open-to-closed conformational change. *J. Cell Biology, 172*, 1009-1022.

Albaugh, B. N., Arnold, K. M., Lee, S., & Denu, J. M. (2011). Autoacetylation of the histone acetyltransferase Rtt109. *Journal of Biological Chemistry, 286*(28), 24694-24701.

Alonso, A., D'Silva, S., Rahman, M., Meluh, P. B., Keeling, J., Meednu, N., . . . Miller, R. K. (2012). The yeast homologue of the microtubule-associated protein Lis1 interacts with the sumoylation machinery and a SUMO-targeted ubiquitin ligase. *Molecular biology of the cell, 23*(23), 4552-4566. doi:10.1091/mbc.E12-03-0195

Alonso, A., Greenlee, M., Matts, J., Kline, J., Davis, K.J., and Miller, R.K. (2015). Emerging roles of sumoylation in the regulation of actin, microtubules, intermediate filaments, and septins. Cytoskeleton (Hoboken, N.J.) 72, 305-339.

Alushin, G. M., Lander, G. C., Kellogg, E. H., Zhang, R., Baker, D., & Nogales, E. (2014). High-resolution microtubule structures reveal the structural transitions in αβ-tubulin upon GTP hydrolysis. *Cell, 157*(5), 1117-1129. doi:10.1016/j.cell.2014.03.053

Anamika, & Spyracopoulos, L. (2016). Molecular Basis for Phosphorylation-dependent SUMO Recognition by the DNA Repair Protein RAP80. *The Journal of Biological Chemistry, 291*(9), 4417-4428. doi:10.1074/jbc.M115.705061

Anders, K. R., & Botstein, D. (2001). Dominant-lethal α-tubulin mutants defective in microtubule depolymerization in yeast. *Mol Biol Cell, 12*(12), 3973-3986.

Aoki, K., Nakaseko, Y., Kinoshita, K., Goshima, G., & Yanagida, M. (2006). CDC2 phosphorylation of the fission yeast dis1 ensures accurate chromosome segregation. *Curr Biol, 16*(16), 1627-1635. doi:10.1016/j.cub.2006.06.065

Aravamudhan, P., Felzer-Kim, I., Gurunathan, K., & Joglekar, A. P. (2014). Assembling the protein architecture of the budding yeast kinetochore-microtubule attachment using FRET. *Curr Biol, 24*(13), 1437-1446. doi:10.1016/j.cub.2014.05.014

Asbury, C. L., Gestaut, D. R., Powers, A. F., Franck, A. D., & Davis, T. N. (2006). The Dam1 kinetochore complex harnesses microtubule dynamics to produce force and movement. *Proc Natl Acad Sci U S A, 103*(26), 9873-9878. doi:10.1073/pnas.0602249103

Ayaz, P., Munyoki, S., Geyer, E. A., Piedra, F.-A., Vu, E. S., Bromberg, R., . . . Rice, L. M. (2014). A tethered delivery mechanism explains the catalytic action of a microtubule polymerase. *Elife, 3*, e03069.

Ayaz, P., Ye, X., Huddleston, P., Brautigam, C. A., & Rice, L. M. (2012). A TOG: alpha-beta tubulin complex structure reveals conformational-based mechanisms for a microtubule polymerase. *Science, 337*, 857-860.

Baas, P. W., & Lin, S. (2011). Hooks and comets: the story of microtubule polarity orientation in the neuron. *Developmental neurobiology, 71*(6), 403-418.

Balakirev, M. Y., Mullally, J. E., Favier, A., Assard, N., Sulpice, E., Lindsey, D. F., . . . Wilkinson, K. D. (2015). Wss1 metalloprotease partners with Cdc48/Doa1 in processing genotoxic SUMO conjugates. *Elife, 4*, e06763.

Barbier, P., Zejneli, O., Martinho, M., Lasorsa, A., Belle, V., Smet-Nocca, C., . . . Landrieu, I. (2019). Role of Tau as a microtubule associated protein: structural and functional aspects. *Frontiers in aging neuroscience, 11*, 204.

Barlan, K., & Gelfand, V. I. (2017). Microtubule-Based Transport and the Distribution, Tethering, and Organization of Organelles. *Cold Spring Harbor perspectives in biology, 9*(5), a025817. doi:10.1101/cshperspect.a025817

Barsnes, H., & Vaudel, M. (2018). SearchGUI: A Highly Adaptable Common Interface for Proteomics Search and de Novo Engines. *Journal of Proteome Research, 17*(7), 2552-2555. doi:10.1021/acs.jproteome.8b00175

Bayer, P., Arndt, A., Metzger, S., Mahajan, R., Melchior, F., & Becker, J. (1998). Structure determination of the small ubiquitin-related modifier SUMO-1. *J Mol Biol 280*, 275-286.

Bedalov, A., Hirao, M., Posakony, J., Nelson, M., & Simon, J. A. (2003). NAD+-dependent deacetylase Hst1p controls biosynthesis and cellular NAD+ levels in Saccharomyces cerevisiae. *Molecular and Cellular Biology, 23*(19), 7044-7054.

Bellanger, J. M., & Gönczy, P. (2003). TAC-1 and ZYG-9 form a complex that promotes microtubule assembly in C. elegans embryos. *Curr Biol, 13*(17), 1488-1498. doi:10.1016/s0960-9822(03)00582-7

Bencsath, K.P., Podgorski, M.S., Pagala, V.R., Slaughter, C.A., and Schulman, B.A. (2002). Identification of a multifunctional binding site on Ubc9p required for Smt3p conjugation. J Biol Chem 277, 47938-47945.

Bermúdez-López, M., Ceschia, A., de Piccoli, G., Colomina, N., Pasero, P., Aragón, L., & Torres-Rosell, J. (2010). The Smc5/6 complex is required for dissolution of DNA-mediated sister chromatid linkages. *Nucleic Acids Res, 38*(19), 6502-6512.

Berndsen, C. E., Albaugh, B. N., Tan, S., & Denu, J. M. (2007). Catalytic mechanism of a MYST family histone acetyltransferase. *Biochemistry, 46*(3), 623-629.

Biggins, S. (2013). The composition, functions, and regulation of the budding yeast kinetochore. *Genetics, 194*(4), 817-846.

Blake-Hodek, K. A., Cassimeris, L., & Huffaker, T. C. (2010). Regulation of microtubule dynamics by Bim1 and Bik1, the budding yeast members of the EB1 and CLIP-170 families of plus-end tracking proteins. *Molecular biology of the cell, 21*(12), 2013-2023. doi:10.1091/mbc.E10-02-0083

Blander, G., & Guarente, L. (2004). The Sir2 family of protein deacetylases. *Annu Rev Biochem, 73*(1), 417-435.

Bloom, K. (2000). It's a kar9ochore to capture microtubules. Nat Cell Biol 2, E96-98.

Bossis, G., Malnou, C.E., Farras, R., Andermarcher, E., Hipskind, R., Rodriguez, M., Schmidt, D., Muller, S., Jariel-Encontre, I., and Piechaczyk, M. (2005). Down-regulation of c-Fos/c-Jun AP-1 dimer activity by sumoylation. Mol Cell Biol 25, 6964-6979.

Borges, V., Lehane, C., Lopez-Serra, L., Flynn, H., Skehel, M., Ben-Shahar, T. R., & Uhlmann, F. (2010). Hos1 deacetylates Smc3 to close the cohesin acetylation cycle. *Molecular Cell, 39*(5), 677-688.

Brouhard, G. J., Stear, J. H., Noetzel, T. L., Al-Bassam, J., Kinoshita, K., Harrison, S. C., . . . Hyman, A. A. (2008). XMAP215 is a processive microtubule polymerase. *Cell, 132*(1), 79-88. doi:10.1016/j.cell.2007.11.043

Burgess, R. J., Zhou, H., Han, J., & Zhang, Z. (2010). A Role for Gcn5 in Replication-Coupled Nucleosome Assembly. *Molecular Cell, 37*(4), 469-480. doi:10.1016/j.molcel.2010.01.020

Burke, D., Gasdaska, P., and Hartwell, L. (1989). Dominant effects of tubulin overexpression in Saccharomyces cerevisiae. Mol Cell Biol 9, 1049-1059.

Bylebyl, G.R., Belichenko, I., and Johnson, E.S. (2003). The SUMO isopeptidase Ulp2 prevents accumulation of SUMO chains in yeast. J Biol Chem 278, 44113-44120.

Cai, L., Sutter, Benjamin M., Li, B., & Tu, Benjamin P. (2011). Acetyl-CoA Induces Cell Growth and Proliferation by Promoting the Acetylation of Histones at Growth Genes. *Molecular Cell, 42*(4), 426-437. doi:10.1016/j.molcel.2011.05.004

Cairns, N. J., Bigio, E. H., Mackenzie, I. R., Neumann, M., Lee, V. M.-Y., Hatanpaa, K. J., . . . Halliday, G. (2007). Neuropathologic diagnostic and nosologic criteria for frontotemporal lobar degeneration: consensus of the Consortium for Frontotemporal Lobar Degeneration. *Acta Neuropathol, 114*(1), 5-22.

Cappadocia, L., Mascle, X. H., Bourdeau, V., Tremblay-Belzile, S., Chaker-Margot, M., Lussier-Price, M., . . . Ferbeyre, G. (2015). Structural and functional characterization of the phosphorylation-dependent interaction between PML and SUMO1. *Structure, 23*(1), 126-138.

Carle, G. F., & Olson, M. V. (1985). An electrophoretic karyotype for yeast. *Proceedings of the National Academy of Sciences, 82*(11), 3756-3760. doi:10.1073/pnas.82.11.3756

Carlier, M. F., & Pantaloni, D. (1981). Kinetic analysis of guanosine 5'-triphosphate hydrolysis associated with tubulin polymerization. *Biochemistry, 20*(7), 1918-1924.

Carmen, A. A., Griffin, P. R., Calaycay, J. R., Rundlett, S. E., Suka, Y., & Grunstein, M. (1999). Yeast HOS3 forms a novel trichostatin A-insensitive homodimer with intrinsic histone deacetylase activity. *Proceedings of the National Academy of Sciences, 96*(22), 12356-12361. doi:10.1073/pnas.96.22.12356

Carrozza, M. J., Utley, R. T., Workman, J. L., & Côté, J. (2003). The diverse functions of histone acetyltransferase complexes. *Trends in Genetics, 19*(6), 321-329.

Chambers, M. C., Maclean, B., Burke, R., Amodei, D., Ruderman, D. L., Neumann, S., . . . Mallick, P. (2012). A cross-platform toolkit for mass spectrometry and proteomics. *Nature Biotechnology, 30*(10), 918-920. doi:10.1038/nbt.2377

Chang, C.-C., Naik, Mandar T., Huang, Y.-S., Jeng, J.-C., Liao, P.-H., Kuo, H.-Y., . . . Shih, H.-M. (2011). Structural and Functional Roles of Daxx SIM Phosphorylation in SUMO Paralog-Selective Binding and Apoptosis Modulation. *Molecular Cell, 42*(1), 62-74. doi:https://doi.org/10.1016/j.molcel.2011.02.022

Charrasse, S., Schroeder, M., Gauthier-Rouviere, C., Ango, F., Cassimeris, L., Gard, D. L., & Larroque, C. (1998). The TOGp protein is a new human microtubule-associated protein homologous to the Xenopus XMAP215. *Journal of Cell Science, 111*(10), 1371-1383.

Chen, X. P., Yin, H., & Huffaker, T. C. (1998). The yeast spindle pole body component Spc72p interacts with Stu2p and is required for proper microtubule assembly. *The Journal of cell biology, 141*(5), 1169-1179. Retrieved from http://www.ncbi.nlm.nih.gov/cgi-bin/Entrez/referer?http://www.jcb.org/cgi/content/full/141/5/1169

Cheng, C. H., Lo, Y. H., Liang, S. S., Ti, S. C., Lin, F. M., Yeh, C. H., . . . Wang, T. F. (2006). SUMO modifications control assembly of synaptonemal complex and polycomplex in meiosis of Saccharomyces cerevisiae. *Genes Dev, 20*(15), 2067-2081. doi:10.1101/gad.1430406

Choudhary, C., Kumar, C., Gnad, F., Nielsen, M. L., Rehman, M., Walther, T. C., . . . Mann, M. (2009). Lysine acetylation targets protein complexes and co-regulates major cellular functions. *Science, 325*(5942), 834-840.

Chung, I., & Zhao, X. (2013). A STUbL wards off telomere fusions. *EMBO J, 32*(6), 775-777. doi:10.1038/emboj.2013.39

Ciechanover, A. (1994). The ubiquitin-proteasome proteolytic pathway. *Cell, 79*(1), 13-21. doi:10.1016/0092-8674(94)90396-4

Cohen, T. J., Guo, J. L., Hurtado, D. E., Kwong, L. K., Mills, I. P., Trojanowski, J. Q., & Lee, V. M. (2011). The acetylation of tau inhibits its function and promotes pathological tau aggregation. *Nature communications, 2*(1), 1-9.

Coquelle, F.M., Caspi, M., Cordelieres, F.P., Dompierre, J.P., Dujardin, D.L., Koifman, C., Martin, P., Hoogenraad, C.C., Akhmanova, A., Galjart, N., et al. (2002). LIS1, CLIP-170's key to the dynein/dynactin pathway. Molecular and Cellular Biology 22, 3089-3102.

Cullen, C. F., Deák, P., Glover, D. M., & Ohkura, H. (1999). mini spindlesa gene encoding a conserved microtubule-associated protein required for the integrity of the mitotic spindle in Drosophila. *Journal of Cell Biology, 146*(5), 1005-1018.

Cullen, C. F., & Ohkura, H. (2001). Msps protein is localized to acentrosomal poles to ensure bipolarity of Drosophila meiotic spindles. *Nature Cell Biology, 3*(7), 637-642. doi:10.1038/35083025

Desai, A., & Mitchison, T. J. (1997). Microtubule polymerization dynamics. *Annu Rev Cell Dev Biol, 13*, 83-117. doi:10.1146/annurev.cellbio.13.1.83

Desterro, J. M., Rodriguez, M. S., Kemp, G. D., & Hay, R. T. (1999). Identification of the enzyme required for activation of the small ubiquitin-like protein SUMO-1. *J Biol Chem, 274*(15), 10618-10624. Retrieved from http://www.ncbi.nlm.nih.gov/pubmed/10187858

Dohmen, R. J., Stappen, R., McGrath, J. P., Forrova, H., Kolarov, J., Goffeau, A., & Varshavsky, A. (1995). An essential yeast gene encoding a homolog of ubiquitin-activating enzyme. *J Biol Chem, 270*(30), 18099-18109. Retrieved from http://www.ncbi.nlm.nih.gov/pubmed/7629121

Dorval, V., & Fraser, P. E. (2006). Small ubiquitin-like modifier (SUMO) modification of natively unfolded proteins tau and alpha-synuclein. *J Biol Chem, 281*(15), 9919-9924.

Driscoll, R., Hudson, A., & Jackson, S. P. (2007). Yeast Rtt109 Promotes Genome Stability by Acetylating Histone H3 on Lysine 56. *Science, 315*(5812), 649-652. doi:10.1126/science.1135862

Duan, X., Holmes, W. B., & Ye, H. (2011). Interaction mapping between *Saccharomyces cerevisiae* Smc5 and SUMO E3 ligase Mms21. *Biochemistry, 50*(46), 10182-10188. doi:10.1021/bi201376e

Duffy, S. K., Friesen, H., Baryshnikova, A., Lambert, J.-P., Chong, Y. T., Figeys, D., & Andrews, B. (2012). Exploring the yeast acetylome using functional genomics. *Cell, 149*(4), 936-948.

Elmore, Z.C., Donaher, M., Matson, B.C., Murphy, H., Westerbeck, J.W., and Kerscher, O. (2011). SUMO-dependent substrate targeting of the SUMO protease Ulp1. BMC Biol 9, 74.

Elia, A. E., Boardman, A. P., Wang, D. C., Huttlin, E. L., Everley, R. A., Dephoure, N., . . . Elledge, S. J. (2015). Quantitative proteomic atlas of ubiquitination and acetylation in the DNA damage response. *Molecular Cell, 59*(5), 867-881.

Escobar-Ramirez, A., Vercoutter-Edouart, A.-S., Mortuaire, M., Huvent, I., Hardivillé, S., Hoedt, E., . . . Pierce, A. (2015). Modification by SUMOylation controls both the transcriptional activity and the stability of delta-lactoferrin. *PLoS One, 10*(6).

Eshel, D., Urrestarazu, L. A., Vissers, S., Jauniaux, J. C., van Vliet-Reedijk, J. C., Planta, R. J., & Gibbons, I. R. (1993). Cytoplasmic dynein is required for normal nuclear segregation in yeast. *Proceedings of the National Academy of Sciences of the United States of America, 90*(23), 11172-11176.

Eshun-Wilson, L., Zhang, R., Portran, D., Nachury, M. V., Toso, D. B., Löhr, T., . . . Nogales, E. (2019). Effects of α-tubulin acetylation on microtubule structure and stability. *Proceedings of the National Academy of Sciences, 116*(21), 10366-10371.

Fang, S., & Weissman, A. M. (2004). A field guide to ubiquitylation. *Cell Mol Life Sci, 61*(13), 1546-1561. doi:10.1007/s00018-004-4129-5

Finkbeiner, E., Haindl, M., Raman, N., & Muller, S. (2011). SUMO routes ribosome maturation. *Nucleus, 2*(6), 527-532.

Finkel, T., Deng, C.-X., & Mostoslavsky, R. (2009). Recent progress in the biology and physiology of sirtuins. *Nature, 460*(7255), 587-591.

Franck, A. D., Powers, A. F., Gestaut, D. R., Gonen, T., Davis, T. N., & Asbury, C. L. (2007). Tension applied through the Dam1 complex promotes microtubule elongation providing a direct mechanism for length control in mitosis. *Nature Cell Biology, 9*(7), 832-837.

Galdieri, L., Zhang, T., Rogerson, D., Lleshi, R., & Vancura, A. (2014). Protein acetylation and acetyl coenzyme a metabolism in budding yeast. *Eukaryotic Cell, 13*(12), 1472-1483.

Garcia-Domiquez, M., & Reyes, J. C. (2009). SUMO association with repressor complexes, emerging routes for transcriptional control. *Biochim Biophys Acta, 1789*, 451-459.

Garcia, M. A., Vardy, L., Koonrugsa, N., & Toda, T. (2001). Fission yeast ch‐TOG/XMAP215 homologue Alp14 connects mitotic spindles with the kinetochore and is a component of the Mad2‐dependent spindle checkpoint. *EMBO J, 20*(13), 3389-3401.

Gareau, J. R., & Lima, C. D. (2010). The SUMO pathway: emerging mechanisms that shape specificity, conjugation and recognition. *Nat Rev Mol Cell Biol, 11*, 861-871.

Geissler, S., Pereira, G., Spang, A., Knop, M., Soues, S., Kilmartin, J., & Schiebel, E. (1996). The spindle pole body component Spc98p interacts with the gamma-tubulin- like Tub4p of Saccharomyces cerevisiae at the sites of microtubule attachment [published erratum appears in EMBO J 1996 Sep 16;15(18):5124]. *Embo J, 15*(15), 3899-3911. Retrieved from http://www.ncbi.nlm.nih.gov/cgi-bin/Entrez/referer?http://www.oup.co.uk/jnls/list/embojo/hdb/Volume_15/Issue_15/153899.sgm.abs.html

Gelperin, D.M., White, M.A., Wilkinson, M.L., Kon, Y., Kung, L.A., Wise, K.J., Lopez-Hoyo, N., Jiang, L., Piccirillo, S., Yu, H., et al. (2005). Biochemical and genetic analysis of the yeast proteome with a movable ORF collection. Genes Dev 19, 2816-2826.

Gombos, L., Neuner, A., Berynskyy, M., Fava, L. L., Wade, R. C., Sachse, C., & Schiebel, E. (2013). GTP regulates the microtubule nucleation activity of γ-tubulin. *Nature Cell Biology, 15*(11), 1317-1327.

Greenberg, C. H., Kollman, J., Zelter, A., Johnson, R., MacCoss, M. J., Davis, T. N., . . . Sali, A. (2016). Structure of γ-tubulin small complex based on a cryo-EM map, chemical cross-links, and a remotely related structure. *Journal of structural biology, 194*(3), 303-310.

Greenlee, M., Alonso, A., M., R., Meednu, N., Davis, K., Crawford, R., & Miller, R. K. (2018). the TOG protein Stu2/XMAP215 binds covalently and non-covalently to SUMO. *Cytoskeleton (Hoboken)*.

Grishchuk, E. L., Efremov, A. K., Volkov, V. A., Spiridonov, I. S., Gudimchuk, N., Westermann, S., . . . Ataullakhanov, F. I. (2008). The Dam1 ring binds microtubules strongly enough to be a processive as well as energy-efficient coupler for chromosome motion. *Proc Natl Acad Sci U S A, 105*(40), 15423-15428. doi:10.1073/pnas.0807859105

Gu, W., & Roeder, R. G. (1997). Activation of p53 sequence-specific DNA binding by acetylation of the p53 C-terminal domain. *Cell, 90*(4), 595-606.

Gundersen, G.G., and Bretscher, A. (2003). Microtubule Asymmetry. Science 300, 2040.

Gunzelmann, J., Rüthnick, D., Lin, T.-c., Zhang, W., Neuner, A., Jäkle, U., & Schiebel, E. (2018). The microtubule polymerase Stu2 promotes oligomerization of the γ-TuSC for cytoplasmic microtubule nucleation. *Elife, 7*, e39932.

Guzzo, C. M., Berndsen, C. E., Zhu, J., Gupta, V., Datta, A., Greenberg, R. A., . . . Matunis, M. J. (2012). RNF4-dependent hybrid SUMO-ubiquitin chains are signals for RAP80 and thereby mediate the recruitment of BRCA1 to sites of DNA damage. *Sci Signal, 5*(253), ra88. doi:10.1126/scisignal.2003485

Haase, K.P., Fox, J.C., Byrnes, A.E., Adikes, R.C., Speed, S.K., Haase, J., Friedman, B., Cook, D.M., Bloom, K., Rusan, N.M., et al. (2017). Stu2 uses a 15 nm parallel coiled coil for kinetochore localization and concomitant regulation of the mitotic spindle. Mol Biol Cell.

Hannich, J. T., Lewis, A., Kroetz, M. B., Li, S.-J., Heide, H., Emili, A., & Hochstrasser, M. (2005). Defining the SUMO-modified proteome by multiple approaches in Saccharomyces cerevisiae. *Journal of Biological Chemistry, 280*(6), 4102-4110.

Hecker, C. M., Rabiller, M., Haglund, K., Bayer, P., & Dikic, I. (2006). Specification of SUMO1- and SUMO2-interacting motifs. *J Biol Chem, 281*(23), 16117-16127. doi:10.1074/jbc.M512757200

Heideker, J., Prudden, J., Perry, J. J. P., Tainer, J. A., & Boddy, M. N. (2011). SUMO-targeted ubiquitin ligase, Rad60, and Nse2 SUMO ligase suppress spontaneous Top1-mediated DNA damage and genome instability. *PLOS Genetics, 7*(3), e10001320.

Hendriks, I. A., Lyon, D., Young, C., Jensen, L. J., Vertegaal, A. C., & Nielsen, M. L. (2017). Site-specific mapping of the human SUMO proteome reveals co-modification with phosphorylation. *Nat Struct Mol Biol, 24*(3), 325-336. doi:10.1038/nsmb.3366

Henriksen, P., Wagner, S. A., Weinert, B. T., Sharma, S., Bačinskaja, G., Rehman, M., . . . Choudhary, C. (2012). Proteome-wide analysis of lysine acetylation suggests its broad regulatory scope in Saccharomyces cerevisiae. *Molecular & Cellular Proteomics, 11*(11), 1510-1522.

Hochstrasser, M. (2001). SP-RING for SUMO: new functions bloom for a ubiquitin-like protein. *Cell, 107*(1), 5-8.

Hoege, C., Pfander, B., Moldovan, G. L., Pyrowolakis, G., & Jentsch, S. (2002). RAD6-dependent DNA repair is linked to modification of PCNA by ubiquitin and SUMO. *Nature, 419*(6903), 135-141. doi:10.1038/nature00991

Hofmann, K., & Falquet, L. (2001). A ubiquitin-interacting motif conserved in components of the proteasomal and lysosomal protein degradation systems. *Trends Biochem Sci, 26*(6), 347-350. doi:10.1016/s0968-0004(01)01835-7

Horigome, C., Bustard, D. E., Marcomini, I., Delgoshaie, N., Tsai-Pflugfelder, M., Cobb, J. A., & Gasser, S. M. (2016). PolySUMOylation by Siz2 and Mms21 triggers relocation of DNA breaks to nuclear pores through the Slx5/Slx8 STUbL. *Genes Dev, 30*(8), 931-945.

Howe, L., Auston, D., Grant, P., John, S., Cook, R. G., Workman, J. L., & Pillus, L. (2001). Histone H3 specific acetyltransferases are essential for cell cycle progression. *Genes Dev, 15*(23), 3144-3154.

Howes, S. C., Geyer, E. A., LaFrance, B., Zhang, R., Kellogg, E. H., Westermann, S., . . . Nogales, E. (2017). Structural differences between yeast and mammalian microtubules revealed by cryo-EM. *Journal of Cell Biology, 216*(9), 2669-2677.

Hu, X., Paul, A., & Wang, B. (2012). Rap80 protein recruitment to DNA double-strand breaks requires binding to both small ubiquitin-like modifier (SUMO) and ubiquitin conjugates. *Journal of Biological Chemistry, 287*(30), 25510-25519.

Huffaker, T. C., Thomas, J. H., & Botstein, D. (1988). Diverse effects of beta-tubulin mutations on microtubule formation and function. *The Journal of cell biology, 106*(6), 1997-2010.

Humphrey, L., Felzer-Kim, I., & Joglekar, A. P. (2018). Stu2 acts as a microtubule destabilizer in metaphase budding yeast spindles. *Mol Biol Cell, 29*(3), 247-255.

Hutton, M., Lendon, C. L., Rizzu, P., Baker, M., Froelich, S., Houlden, H., . . . Grover, A. (1998). Association of missense and 5′ -splice-site mutations in tau with the inherited dementia FTDP-17. *Nature, 393*(6686), 702-705.

Hyman, A. A., Salser, S., Drechsel, D. N., Unwin, N., & Mitchison, T. J. (1992). Role of GTP hydrolysis in microtubule dynamics: information from a slowly hydrolyzable analogue, GMPCPP. *Molecular biology of the cell, 3*(10), 1155-1167. Retrieved from http://www.ncbi.nlm.nih.gov/htbin-post/Entrez/query?db=m&form=6&dopt=r&uid=1421572

Irwin, D. J., Cohen, T. J., Grossman, M., Arnold, S. E., Xie, S. X., Lee, V. M.-Y., & Trojanowski, J. Q. (2012). Acetylated tau, a novel pathological signature in Alzheimer's disease and other tauopathies. *Brain, 135*(3), 807-818.

Irwin, D. J., Lee, V. M.-Y., & Trojanowski, J. Q. (2013). Parkinson's disease dementia: convergence of α-synuclein, tau and amyloid-β pathologies. *Nature Reviews Neuroscience, 14*(9), 626-636.

James, P., Halladay, J., and Craig, E.A. (1996). Genomic libraries and a host strain designed for highly efficient two- hybrid selection in yeast. Genetics 144, 1425-1436.

Jardin, C., Horn, A.H., and Sticht, H. (2015). Binding properties of SUMO-interacting motifs (SIMs) in yeast. J Mol Model 21, 50.

Johnson, E. S. (2004). Protein Modification by SUMO. *Annu Rev Biochem, 73*, 355-382.

Johnson, E. S., & Blobel, G. (1997). Ubc9p is the conjugating enzyme for the ubiquitin-like protein Smt3p. *J Biol Chem, 272*(43), 26799-26802.

Johnson, E. S., & Blobel, G. (1999). Cell cycle-regulated attachment of the ubiquitin-related protein SUMO to the yeast septins. *The Journal of cell biology, 147*(5), 981-994.

Johnson, E. S., & Gupta, A. A. (2001). An E3-like factor that promotes SUMO conjugation to the yeast septins. *Cell, 106*, 735-744.

Johnson, E. S., Schwienhorst, Dohmen, R. J., & and Blobel, G. (1997). The ubiquitin-like protein Smt3p is activated for conjugation to other proteins by an Aos1p/Uba2p heterodimer. *EMBO J, 16*(18), 5509-5519.

Kagey, M. H., Melhuish, T. A., & Wotton, D. (2003). The polycomb protein Pc2 is a SUMO E3. *Cell, 113*(1), 127-137. Retrieved from http://www.ncbi.nlm.nih.gov/pubmed/12679040

Katz, W., Weinstein, B., and Solomon, F. (1990). Regulation of tubulin levels and microtubule assembly in Saccharomyces cerevisiae: consequences of altered tubulin gene copy number. Mol Cell Biol 10, 5286-5294.

Kaul, N., Soppina, V., & Verhey, K. J. (2014). Effects of α-tubulin K40 acetylation and detyrosination on kinesin-1 motility in a purified system. *Biophysical journal, 106*(12), 2636-2643.

Kersher, O., Felberbaum, R., and Hochstrasser, M. (2006). Modification of proteins by ubiquitin and ubiquitin-like proteins. Ann. Rev. Cell Dev. Biol 22, 159-180.

Kerscher, O. (2007). SUMO junction-what's your function? New insights through SUMO-interacting motifs. *EMBO Rep, 8*(6), 550-555. doi:10.1038/sj.embor.7400980

Kim, D.-H., Harris, B., Wang, F., Seidel, C., McCroskey, S., & Gerton, J. L. (2016). Mms21 SUMO ligase activity promotes nucleolar function in Saccharomyces cerevisiae. *Genetics, 204*(2), 645-658.

Kim, E. T., Kim, K. K., Matunis, M. J., & Ahn, J.-H. (2009). Enhanced SUMOylation of proteins containing a SUMO-interacting motif by SUMO-Ubc9 fusion. *Biochem Biophys Res Commun, 388*(1), 41-45.

Kim, H.-S., Vassilopoulos, A., Wang, R.-H., Lahusen, T., Xiao, Z., Xu, X., . . . Yu, H. (2011). SIRT2 maintains genome integrity and suppresses tumorigenesis through regulating APC/C activity. *Cancer Cell, 20*(4), 487-499.

Kim, S. C., Sprung, R., Chen, Y., Xu, Y., Ball, H., Pei, J., . . . Xiao, L. (2006). Substrate and functional diversity of lysine acetylation revealed by a proteomics survey. *Molecular Cell, 23*(4), 607-618.

Kim, W., Bennett, E. J., Huttlin, E. L., Guo, A., Li, J., Possemato, A., . . . Comb, M. J. (2011). Systematic and quantitative assessment of the ubiquitin-modified proteome. *Molecular Cell, 44*(2), 325-340.

Kimura, A., Umehara, T., & Horikoshi, M. (2002). Chromosomal gradient of histone acetylation established by Sas2p and Sir2p functions as a shield against gene silencing. *Nat Genet, 32*(3), 370-377.

Kinoshita, K., Noetzel, T. L., Pelletier, L., Mechtler, K., Drechsel, D. N., Schwager, A., . . . Hyman, A. A. (2005). Aurora A phosphorylation of TACC3/maskin is required for centrosome-dependent microtubule assembly in mitosis. *J Cell Biol, 170*(7), 1047-1055. doi:10.1083/jcb.200503023

Kitamura, E., Tanaka, K., Komoto, S., Kitamura, Y., Antony, C., and Tanaka, T.U. (2010). Kinetochores generate microtubules with distal plus ends: their roles and limited lifetime in mitosis. Dev Cell 18, 248-259.

Knipscheer, P., Flotho, A., Klug, H., Olsen, J. V., van Dijk, W. J., Fish, A., . . . Pichler, A. (2008). Ubc9 sumoylation regulates SUMO target discrimination. *Mol Cell, 31*(3), 371-382. doi:10.1016/j.molcel.2008.05.022

Knop, M., Pereira, G., Geissler, S., Grein, K., & Schiebel, E. (1997). The spindle pole body component Spc97p interacts with the gamma-tubulin of Saccharomyces cerevisiae and functions in microtubule organization and spindle pole body duplication. *Embo J, 16*(7), 1550-1564. Retrieved from http://www.ncbi.nlm.nih.gov/cgi-bin/Entrez/referer?http://www.emboj.org/cgi/content/full/16/7/1550

Kollman, J. M., Merdes, A., Mourey, L., & Agard, D. A. (2011). Microtubule nucleation by γ-tubulin complexes. *Nature Reviews Molecular Cell Biology, 12*(11), 709-721.

Kollman, J. M., Polka, J. K., Zelter, A., Davis, T. N., & Agard, D. A. (2010). Microtubule nucleating γ-TuSC assembles structures with 13-fold microtubule-like symmetry. *Nature, 466*(7308), 879-882.

Kollman, J. M., Zelter, A., Muller, E. G., Fox, B., Rice, L. M., Davis, T. N., & Agard, D. A. (2008). The structure of the gamma-tubulin small complex: implications of its architecture and flexibility for microtubule nucleation. *Molecular biology of the cell, 19*(1), 207-215. doi:10.1091/mbc.e07-09-0879

Kosco, K.A., Pearson, C.G., Maddox, P.S., Wang, P.J., Adams, I.R., Salmon, E.D., Bloom, K., and Huffaker, T.C. (2001a). Control of microtubule dynamics by Stu2p is essential for spindle orientation and metaphase chromosome alignment in yeast. Mol Biol Cell 12, 2870-2880.

Kosco, K.A., Pearson, C.G., Maddox, P.S., Wang, P.J., Adams, I.R., Salmon, E.D., Bloom, K., and Huffaker, T.C. (2001b). Control of microtubule dynamics by Stu2p is essential for spindle orientation and metaphase chromosome alignment in yeast. Mol Biol Cell 12, 2870-2880.

Krebs, J. E. (2007). Moving marks: dynamic histone modifications in yeast. *Molecular BioSystems, 3*(9), 590-597.

Kroetz, M. B., & Hochstrasser, M. (2009). Identification of SUMO-interacting proteins by yeast two-hybrid analysis. *Methods Mol Biol, 497*, 107-120. doi:10.1007/978-1-59745-566-4_7

Kroll, E. S., Hyland, K. M., Hieter, P., & Li, J. J. (1996). Establishing genetic interactions by a synthetic dosage lethality phenotype. *Genetics, 143*(1), 95-102. Retrieved from https://pubmed.ncbi.nlm.nih.gov/8722765

Kurihara, L. J., Beh, C. T., Latterich, M., Schekman, R., & Rose, M. D. (1994). Nuclear congression and membrane fusion: two distinct events in the yeast karyogamy pathway. *J Cell Biol, 126*(4), 911-923. doi:10.1083/jcb.126.4.911

Lampert, F., Hornung, P., & Westermann, S. (2010). The Dam1 complex confers microtubule plus end-tracking activity to the Ndc80 kinetochore complex. *J Cell Biol, 189*(4), 641-649. doi:10.1083/jcb.200912021

Larsen, C. N., Krantz, B. A., & Wilkinson, K. D. (1998). Substrate specificity of deubiquitinating enzymes: ubiquitin C-terminal hydrolases. *Biochemistry, 37*(10), 3358-3368. doi:10.1021/bi972274d

Lee, L., Tirnauer, J.S., Li, J., Schuyler, S.C., Liu, J.Y., and Pellman, D. (2000). Positioning of the mitotic spindle by a cortical-microtubule capture mechanism. Science 287, 2260-2262.

Lee, M. J., Gergely, F., Jeffers, K., Peak-Chew, S. Y., & Raff, J. W. (2001). Msps/XMAP215 interacts with the centrosomal protein D-TACC to regulate microtubule behaviour. *Nature Cell Biology, 3*(7), 643-649. doi:10.1038/35083033

Lee, W.-L., Oberle, J. R., & Cooper, J. A. (2003). The role of the lissencephaly protein Pac1 during nuclear migration in budding yeast. *J Cell Biol, 160*, 355-364.

Leisner, C., Kammerer, D., Denoth, A., Britschi, M., Barral, Y., & Liakopoulos, D. (2008). Regulation of mitotic spindle asymmetry by SUMO and the spindle-assembly checkpoint in yeast. *Curr Biol, 18*, 1249-1255.

Lescasse, R., Pobiega, S., Callebaut, I., & Marcand, S. (2013). End-joining inhibition at telomeres requires the translocase and polySUMO-dependent ubiquitin ligase Uls1. *EMBO J, 32*(6), 805-815. doi:10.1038/emboj.2013.24

Li, D., Sun, X., Zhang, L., Yan, B., Xie, S., Liu, R., . . . Zhou, J. (2014). Histone deacetylase 6 and cytoplasmic linker protein 170 function together to regulate the motility of pancreatic cancer cells. *Protein & cell, 5*(3), 214-223.

Li, S.-J., & Hochstrasser, M. (1999). A new protease required for cell-cycle progression in yeast. *Nature, 398*, 246-251.

Li, S. J., & Hochstrasser, M. (2000). The yeast *ULP2 (SMT4*) gene encodes a novel protease specific for the ubiquitin-like Smt3 protein. *Mol Cell Biol, 20*(7), 2367-2377.

Li, W., & Ye, Y. (2008). Polyubiquitin chains: functions, structures, and mechanisms. *Cell Mol Life Sci, 65*(15), 2397-2406. doi:10.1007/s00018-008-8090-6

Liakopoulos, D., Kusch, J., Grava, S., Vogel, J., and Barral, Y. (2003). Asymmetric loading of Kar9 onto spindle poles and microtubules ensures proper spindle alignment. Cell 112, 561-574.

Lin, Y.-y., Lu, J.-y., Zhang, J., Walter, W., Dang, W., Wan, J., . . . Boeke, J. D. (2009). Protein acetylation microarray reveals that NuA4 controls key metabolic target regulating gluconeogenesis. *Cell, 136*(6), 1073-1084.

Lin, Y.-y., Qi, Y., Lu, J.-y., Pan, X., Yuan, D. S., Zhao, Y., . . . Boeke, J. D. (2008). A comprehensive synthetic genetic interaction network governing yeast histone acetylation and deacetylation. *Genes Dev, 22*(15), 2062-2074.

Liu, S. S., Hockenberry, A. J., Lancichinetti, A., Jewett, M. C., & Amaral, L. A. N. (2016). NullSeq: A Tool for Generating Random Coding Sequences with Desired Amino Acid and GC Contents. *PLOS Computational Biology, 12*(11), e1005184. doi:10.1371/journal.pcbi.1005184

Lowe, J., Li, H., Downing, K., & Nogales, E. (2001). Refined structure of abtubulin at 3.5 A. *J. Mol. Biol, 313*.

Ludolph, A., Kassubek, J., Landwehrmeyer, B., Mandelkow, E., Mandelkow, E. M., Burn, D., . . . Gasser, T. (2009). Tauopathies with parkinsonism: clinical spectrum, neuropathologic basis, biological markers, and treatment options. *European Journal of Neurology, 16*(3), 297-309.

Lundin, C., North, M., Erixon, K., Walters, K., Jenssen, D., Goldman, A. S., & Helleday, T. (2005). Methyl methanesulfonate (MMS) produces heat-labile DNA damage but no detectable in vivo DNA double-strand breaks. *Nucleic Acids Res, 33*(12), 3799-3811.

Ma, L., McQueeen, J., Cuschieri, L., Vogel, J., and Measday, V. (2007). Spc24 and Stu2 promote spindle integrity when DNA replication is stalled. Molecular Biology of the Cell 18, 2805-2816.

Manka, S. W., & Moores, C. A. (2018). The role of tubulin–tubulin lattice contacts in the mechanism of microtubule dynamic instability. *Nature structural & molecular biology, 25*(7), 607-615.

Markus, S.M., Plevock, K.M., St. Germain, B.J., Punch, J.J., Meaden, C.W., and Lee, W.L. (2011). Quantitative analysis of Pac1/Lis1-mediated dynein targeting: Implications for regulation of dynein activity in budding yeast. Cytoskeleton (Hoboken, N.J.) 68, 157-174.Matsumoto, M. L., Wickliffe, K. E., Dong, K. C., Yu, C., Bosanac, I., Bustos, D., . . . Rape, M. (2010). K11-linked polyubiquitination in cell cycle control revealed by a K11 linkage-specific antibody. *Molecular Cell, 39*(3), 477-484.

McKinsey, T. A., & Olson, E. N. (2004). Cardiac histone acetylation–therapeutic opportunities abound. *Trends in Genetics, 20*(4), 206-213.

Meednu, N., Hoops, H., D'Silva, S., Pogorzala, L., Wood, S., Farkas, D., . . . Miller, R. K. (2008). The spindle positioning protein Kar9p interacts with the sumoylation machinery in *Saccharomyces cerevisiae. Genetics, 180*, 2033-2055.

Melchior, F. (2000). SUMO-nonclassical ubiquitin. *Annu Rev Cell Dev Biol, 16*, 591-626.

Mevissen, T. E. T., & Komander, D. (2017). Mechanisms of Deubiquitinase Specificity and Regulation. *Annu Rev Biochem, 86*, 159-192. doi:10.1146/annurev-biochem-061516-044916

Millar, C. B., & Grunstein, M. (2006). Genome-wide patterns of histone modifications in yeast. *Nature Reviews Molecular Cell Biology, 7*(9), 657-666. doi:10.1038/nrm1986

Miller, M. P., Asbury, C. L., & Biggins, S. (2016). A TOG protein confers tension sensitivity to kinetochore-microtubule attachments. *Cell, 165*(6), 1428-1439. doi:10.1016/j.cell.2016.04.030

Miller, M. P., Evans, R. K., Zelter, A., Geyer, E. A., MacCoss, M. J., Rice, L. M., . . . Biggins, S. (2019). Kinetochore-associated Stu2 promotes chromosome biorientation in vivo. *PLoS Genet, 15*(10), e1008423. doi:10.1371/journal.pgen.1008423

Miller, R.K., Cheng, S.-C., and Rose, M.D. (2000). Bim1p/Yeb1p mediates the Kar9p-dependent cortical attachment of cytoplasmic microtubules. Mol Biol Cell 11, 2949-2959.

Miller, R.K., Matheos, D., and Rose, M.D. (1999). The cortical localization of the microtubule orientation protein, Kar9p, is dependent upon actin and proteins required for polarization. J Cell Biol 144, 963-975.

Miller, R. K., & Rose, M. D. (1998). Kar9p is a novel cortical protein required for cytoplasmic microtubule orientation in yeast. *The Journal of cell biology, 140*(2), 377-390. Retrieved from http://www.ncbi.nlm.nih.gov/cgi-bin/Entrez/referer?http://www.jcb.org/cgi/content/full/140/2/377

Min, S.-W., Chen, X., Tracy, T. E., Li, Y., Zhou, Y., Wang, C., . . . Mok, S. A. (2015). Critical role of acetylation in tau-mediated neurodegeneration and cognitive deficits. *Nature medicine, 21*(10), 1154.

Min, S.-W., Cho, S.-H., Zhou, Y., Schroeder, S., Haroutunian, V., Seeley, W. W., . . . Gan, L. (2010). Acetylation of tau inhibits its degradation and contributes to tauopathy. *Neuron, 67*(6), 953-966. doi:10.1016/j.neuron.2010.08.044

Minty, A., Dumont, X., Kaghad, M., & Caput, D. (2000). Covalent modification of p73alpha by SUMO-1. Two-hybrid screening with p73 identifies novel SUMO-1-interacting proteins and a SUMO-1 interaction motif. *J Biol Chem, 275*(46), 36316-36323. doi:10.1074/jbc.M004293200

Miranda, M., & Sorkin, A. (2007). Regulation of receptors and transporters by ubiquitination: new insights into surprisingly similar mechanisms. *Mol Interv, 7*(3), 157-167. doi:10.1124/mi.7.3.7

Mitchison, T., & Kirschner, M. (1984a). Dynamic instability of microtubule growth. *Nature, 312*(5991), 237-242.

Mitchison, T., & Kirschner, M. (1984b). Microtubule assembly nucleated by isolated centrosomes. *Nature, 312*(5991), 232-237.

Montelone, B. A., & Koelliker, K. J. (1995). Interactions among mutations affecting spontaneous mutation, mitotic recombination, and DNA repair in yeast. *Current genetics, 27*(2), 102-109.

Montpetit, B., Hazbun, T. R., Fields, S., & Hieter, P. (2006). Sumoylation of the budding yeast kinetochore protein Ndc10 is required for Ndc10 spindle localization and regulation of anaphase spindle elongation. *The Journal of cell biology, 174*(5), 653-663.

Moore, J.K., D'Silva, S., and Miller, R.K. (2006). The CLIP-170 homologue Bik1p promotes the phosphorylation and asymmetric localization of Kar9p. Mol Biol Cell 17, 178-191.

Moore, J.K., Li, J., and Cooper, J.A. (2008). Dynactin function in mitotic spindle positioning. Traffic 9, 510-527.

Moore, J.K., and Miller, R.K. (2007). The cyclin-dependent kinase Cdc28p regulates multiple aspects of Kar9p function in yeast. Mol Biol Cell 18, 1187-1202.

Morris, J. R., & Solomon, E. (2004). BRCA1: BARD1 induces the formation of conjugated ubiquitin structures, dependent on K6 of ubiquitin, in cells during DNA replication and repair. *Human Molecular Genetics, 13*(8), 807-817.

Mullen, J. R., Kaliraman, V., Ibrahim, S. S., & Brill, S. J. (2001). Requirement for three novel protein complexes in the absence of the Sgs1 DNA helicase in Saccharomyces cerevisiae. *Genetics, 157*(1), 103-118. Retrieved from http://www.ncbi.nlm.nih.gov/pubmed/11139495

Nagai, S., Davoodi, N., & Gasser, S. M. (2011). Nuclear organization in genome stability: SUMO connections. *Cell Res, 21*(3), 474-485. doi:10.1038/cr.2011.31

Naik, M. T., Kang, M., Ho, C.-C., Liao, P.-H., Hsieh, Y.-L., Naik, N. M., . . . Huang, T.-H. (2017). Molecular mechanism of K65 acetylation-induced attenuation of Ubc9 and the NDSM interaction. *Scientific Reports, 7*(1), 17391. doi:10.1038/s41598-017-17465-0

Namanja, A. T., Li, Y.-J., Su, Y., Wong, S., Lu, J., Colson, L. T., . . . Chen, Y. (2012). Insights into high affinity small ubiquitin-like modifier (SUMO) recognition by SUMO-interacting motifs (SIMs) revealed by a combination of NMR and peptide array analysis. *Journal of Biological Chemistry, 287*(5), 3231-3240.

Newman, H.A., Meluh, P.B., Lu, J., Vidal, J., Carson, C., Lagesse, E., Gray, J.J., Boeke, J.D., and Matunis, M.J. (2017). A high throughput mutagenic analysis of yeast sumo structure and function. PLoS Genet 13, e1006612.

Nguyen, T., Vinh, D. B., Crawford, D. K., & Davis, T. N. (1998). A genetic analysis of interactions with Spc110p reveals distinct functions of Spc97p and Spc98p, components of the yeast gamma-tubulin complex. *Mol Biol Cell, 9*(8), 2201-2216. doi:10.1091/mbc.9.8.2201

Nishikawa, H., Ooka, S., Sato, K., Arima, K., Okamoto, J., Klevit, R. E., . . . Ohta, T. (2004). Mass spectrometric and mutational analyses reveal Lys-6-linked polyubiquitin chains catalyzed by BRCA1-BARD1 ubiquitin ligase. *Journal of Biological Chemistry, 279*(6), 3916-3924.

Nithianantham, S., Cook, B. D., Beans, M., Guo, F., Chang, F., & Al-Bassam, J. (2018). Structural basis of tubulin recruitment and assembly by microtubule polymerases with tumor overexpressed gene (TOG) domain arrays. *Elife, 7*, e38922. doi:10.7554/eLife.38922

Nogales, E. WS (1998). Structure of the alpha beta tubulin dimer by electron crystallography. In: Nauture.

Nogales, E., & Wang, H.-W. (2006). Structural mechanisms underlying nucleotide-dependent self-assembly of tubulin and its relatives. *Current opinion in structural biology, 16*(2), 221-229.

North, B. J., & Verdin, E. (2004). Sirtuins: Sir2-related NAD-dependent protein deacetylases. *Genome Biol, 5*(5), 224-224. doi:10.1186/gb-2004-5-5-224

Okada, N., Toda, T., Yamamoto, M., & Sato, M. (2014). CDK-dependent phosphorylation of Alp7-Alp14 (TACC-TOG) promotes its nuclear accumulation and spindle microtubule assembly. *Mol Biol Cell, 25*(13), 1969-1982. doi:10.1091/mbc.E13-11-0679

Okuma, T., Honda, R., Ichikawa, G., Tsumagari, N., & Yasuda, H. (1999). In vitro SUMO-1 modification requires two enzymatic steps, E1 and E2. *Biochemical & Biophysical Research Communications, 254*(3), 693-698.

Ouspenski, I. I., Elledge, S. J., & Brinkley, B. (1999). New yeast genes important for chromosome integrity and segregation identified by dosage effects on genome stability. *Nucleic Acids Res, 27*(15), 3001-3008.

Ouyang, J., Valin, A., & Gill, G. (2009). Regulation of transcription factor activity by SUMO modification. *Methods Mol Biol, 497*, 141-152.

Ozkaynak, E., Finley, D., Solomon, M. J., & Varshavsky, A. (1987). The yeast ubiquitin genes: a family of natural gene fusions. *EMBO J, 6*(5), 1429-1439. Retrieved from http://www.ncbi.nlm.nih.gov/pubmed/3038523

Papouli, E., Chen, S., Davies, A. A., Huttner, D., Krejci, L., Sung, P., & Ulrich, H. D. (2005). Crosstalk between SUMO and ubiquitin on PCNA is mediated by recruitment of the helicase Srs2p. *Molecular Cell, 19*(1), 123-133.

Park, C.J., Park, J.-E., Karpova, T.S., Soung, N.-K., Yu, L.-R., Song, S., Lee, K.H., Xia, X., Kang, E., Dabanoglu, I., et al. (2008). Requirement for the budding yeast polo kinase Cdc5 in proper microtubule growth and dynamics. Eukaryot Cell 7, 444-453.

Parthun, M. R., Widom, J., & Gottschling, D. E. (1996). The Major Cytoplasmic Histone Acetyltransferase in Yeast: Links to Chromatin Replication and Histone Metabolism. *Cell, 87*(1), 85-94. doi:10.1016/S0092-8674(00)81325-2

Pearson, C.G., Maddox, P.S., Zarzar, T.R., Salmon, E.D., and Bloom, K. (2003). Yeast kinetochores do not stabilize Stu2p-dependent spindle microtubule dynamics. Mol Biol Cell. 14, 4181-4195.

Perry, J. J., Tainer, J. A., & Boddy, M. N. (2008). A SIM-ultaneous role for SUMO and ubiquitin. *Trends Biochem Sci, 33*(5), 201-208. doi:10.1016/j.tibs.2008.02.001

Pichler, A., Gast, A., Seeler, J. S., Dejean, A., & Melchior, F. (2002). The nucleoporin RanBP2 has SUMO1 E3 ligase activity. *Cell, 108*(1), 109-120. Retrieved from http://www.ncbi.nlm.nih.gov/pubmed/11792325

Pickart, C. M., & Fushman, D. (2004). Polyubiquitin chains: polymeric protein signals. *Curr Opin Chem Biol, 8*(6), 610-616.

Pijnappel, W. W., Schaft, D., Roguev, A., Shevchenko, A., Tekotte, H., Wilm, M., . . . Stewart, A. F. (2001). The S. cerevisiae SET3 complex includes two histone deacetylases, Hos2 and Hst1, and is a meiotic-specific repressor of the sporulation gene program. *Genes Dev, 15*(22), 2991-3004. doi:10.1101/gad.207401

Pinder, J. B., McQuaid, M. E., & Dobson, M. J. (2013). Deficient sumoylation of yeast 2-micron plasmid proteins Rep1 and Rep2 associated with their loss from the plasmid-partitioning locus and impaired plasmid inheritance. *PLoS One, 8*(3), e60384. doi:10.1371/journal.pone.0060384

Podolski, M., Mahamdeh, M., & Howard, J. (2014). Stu2, the budding yeast XMAP215/Dis1 homolog, promotes assembly of yeast microtubles by increasing growth rate and decreasing catastrophe frequency. *Journal of Biological Chemistry, 289*(41), 28087-28093.

Poulsen, S. L., Hansen, R. K., Wagner, S. A., van Cuijk, L., van Belle, G. J., Streicher, W., . . . Mailand, N. (2013). RNF111/Arkadia is a SUMO-targeted ubiquitin ligase that facilitates the DNA damage response. *The Journal of cell biology, 201*(6), 797-807. doi:10.1083/jcb.201212075

Powers, A. F., Franck, A. D., Gestaut, D. R., Cooper, J., Gracyzk, B., Wei, R. R., . . . Asbury, C. L. (2009). The Ndc80 kinetochore complex forms load-bearing attachments to dynamic microtubule tips via biased diffusion. *Cell, 136*(5), 865-875. doi:10.1016/j.cell.2008.12.045

Praefcke, G.J., Hofmann, K., and Dohmen, R.J. (2012). SUMO playing tag with ubiquitin. Trends Biochem Sci 37, 23-31.

Prakash, S., & Prakash, L. (1977). Increased spontaneous mitotic segregation in MMS-sensitive mutants of Saccharomyces cerevisiae. *Genetics, 87*(2), 229-236. Retrieved from http://www.ncbi.nlm.nih.gov/pubmed/200524

Prudden, J., Perry, J. J., Nie, M., Vashisht, A. A., Arvai, A. S., Hitomi, C., . . . Boddy, M. N. (2011). DNA repair and global sumoylation are regulated by distinct Ubc9 noncovalent complexes. *Mol Cell Biol, 31*(11), 2299-2310.

Puig, O., Caspary, F., Rigaut, G., Rutz, B., Bouveret, E., Bragado-Nilsson, E., Wilm, M., and Seraphin, B. (2001). The tandem affinity purification (TAP) method: a general procedure of protein complex purification. Methods 24, 218-229.

Rabellino, A., Carter, B., Konstantinidou, G., Wu, S.-Y., Rimessi, A., Byers, L. A., . . . Teruya-Feldstein, J. (2012). The SUMO E3-ligase PIAS1 regulates the tumor suppressor PML and its oncogenic counterpart PML-RARA. *Cancer Research, 72*(9), 2275-2284.

Ramaswamy, V., Williams, J. S., Robinson, K. M., Sopko, R. L., & Schultz, M. C. (2003). Global control of histone modification by the anaphase-promoting complex. *Molecular and Cellular Biology, 23*(24), 9136-9149.

Rando, O. J., & Winston, F. (2012). Chromatin and transcription in yeast. *Genetics, 190*(2), 351-387.

Reifsnyder, C., Lowell, J., Clarke, A., & Pillus, L. (1996). Yeast SAS silencing genes and human genes associated with AML and HIV–1 Tat interactions are homologous with acetyltransferases. *Nat Genet, 14*(1), 42-49.

Reindle, A., Belichenko, I., Bylebyl, G. R., Chen, X. L., Gandhi, N., & Johnson, E. S. (2006). Multiple domains in Siz SUMO ligases contribute to substrate selectivity. *J Cell Sci, 119*, 4749-4757.

Rice, L. M., Montabana, E. A., & Agard, D. A. (2008). The lattice as allosteric effector: structural studies of αβ-and γ-tubulin clarify the role of GTP in microtubule assembly. *Proceedings of the National Academy of Sciences, 105*(14), 5378-5383.

Robbins, N., Leach, M. D., & Cowen, L. E. (2012). Lysine deacetylases Hda1 and Rpd3 regulate Hsp90 function thereby governing fungal drug resistance. *Cell reports, 2*(4), 878-888. doi:10.1016/j.celrep.2012.08.035

Rock, K. L., Gramm, C., Rothstein, L., Clark, K., Stein, R., Dick, L., . . . Goldberg, A. L. (1994). Inhibitors of the proteasome block the degradation of most cell proteins and the generation of peptides presented on MHC class I molecules. *Cell, 78*(5), 761-771. doi:10.1016/s0092-8674(94)90462-6

Rockmill, B., & Fogel, S. (1988). DIS1: a yeast gene required for proper meiotic chromosome disjunction. *Genetics, 119*(2), 261-272.

Rojas-Fernandez, A., Plechanovova, A., Hattersley, N., Jaffray, E., Tatham, M.H., and Hay, R.T. (2014). SUMO chain-induced dimerization activates RNF4. Mol Cell 53, 880-892.

Ronau, J. A., Beckmann, J. F., & Hochstrasser, M. (2016). Substrate specificity of the ubiquitin and Ubl proteases. *Cell Res, 26*(4), 441-456. doi:10.1038/cr.2016.38

Roth, S. Y., Denu, J. M., & Allis, C. D. (2001). Histone Acetyltransferases. *Annu Rev Biochem, 70*(1), 81-120. doi:10.1146/annurev.biochem.70.1.81

Roy, A., Kucukural, A., & Zhang, Y. (2010). I-TASSER: a unified platform for automated protein structure and function prediction. *Nature protocols, 5*(4), 725.

Sanchez, A. D., & Feldman, J. L. (2017). Microtubule-organizing centers: from the centrosome to non-centrosomal sites. *Current Opinion in Cell Biology, 44*, 93-101.

Sandmeier, J. J., French, S., Osheim, Y., Cheung, W. L., Gallo, C. M., Beyer, A. L., & Smith, J. S. (2002). RPD3 is required for the inactivation of yeast ribosomal DNA genes in stationary phase. *EMBO J, 21*(18), 4959-4968.

Sato, M., Vardy, L., Angel Garcia, M., Koonrugsa, N., & Toda, T. (2004). Interdependency of fission yeast Alp14/TOG and coiled coil protein Alp7 in microtubule localization and bipolar spindle formation. *Molecular biology of the cell, 15*(4), 1609-1622. doi:10.1091/mbc.e03-11-0837

Saunders, A., Core, L. J., & Lis, J. T. (2006). Breaking barriers to transcription elongation. *Nature Reviews Molecular Cell Biology, 7*(8), 557-567.

Scaglioni, P. P., Yung, T. M., Cai, L. F., Erdjument-Bromage, H., Kaufman, A. J., Singh, B., . . . Pandolfi, P. P. (2006). A CK2-dependent mechanism for degradation of the PML tumor suppressor. *Cell, 126*(2), 269-283.

Schwarz, S. E., Matuschewski, K., Liakopoulos, D., Scheffner, M., & Jentsch, S. (1998). The ubiquitin-like proteins SMT3 and SUMO-1 are conjugated by the UBC9 E2 enzyme. *Proceedings of the National Academy of Sciences of the United States of America, 95*(2), 560-564.

Schweiggert, J., Stevermann, L., Panigada, D., Kammerer, D., & Liakopoulos, D. (2016). Regulation of a spindle positioning factor at kinetochores by SUMO-targeted ubiquitin ligases. *Dev Cell, 36*(4), 415-427. doi:10.1016/j.devcel.2016.01.011

Schwienhorst, I., Johnson, E. S., & Dohmen, R. J. (2000). SUMO conjugation and deconjugation. *Mol Gen Genet, 263*(5), 771-786. doi:10.1007/s004380000254

Seker, T., Møller, K., & Nielsen, J. (2005). Analysis of acyl CoA ester intermediates of the mevalonate pathway in Saccharomyces cerevisiae. *Applied microbiology and biotechnology, 67*(1), 119-124.

Sekiyama, N., Ikegami, T., Yamane, T., Ikeguchi, M., Uchimura, Y., Baba, D., . . . Shirakawa, M. (2008). Structure of the small ubiquitin-like modifier (SUMO)-interacting motif of MBD1-containing chromatin-associated factor 1 bound to SUMO-3. *Journal of Biological Chemistry, 283*(51), 35966-35975.

Serrentino, M. E., Chaplais, E., Sommermeyer, V., & Borde, V. (2013). Differential association of the conserved SUMO ligase Zip3 with meiotic double-strand break sites reveals regional variations in the outcome of meiotic recombination. *PLoS Genet, 9*(4), e1003416. doi:10.1371/journal.pgen.1003416

Shahbazian, M. D., & Grunstein, M. (2007). Functions of site-specific histone acetylation and deacetylation. *Annu Rev Biochem, 76*.

Shandilya, S., Vertrees, J., & T., H. (2016). ColorByRMSD. *Pymol-script-repo*. Retrieved from https://pymolwiki.org/index.php/ColorByRMSD

Shang, Y., Tsao, C. C., & Gorovsky, M. A. (2005). Mutational analyses reveal a novel function of the nucleotide-binding domain of gamma-tubulin in the regulation of basal body biogenesis. *The Journal of cell biology, 171*(6), 1035-1044. doi:10.1083/jcb.200508184

Shero, J. H., Koval, M., Spencer, F., Palmer, R. E., Hieter, P., & Koshland, D. (1991). [54] Analysis of chromosome segregation in Saccharomyces cerevisiae. In *Methods in Enzymology* (Vol. 194, pp. 749-773): Elsevier.

Shirasu-Hiza, M., Coughlin, P., & Mitchison, T. (2003). Identification of XMAP215 as a microtubule-destabilizing factor in Xenopus egg extract by biochemical purification. *The Journal of cell biology, 161*(2), 349-358. doi:10.1083/jcb.200211095

Shuai, K. (2000). Modulation of STAT signaling by STAT-interacting proteins. *Oncogene, 19*(21), 2638-2644. doi:10.1038/sj.onc.1203522

Sievers, F., & Higgins, D. G. (2018). Clustal Omega for making accurate alignments of many protein sequences. *Protein Science, 27*(1), 135-145.

Sikorski, R. S., & Hieter, P. (1989). A system of shuttle vectors and yeast host strains designed for efficient manipulation of DNA in Saccharomyces cerevisiae. *Genetics, 122*(1), 19-27. Retrieved from https://www.ncbi.nlm.nih.gov/pubmed/2659436

Slaugenhaupt, S. A., Blumenfeld, A., Gill, S. P., Leyne, M., Mull, J., Cuajungco, M. P., . . . Reznik, L. (2001). Tissue-specific expression of a splicing mutation in the IKBKAP gene causes familial dysautonomia. *The American Journal of Human Genetics, 68*(3), 598-605.

Slep, K. C., & Vale, R. D. (2007). Structural basis of microtubule plus end tracking by XMAP215, CLIP-170, and EB1. *Molecular Cell, 27*, 976-991.

Smith, E. R., Eisen, A., Gu, W., Sattah, M., Pannuti, A., Zhou, J., . . . Allis, C. D. (1998). ESA1 is a histone acetyltransferase that is essential for growth in yeast. *Proceedings of the National Academy of Sciences, 95*(7), 3561-3565.

Sobel, R. E., Cook, R. G., Perry, C. A., Annunziato, A. T., & Allis, C. D. (1995). Conservation of deposition-related acetylation sites in newly synthesized histones H3 and H4. *Proceedings of the National Academy of Sciences, 92*(4), 1237-1241. doi:10.1073/pnas.92.4.1237

Song, J., Durrin, L. K., Wilkinson, T. A., Krontiris, T. G., & Chen, Y. (2004). Identification of a SUMO-binding motif that recognizes SUMO-modified proteins. *Proceedings of the National Academy of Sciences of the United States of America, 101*(40), 14373-14378. doi:10.1073/pnas.0403498101

Song, J., Zhang, Z., Hu, W., & Chen, Y. (2005). Small Ubiquitin-like Modifier (SUMO) Recognition of a SUMO Binding Motif a reversal of the bound orientation. *Journal of Biological Chemistry, 280*(48), 40122-40129.

Spillantini, M. G., Murrell, J. R., Goedert, M., Farlow, M. R., Klug, A., & Ghetti, B. (1998). Mutation in the tau gene in familial multiple system tauopathy with presenile dementia. *Proceedings of the National Academy of Sciences, 95*(13), 7737-7741.

Stankovic-Valentin, N., Deltour, S., Seeler, J., Pinte, S., Vergoten, G., Guérardel, C., . . . Leprince, D. (2007). An acetylation/deacetylation-SUMOylation switch through a phylogenetically conserved ψKXEP motif in the tumor suppressor HIC1 regulates transcriptional repression activity. *Molecular and Cellular Biology, 27*(7), 2661-2675.

Starai, V. J., Takahashi, H., Boeke, J. D., & Escalante-Semerena, J. C. (2003). Short-chain fatty acid activation by acyl-coenzyme A synthetases requires SIR2 protein function in Salmonella enterica and Saccharomyces cerevisiae. *Genetics, 163*(2), 545-555.

Stead, K., Aguilar, C., Hartman, T., Drexel, M., Meluh, P., & Guacci, V. (2003). Pds5p regulates the maintenance of sister chromatid cohesion and is sumoylated to promote the dissolution of cohesion. *J Cell Biol, 163*(4), 729-741.

Stehmeier, P., & Muller, S. (2009). Phospho-regulated SUMO interaction modules connect the SUMO system to CK2 signaling. *Molecular Cell, 33*(3), 400-409.

Stephan, A. K., Kliszczak, M., & Morrison, C. G. (2011). The Nse2/Mms21 SUMO ligase of the Smc5/6 complex in the maintenance of genome stability. *FEBS Lett, 585*(18), 2907-2913. doi:10.1016/j.febslet.2011.04.067

Sterner, D. E., & Berger, S. L. (2000). Acetylation of Histones and Transcription-Related Factors. *Microbiology and Molecular Biology Reviews, 64*(2), 435-459. doi:10.1128/mmbr.64.2.435-459.2000

Su, D., & Hochstrasser, M. (2010). A WLM protein with SUMO-directed protease activity. *Mol Cell Biol, 30*(15), 3734-3736.

Su, Y. F., Yang, T., Huang, H., Liu, L. F., & Hwang, J. (2012). Phosphorylation of Ubc9 by Cdk1 enhances SUMOylation activity. *PLoS One, 7*(4), e34250. doi:10.1371/journal.pone.0034250

Suka, N., Luo, K., & Grunstein, M. (2002). Sir2p and Sas2p opposingly regulate acetylation of yeast histone H4 lysine16 and spreading of heterochromatin. *Nat Genet, 32*(3), 378-383.

Sung, M.K., Lim, G., Yi, D.G., Chang, Y.J., Yang, E.B., Lee, K., and Huh, W.K. (2013). Genome-wide bimolecular fluorescence complementation analysis of SUMO interactome in yeast. Genome Res 23, 736-746.

Suzuki, A., Badger, B.L., Haase, J., Ohashi, T., Erickson, H.P., Salmon, E.D., and Bloom, K. (2016). How the kinetochore couples microtubule force and centromere stretch to move chromosomes. Nat Cell Biol 18, 382-392.

Svejstrup, J. Q. (2007). Elongator complex: how many roles does it play? *Current Opinion in Cell Biology, 19*(3), 331-336.

Tai, C.Y., Dujardin, D.L., Faulkner, N.E., and Vallee, R.B. (2002). The role of dynein, dynactin, and CLIP-170 interactions in LIS1 kinetochore function. J Cell Biol 156, 959-968.

Takahashi, H., McCaffery, J. M., Irizarry, R. A., & Boeke, J. D. (2006). Nucleocytosolic Acetyl-Coenzyme A Synthetase Is Required for Histone Acetylation and Global Transcription. *Molecular Cell, 23*(2), 207-217. doi:10.1016/j.molcel.2006.05.040

Takahashi, Y., Kahyo, T., Toh-E., A., Yasuda, H., & Kikuchi, Y. (2001). Yeast Ull1/Siz1 is a novel SUMO1/Smt3 ligase for septin components and functions as an adaptor between conjugating enzyme and substrates. *J Biol Chem, 276*(52), 48973-48977.

Takahashi, Y., Toh-e, A., & Kikuchi, Y. (2001). A novel factor required for the SUMO1/Smt3 conjugation of yeast septins. *Gene, 275*(2), 223-231.

Tanner, K. G., Langer, M. R., Kim, Y., & Denu, J. M. (2000). Kinetic mechanism of the histone acetyltransferase GCN5 from yeast. *Journal of Biological Chemistry, 275*(29), 22048-22055.

Tatham, M. H., Kim, S., Jaffray, E., Song, J., Chen, Y., & Hay, R. T. (2005). Unique binding interactions among Ubc9, SUMO and RanBP2 reveal a mechanism for SUMO paralog selection. *Nature structural & molecular biology, 12*(1), 67-74.

Teixidó-Travesa, N., Roig, J., & Lüders, J. (2012). The where, when and how of microtubule nucleation–one ring to rule them all. *Journal of Cell Science, 125*(19), 4445-4456.

Thawani, A., Kadzik, R. S., & Petry, S. (2018). XMAP215 is a microtubule nucleation factor that functions synergistically with the γ-tubulin ring complex. *Nature Cell Biology, 20*(5), 575-585.

Theodorakis, N.G., and Cleveland, D.W. (1992). Physical evidence for cotranslational regulation of beta-tubulin mRNA degradation. Mol Cell Biol 12, 791-799.

Tien, J. F., Umbreit, N. T., Gestaut, D. R., Franck, A. D., Cooper, J., Wordeman, L., . . . Davis, T. N. (2010). Cooperation of the Dam1 and Ndc80 kinetochore complexes enhances microtubule coupling and is regulated by aurora B. *J Cell Biol, 189*(4), 713-723. doi:10.1083/jcb.200910142

Tolić, I. M. (2018). Mitotic spindle: kinetochore fibers hold on tight to interpolar bundles. *European Biophysics Journal, 47*(3), 191-203.

Tóth, K. F., Knoch, T. A., Wachsmuth, M., Frank-Stöhr, M., Stöhr, M., Bacher, C. P., . . . Rippe, K. (2004). Trichostatin A-induced histone acetylation causes decondensation of interphase chromatin. *Journal of Cell Science, 117*(18), 4277. doi:10.1242/jcs.01293

Tracy, T. E., Sohn, P. D., Minami, S. S., Wang, C., Min, S.-W., Li, Y., . . . Ponnusamy, R. (2016). Acetylated tau obstructs KIBRA-mediated signaling in synaptic plasticity and promotes tauopathy-related memory loss. *Neuron, 90*(2), 245-260.

Trogden, K. P., & Rogers, S. L. (2015). TOG proteins are spatially regulated by Rac-GSK3beta to control interphase microtubule dynamics. *PLoS One, 10*(9), e0138966. doi:10.1371/journal.pone.0138966

Ullmann, R., Chien, C. D., Avantaggiati, M. L., & Muller, S. (2012). An acetylation switch regulates SUMO-dependent protein interaction networks. *Molecular Cell, 46*(6), 759-770.

Ulrich, H. D. (2008). The fast-growing business of SUMO chains. *Mol Cell, 32*(3), 301-305. doi:10.1016/j.molcel.2008.10.010

Usui, T., Maekawa, H., Pereira, G., & Schiebel, E. (2003). The XMAP215 homologue Stu2 at yeast spindle pole bodies regulates microtubule dynamics and anchorage. *EMBO J, 22*(18), 4779-4793. doi:10.1093/emboj/cdg459

Uzunova, K., Gottsche, K., Miteva, M., Weisshaar, S.R., Glanemann, C., Schnellhardt, M., Niessen, M., Scheel, H., Hofmann, K., Johnson, E.S., et al. (2007). Ubiquitin-dependent proteolytic control of SUMO conjugates. J Biol Chem 282, 34167-34175.

van Breugel, M., Dreschsel, D., & Hyman, A. A. (2003). Stu2p, the budding yeast member of the conserved Dis1/XMAP215 family of microtubule-associated proteins is a plus end-binding microtubule destabilizer. *Journal of Cell Biology, 161*(2), 359-369.

Vidali, G., Gershey, E., & Allfrey, V. (1968). Chemical studies of histone acetylation the distribution of ε-N-acetyllysine in calf thymus histones. *Journal of Biological Chemistry, 243*(24), 6361-6366.

Volkov, V. A., Zaytsev, A. V., Gudimchuk, N., Grissom, P. M., Gintsburg, A. L., Ataullakhanov, F. I., . . . Grishchuk, E. L. (2013). Long tethers provide high-force coupling of the Dam1 ring to shortening microtubules. *Proc Natl Acad Sci U S A, 110*(19), 7708-7713. doi:10.1073/pnas.1305821110

Wagner, S. A., Beli, P., Weinert, B. T., Nielsen, M. L., Cox, J., Mann, M., & Choudhary, C. (2011). A proteome-wide, quantitative survey of in vivo ubiquitylation sites reveals widespread regulatory roles. *Molecular & Cellular Proteomics, 10*(10).

Wang, H.-W., & Nogales, E. (2005). Nucleotide-dependent bending flexibility of tubulin regulates microtubule assembly. *Nature, 435*(7044), 911-915.

Wang, P. J., & Huffaker, T. C. (1997). Stu2p: A microtubule-binding protein that is an essential component of the yeast spindle pole body. *The Journal of cell biology, 139*(5), 1271-1280. Retrieved from http://www.ncbi.nlm.nih.gov/cgi-bin/Entrez/referer?http://www.jcb.org/cgi/content/full/139/5/1271

Wang, Y. E., Pernet, O., & Lee, B. (2012). Regulation of the nucleocytoplasmic trafficking of viral and cellular proteins by ubiquitin and small ubiquitin-related modifiers. *Biol Cell, 104*, 121-138. doi:10.1111/b0c.201100105

Warren, C. D., Brady, D. M., Johnston, R. C., Hanna, J. S., Hardwick, K. G., & Spencer, F. A. (2002). Distinct Chromosome Segregation Roles for Spindle Checkpoint Proteins. *Mol Biol Cell, 13*(9), 3029-3041. doi:10.1091/mbc.e02-04-0203

Weinert, B. T., Iesmantavicius, V., Moustafa, T., Schölz, C., Wagner, S. A., Magnes, C., . . . Choudhary, C. (2014). Acetylation dynamics and stoichiometry in Saccharomyces cerevisiae. *Mol Syst Biol, 10*(1), 716. doi:https://doi.org/10.1002/msb.134766

Weinstein, B., and Solomon, F. (1990). Phenotypic consequences of tubulin overproduction in Saccharomyces cerevisiae: differences between alpha-tubulin and beta-tubulin. Mol Cell Biol 10, 5295-5304.

Wellen, K. E., Hatzivassiliou, G., Sachdeva, U. M., Bui, T. V., Cross, J. R., & Thompson, C. B. (2009). ATP-Citrate Lyase Links Cellular Metabolism to Histone Acetylation. *Science, 324*(5930), 1076-1080. doi:10.1126/science.1164097

Whittington, A. T., Vugrek, O., Wei, K. J., Hasenbein, N. G., Sugimoto, K., Rashbrooke, M. C., & Wasteneys, G. O. (2001). MOR1 is essential for organizing cortical microtubules in plants. *Nature, 411*(6837), 610-613.

Widlund, P. O., Stear, J. H., Pozniakovsky, A., Zanic, M., Reber, S., Brouhard, G. J., . . . Howard, J. (2011). XMAP215 polymerase activity is built by combining multiple tubulin-binding TOG domains and a basic lattice-binding region. *Proceedings of the National Academy of Sciences of the United States of America, 108*(7), 2741-2746. doi:10.1073/pnas.1016498108

Wieczorek, M., Bechstedt, S., Chaaban, S., and Brouhard, G.J. (2015). Microtuble-associated proteins control the kinetics of microtubule nucleation. Nature Cell Biology 17, 907-916.

Wiese, C., & Zheng, Y. (2006). Microtubule nucleation: γ-tubulin and beyond. *Journal of Cell Science, 119*(20), 4143-4153.

Wilkinson, K. D. (1997). Regulation of ubiquitin-dependent processes by deubiquitinating enzymes. *FASEB J, 11*(14), 1245-1256. Retrieved from http://www.ncbi.nlm.nih.gov/pubmed/9409543

Winey, M., & Bloom, K. (2012). Mitotic spindle form and function. *Genetics, 190*(4), 1197-1224. doi:10.1534/genetics.111.128710

Wolyniak, M. J., Blake-Hodek, K., Kosco, K., Hwang, E., You, L., & Huffaker, T. C. (2006). The regulation of microtubule dynamics in *Saccharomyces cerevisiae* by three interacting plus end tracking proteins. *Mol. Biol. Cell, 17*(6), 2789-2798.

Wong, J., Nakajima, Y., Westermann, S., Shang, C., Kang, J.-S., ., Goodner, C., Houshmand, P., Fields, S., Chan, C.S.M., Drubin, D., et al. (2007). A protein interaction map of the mitotic spindle. Molecular Biology of the Cell 18, 3800-3809.

Wu, J., & Akhmanova, A. (2017). Microtubule-organizing centers. *Annual review of cell and developmental biology, 33*, 51-75.

Xia, P., Wang, Z., Liu, X., Wu, B., Wang, J., Ward, T., . . . Yao, X. (2012). EB1 acetylation by P300/CBP-associated factor (PCAF) ensures accurate kinetochore-microtubule interactions in mitosis. *Proc Natl Acad Sci U S A, 109*(41), 16564-16569. doi:10.1073/pnas.1202639109

Xie, S., Yang, Y., Lin, X., Zhou, J., Li, D., & Liu, M. (2018). Characterization of a novel EB1 acetylation site important for the regulation of microtubule dynamics and cargo recruitment. *Journal of cellular physiology, 233*(3), 2581-2589.

Xu, Y., Plechanovová, A., Simpson, P., Marchant, J., Leidecker, O., Kraatz, S., . . . Matthews, S. J. (2014). Structural insight into SUMO chain recognition and manipulation by the ubiquitin ligase RNF4. *Nature communications, 5*(1), 1-12.

Xu, Z.-m., Wang, Y.-q., Mei, Q., Chen, J., Du, J., Wei, Y., & Xu, Y.-c. (2006). Trichostatin a inhibits proliferation, induces apoptosis and cell cycle arrest in HeLa cells. *Chinese Journal of Cancer Research, 18*(3), 188-192. doi:10.1007/s11670-006-0188-5

Yang, J., Yan, R., Roy, A., Xu, D., Poisson, J., & Zhang, Y. (2015). The I-TASSER Suite: protein structure and function prediction. *Nature methods, 12*(1), 7.

Yang, X. J. (2004). The diverse superfamily of lysine acetyltransferases and their roles in leukemia and other diseases. *Nucleic Acids Res, 32*(3), 959-976.

Yong-Gonzales, V., Hang, L. E., Castellucci, F., Branzei, D., & Zhao, X. (2012). The Smc5-Smc6 complex regulates recombination at centromeric regions and affects kinetochore protein sumoylation during normal growth. *PLoS One, 7*(12), e51540. doi:10.1371/journal.pone.0051540

Yoshimura, S. H., & Hirano, T. (2016). HEAT repeats – versatile arrays of amphiphilic helices working in crowded environments? *Journal of Cell Science, 129*(21), 3963-3970. doi:10.1242/jcs.185710

Young, P., Deveraux, Q., Beal, R. E., Pickart, C. M., & Rechsteiner, M. (1998). Characterization of two polyubiquitin binding sites in the 26 S protease subunit 5a. *Journal of Biological Chemistry, 273*(10), 5461-5467.

Yu, J.-X., Chen, Q., Yu, Y.-Q., Li, S.-Q., & Song, J.-F. (2016). Upregulation of colonic and hepatic tumor overexpressed gene is significantly associated with the unfavorable prognosis marker of human hepatocellular carcinoma. *American journal of cancer research, 6*(3), 690-700. Retrieved from https://pubmed.ncbi.nlm.nih.gov/27152245

Yuan, H., Rossetto, D., Mellert, H., Dang, W., Srinivasan, M., Johnson, J., . . . Abshiru, N. (2012). MYST protein acetyltransferase activity requires active site lysine autoacetylation. *EMBO J, 31*(1), 58-70.

Yunus, A. A., & Lima, C. D. (2009). Structure of the Siz/PIAS SUMO E3 ligase Siz1 and determinants required for SUMO modification of PCNA. *Molecular Cell, 35*(5), 669-682.

Zhang, X.-D., Goeres, J., Zhang, H., Yen, T. J., Porter, A. C. G., & Matunis, M. J. (2008). SUMO-2/3 modification and binding regulate the association of CENP-E with kinetochores and progression through mitosis. *Mol Cell, 29*, 729-741.

Zhang, Y. (2008). I-TASSER server for protein 3D structure prediction. *BMC Bioinformatics, 9*(1), 40.

Zhao, G., Cheng, Y., Gui, P., Cui, M., Liu, W., Wang, W., . . . Yao, X. (2019). Dynamic acetylation of the kinetochore-associated protein HEC1 ensures accurate microtubule-kinetochore attachment. *The Journal of Biological Chemistry, 294*(2), 576-592. doi:10.1074/jbc.RA118.003844

Zhao, X., & Blobel, G. (2005). A SUMO ligase is part of a nuclear multiprotein complex that affects DNA repair and chromosomal organization. *Proc. Natl. Acad. Sci. USA, 102*(13), 4777-4782.

Zheng, G., & Yang, Y.-C. (2005). Sumoylation and acetylation play opposite roles in the transactivation of PLAG1 and PLAGL2. *Journal of Biological Chemistry, 280*(49), 40773-40781.

VITA

Matt Alec Greenlee

Candidate for the Degree of

Doctor of Philosophy

Dissertation: THE TOG PROTEIN STU2/XMAP215 IS REGULATED BY ACETYLATION AND SUMOYLATION

Major Field: Biochemistry and Molecular Biology

Biographical:

Education:

Completed the requirements for the Doctor of Philosophy in Biochemistry and Molecular Biology at Oklahoma State University, Stillwater, Oklahoma in May 2021.

Completed the requirements for the Bachelor of Science in Biochemistry and Molecular Biology at Oklahoma State University, Stillwater, Oklahoma in Spring 2011.

Experience:

Research Associate, Professor Rita K. Miller, Oklahoma State University, Stillwater, Oklahoma, January 2012-Present

Undergraduate Research Assistant, Professor Junpeng Deng, Oklahoma State University, Stillwater, Oklahoma, January 2008-August 2010

Undergraduate Research Assistant, Professor Jack W. Dillwith, Oklahoma State University, Stillwater, Oklahoma, August 2010-May 2011

Sergeant, United States Army Reserves, 401st Engineering Brigade, Enid, Oklahoma, March 2009-March 2017